Assessment of structural damage using operational time responses

by

Harry Magadhlela Ngwangwa

submitted in partial fulfilment of the requirements
for the degree

MSc: Mechanics

in the Faculty of Engineering, Built Environment
and Information Technology

University of Pretoria

Pretoria

November 2004

Assessment of structural damage using operational time responses

By

Harry Magadhlela Ngwangwa

Supervisors: Prof. P.S. Heyns, Mr F. van Tonder

Department: Mechanical and Aeronautical Engineering

Degree: MSc:Mechanics

Summary

The problem of vibration induced structural faults has been a real one in engineering over the years. If left unchecked it has led to the unexpected failures of so many structures. Needless to say, this has caused both economic and human life losses.

Therefore for over forty years, structural damage identification has been one of the important research areas for engineers. There has been a thrust to develop global structural damage identification techniques to complement and/or supplement the long-practised local experimental techniques. In that respect, studies have shown that vibration-based techniques prove to be more potent.

Most of the existing vibration-based techniques monitor changes in modal properties like natural frequencies, damping factors and mode shapes of the structural system to infer the presence of structural damage. Literature also reports other techniques which monitor changes in other vibration quantities like the frequency response functions, transmissibility functions and time-domain responses. However, none of these techniques provide a complete identification of structural damage.

This study presents a damage detection technique based on operational response monitoring, which can identify all the four levels of structural damage and be implemented as a continuous structural health monitoring technique. The technique is based on monitoring changes in internal data variability measured by a test statistic χ_0^2 value. Structural normality is assumed when the χ_{0m}^2value calculated from a fresh set of measured data is within the limits prescribed by a threshold χ_{0TH}^2 value . On the other hand, abnormality is assumed when this threshold value has been exceeded. The quantity of damage is determined by matching the χ_{0m}^2 value with the χ_{0p}^2 values predicted using a benchmark finite element model.

The use of χ_0^2 values is noted to provide better sensitivity to structural damage than the natural frequency shift technique. The analysis carried out on a numerical study showed that the sensitivity of the proposed technique ranged from three to thousand times as much as the sensitivity of the natural frequencies. The results from a laboratory structure showed that accurate estimates of damage quantity and remaining service life could be achieved for crack lengths of less than 0.55 the structural thickness. This was due to the fact that linear elastic fracture mechanics theory was applicable up to this value.

Therefore, the study achieved its main objective of identifying all four levels of structural damage using operational response changes.

Keywords: structural damage identification, vibration-based technique, operational response monitoring, continuous structural health monitoring, internal data variability, test statistic, damage quantification, crack ratio, remaining service life, crack propagation.

CONTENTS

List of figures

List of tables

Nomenclature

Symbol	Meaning	Units
a	crack length	m
A	cross-sectional area	m^2
$\bar{a}$	crack ratio	
b	material width	m
C	crack growth coefficient	$MPa(\sqrt{m})$
$[C]$	viscous damping matrix	Ns/m
$[\Delta C]$	change in viscous damping matrix	Ns/m
C_0	corrected crack growth coefficient	$MPa(\sqrt{m})$
d_{Ks}	reduction factor	
E	Young's modulus of elasticity	Pa
f	frequency	Hz
$f(g)$	crack geometry factor	
$\{F\}$	force vector	N
F_0	test statistics for equality of means	
$F(t)$	force as a function of time	N
H	thickness or material depth	m

$[H]$	structural damping matrix	N/m
H_0	null hypothesis	
H_1	alternative hypothesis	
i	$\sqrt{-1}$	
I	second moment of area	m^4
$[ke]$	element stiffness matrix	N/m
$[K]$	stiffness matrix	N/m
ΔK	change in stress intensity factor	$Pa\sqrt{m}$
$[\Delta K]$	change in stiffness matrix	N/m
L	length	m
m	crack growth exponent	
$[M]$	mass matrix	kg
N_a	Crack propagation life to crack length a	$cycles$
N_f	Progation life to failure or final crack length a_f	$cycles$
RSL_a	Remaining service life at crack length a	$cycles$
S^2	sample variance	
$[S]$	sensitivity matrix	

Symbol	Meaning	Units
t	time	s
x, y, z	translational degrees of freedom	m
χ_0^2	test statistics for equality of variances	
ρ	mass density	kg/m^3
ϵ	error	
σ^2	variance	
$\Delta\sigma_{eff}$	effective stress	Pa
μ	sample mean	
ω	circular frequency	rad/s
ω_n	undamped natural frequency	rad/s
ω_d	damped natural frequency	rad/s

Superscripts and Subscripts

d	damaged
i, j, k, l, m, n	integers
m	measured
p	predicted
u	undamaged
0	original or initial

Abbreviations

APC	aproximate parameter change
AR(X)	autoregressive (with eXogeneous inputs) model
ARMA(X)	autoregressive moving average (with eXogeneous inputs) model
DI	damage index method
DSM	damage signature matching
FEM	finite element method
FRF	frequency response function
LEFM	linear elastic fracture mechanics
MIMO	multiple input multiple output
MISO	multiple input single output
MRP	minimum rank perturbation method
PRBS	pseudo-random binary signal
SEE	sensitivity-based element by element method

1. INTRODUCTION AND LITERATURE STUDY

1.1 *Introduction*

Modern practice in structural design often dictates that structural systems be fabricated to minimum weight and cost yet safely sustain the loads applied to them for a pre-established duration. Nevertheless, many structures develop serious structural faults resulting in failure due to unexpected severe loadings or deterioration from exposure to elements. Thus their capacity to perform intended functions is diminished by the faults.

Structural faults may be caused by different mechanisms: corrosion, creep, erosion, fatigue, impact, wear, etc. The present study focuses on structural damage caused by service cyclic loading (fatigue). The problem with this is that the structure can start to develop cracks well below its design stress (especially if the structure was not designed for fatigue). Now, unchecked structural damage leads to structural failure, which can cause economic and life losses. Thus, there is need for continuous monitoring of structures to detect any initiating cracks.

Industry has used regular visual inspections for structural damage detection. These methods are localised and almost always require that the suspect sections of the structure be known. There may also be a need to shut down production or service, and the structure may even have to be disassembled during the inspections. This has an obvious disadvantage of loss of production or services.

Therefore, since the late 1960's, industry has also focussed its investigations on the use of global structural damage detection methods. Vibration-based damage detection methods have been developed under this motivation. Mottershead and Friswell (1993) provided a survey of damage detection methods that are based on FEM updating. Doebling, Farrar, Prime and Shevitz (1996) provided a review of vibration-based damage detection methods.

Vibration-based damage detection methods are developed on the premise that damage will change the structural (mass, stiffness or damping) properties, which further lead to changes in the dynamic characteristics such as natural frequencies, damping loss factors and mode shapes. Since the changes in the characteristics can be measured and studied, in principle, it is possible to trace what structural changes have caused the dynamic characteristics to change (He, 1999).

Rytter (1993) proposed a classification system for damage detection. He identified four levels against which the success of structural damage detection techniques can be

measured:

- **Level 1:** Determining that damage is present in the structure;
- **Level 2:** Determination of the geometric location of the damage;
- **Level 3:** Quantification of the severity of the damage;
- **Level 4:** Prediction of the remaining service life of the structure.

Farrar and Doebling (1997) noted that the modal-based damage detection methods that do not use some structural model, primarily provide Level 1 and Level 2 damage identification. They further noted that, when the modal-based methods are coupled with a structural model, Level 3 damage identification could be provided in some cases. Level 4 is generally associated with the fields of fracture mechanics, fatigue life analysis, or structural design assessment, which are considered outside the vibration analysis.

A review of the most recent literature (see section 1.5) shows that more emphasis has been placed on the derivation and refinement of the algorithms (and schemes) used for damage identification rather than full realisation of these damage identification levels. It may therefore be said that not enough work has been done to bring together vibration analysis and fracture mechanics analysis so that full structural damage identification can be provided within a single package.

Thus, the purpose of this work is to develop a structural damage detection technique, which provides all four levels of damage identification by integrating linear elastic fracture mechanics analysis into vibration analysis. The uniqueness of this work lies in its effort to draw upon structural dynamics analysis, and fracture mechanics analysis to develop a complete damage identification technique at all four levels. The next section presents an overview of the proposed technique.

1.2 Technique overview

The technique uses changes in measured operational time responses to detect structural damage. In order to estimate damage quantity, the changes in measured responses are compared with changes from predicted responses using a test statistic value. More accurate estimates can be determined by performing a sensitivity based procedure, which optimises an error between the measured response and a closest matching predicted response. The entire technique involves the following parts:

- System modelling and force identification
- Structural damage modelling
- Prediction of responses
- Structural damage identification.

These parts are described in more detail in section 1.3.

1.3 Detailed technique description

The proposed technique solves the structural damage problem via the forward problem formulation, in which measured structural time response changes are compared to the predicted time response changes with known structural damage (crack length) and service life. Thus, changes in structural time responses are initially predicted from known structural damage using a FEM. These changes are benchmarked against measured time response changes.

System modelling and force identification

A finite element model of the real structural system is developed. Having ensured that the analytical model is representative of the real system, it is accordingly, simulated with synthetically generated excitation. This results into a multivariable state space model, which is inverted using time domain-based inversion techniques (Raath, 1992).

Then the measured operational responses are applied to the inverse model to calculate, in an offline manner, the operational forces. The identified operational forces are applied to the finite element model to identify stress *hot spots* on the structure. The location of the stress *hot spots* on the model are considered to be likely damage locations.

Structural damage modelling

Structural damage is represented by a crack ratio, which is the ratio of crack length a to the depth of the material H at the critical location (figure 1.1). Taking the worst damage scenario as crack ratio a_f/H, the crack propagation space (from a virgin state to the worst damage state) is scaled into convenient damage scenarios each of which is represented by a crack ratio. An assumption is made that the crack is not branched but

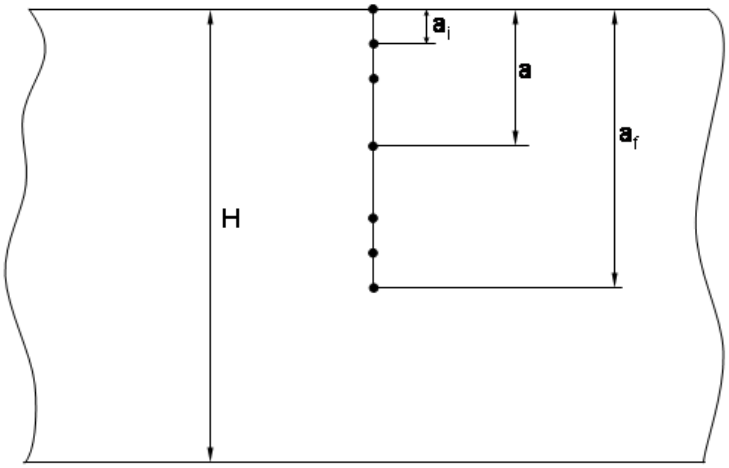

Fig. 1.1: Modelling damage by using crack ratios

grows linearly and uni-axially. This assumption basically aligns itself with fractures under plain strain state.

The Paris law is used to calculate remaining life to failure for each of the damage scenarios. In this way, each damage scenario has both the crack ratio and remaining service life.

Prediction of responses

Operational responses are predicted at each crack ratio using FEM. Then, dynamic sensitivity coefficients of operational responses with respect to crack length changes are used to fine tune the predictions so that a better fit is achieved with measured responses. This is done by using a first order Taylor series expansion.

Structural damage identification

Residual errors are determined by taking the differences between the predicted responses for each damage scenario, and the undamaged structural responses. These are statistically treated in a model, which returns test statistics values for each damage scenario.

These test statistics values are used as features for damage identification. So during the test, measured responses are treated in a similar manner and their calculated test statistics values are compared with the predicted values. Then a sensitivity based

optimisation scheme is used which minimises an error function of the measured response and closest matching predicted response. The result is that at each stage, the model is capable of estimating the amount of structural damage (in crack ratio) and remaining service life of the structure, which satisfies all the four levels of damage identification.

1.4 Historical perspective

Damage detection as determined by the changes in the dynamic properties or response of systems, has been practiced in a qualitative manner using acoustic techniques, since modern man has used tools (Farrar, Doebling & Duffey, 1997). This subject has received considerable attention in the technical literature and a more comprehensive review of the developments in this technology up to 1995 is reported by Doebling, et al. 1996. Some of the more recent work has been presented in this study in section 1.5.

In the literature, four distinct industries are recognised as having driven the development of vibration-based damage detection techniques. They are listed here in ascending order of their relative success in the final implementation of vibration-based damage detection techniques on their structural systems: oil industry, civil engineering industry, aerospace industry and rotating machinery industry.

Oil industry

Efforts to develop vibration-based damage detection for its offshore structures started in the 1970s. However, the efforts were abandoned in the early 1980s, because of problems related to inaccessibility of some parts of the structures for measurement and the ever-changing structural properties due to marine growth.

Civil engineering industry

The civil engineering community started the study of vibration based damage detection in the early 1980s. Research is still on going in this industry and current focus is on installation of online structural health monitoring systems on bridges (Li, Chan & Ko, 2001).

Aerospace industry

Efforts to study the application of vibration based damage detection on its space shuttles began during the late 1970s and early 1980s. They developed the Shuttle Modal Inspection System (SMIS), which is used to detect damage on control surfaces, fuselage

panels and lifting surfaces.

Rotating machinery industry

Over the years, vibration based damage detection methods have developed from academia into an industrial practice in the rotating machinery industry. Today commercial software is available to help the user to systematically apply the technology to the operating environment.

1.5 Review of the existing vibration based damage detection methods

Doebling et al. (1996) categorised structural damage methods based on the type of measured data used, and/or the technique used to identify the damage from the measured data. From their review it is clear that the use of modal property data has dominated structural damage detection. In this section, an attempt is made to review some of the more recent literature on structural damage detection. A new classification called *Statistical based methods* has been added in section 1.5.8 to capture the proliferation of methods that attempt to install continuous health monitoring systems on structures. The detection scheme employed in the present study belongs to this class.

1.5.1 Modal frequency changes

The observation that changes in structural properties cause changes in vibration frequencies was the motivation for using modal frequency changes for damage detection. The employed detection techniques attempt to solve the structural damage problem either as a forward problem or an inverse problem.

The forward problem seeks the solution by calculating frequency shifts from known damage. While the inverse problem calculates structural damage given the frequency shifts (Doebling, et al. 1996). There are a lot of methods reported in the literature which are based on these approaches (Doebling, et al. 1996).

Narayana and Jebaraj (1999) propose a method for detecting crack location and extent on a cantilever beam by using changes in natural frequencies only. They show that when the crack is located at the peak/trough positions of the strain mode shapes, the percentage change in frequency values are higher for corresponding modes. Whereas,

if the crack is located at the nodal points of the strain mode shapes, the percentage change in frequency values are lower for corresponding modes.

1.5.2 ***Mode Shape changes***

Mode shapes reveal information about the deformation pattern of the vibrating structure under some given excitations (Heyns, 2002). Modal Assurance Criterion (MAC) and Co-ordinate Modal Assurance Criterion (COMAC) are two innovations in the use of mode shape data for structural damage detection.

1.5.3 ***Mode shape curvature/Strain mode shape changes***

The method provides a more sensitive and reliable technique (it is stable, because it is not liable to false-positive or -negative results as is the case with the other techniques) (Doebling, et al. 1996). The mode shape curvature methods have mainly been applied to detection of damage in bridge structures.

1.5.4 ***Methods based on dynamically measured flexibility***

Typically, damage is detected using flexibility matrices by comparing the flexibility matrix synthesized using the modes of the damaged structure with the flexibility matrix synthesized using the modes of the undamaged structure or the flexibility matrix from a finite element model. The measured flexibility matrix is noted to be most sensitive to changes in the lower-frequency modes of the structure, because of the inverse relationship to the square of the modal frequencies (Doebling, et al. 1996).

There are five different variants for damage detection based on the dynamically measured flexibility:

- **Comparisons of flexibility changes**: The changes in the dynamically measured flexibility matrices as induced by structural damage are determined and compared with each other.
- **Unity check method**: Structural damage is assumed to occur if the dynamically measured flexibility matrix does not approximate the pseudo inverse of the undamaged structure's stiffness matrix.

- **Stiffness error matrix method**: This is based on the determination of a stiffness error matrix, which is described as a function of the change in dynamically measured flexibility matrix and the stiffness of the undamaged structure.

- **Effects of residual flexibility**: This completes the reciprocity of the dynamically measured flexibility matrix by adding contributions from modes lying outside the desired bandwidth (Doebling, et al. 1996). It is noted that more accuracy is achieved when the residuals are taken into account.

- **Changes in measured stiffness matrix**: This method monitors the changes in a dynamically measured stiffness matrix (a pseudo inverse of the dynamically measured flexibility matrix). The dynamically measured mass and damping can also be monitored.

  Maeck and De Roeck (2003) calculate the modal bending moments and curvatures to derive the bending stiffness at each location on the structure. The basic assumption is that damage can be directly related to a decrease of stiffness in the structure.

1.5.5 ***Matrix update methods***

The basic idea in this approach is that structural damage is indicated in the overall static and/or dynamic response of the system by some diversion from the nominal response (response of the undamaged structure). It is then possible to use the structural equations of motion, the undamaged structure's property matrices, and the structural response to mathematically search for the damaged structure's property matrices that would reproduce the desired structural response as closely as possible. The manner in which this is performed is by forming a constrained optimisation problem which is made up of the structural equations of motion, the original matrices and the desired structural response (Doebling, et al. 1996).

There are five approaches, which are characteristic of this classification.

- **Objective functions and constraints**: The objective functions and constraints are both given by the modal force error, which is defined as the harmonic force excitation that would have to be applied to the undamaged structure at the frequency of the damaged structure so that it would respond with the damaged structure's mode shapes.

  Chou and Ghaboussi (2001) use a genetic algorithm to identify damage in a framed bridge structure. They use the differences between measured and com-

puted static responses (displacements) to identify changes in Young's modulus and cross-sectional areas. The structural damage problem is formulated as an optimisation problem. The output and equation errors are used in the formulation of the optimisation problem, where output error is defined as the discrepancy between measured and computed responses under static loading and equation error is the residual force in the system of equilibrium equations.

Görl and Link (2003) describe an approach to identify the location and the extent of damage introduced into the steel frame, using a two-step procedure. In the first step, the measured dynamic response of the original undamaged structure is used to generate a reference finite element model of the structure. The selected parameters are identified by means of a mathematical optimisation algorithm, minimising an objective function containing the test/analyses differences of the eigenfrequencies and mode shapes. The uncertain parameters have to be chosen with care in order to retain the physical significance of the updated model.

In the next step, the experimental modal data of the damaged structure are used to identify the extent of the damages. This is based on comparing the changes of stiffness parameters identified from the undamaged and the damaged structure. With the identified parameters, the finite element model is able to reproduce the experimental data as close as possible and allow damage quantification.

- **Optimal matrix update methods**: These methods use a closed-form, direct solution to compute the damaged model matrices or the perturbation matrices (Doebling, et al. 1996). The problem is generally formulated as a Lagrange multiplier or penalty-based optimisation, in which an error function of the dynamic matrices is minimised.

- **Sensitivity based update methods**: These methods are based on the solution of a first-order Taylor series that minimises an error function of the matrix perturbations (Doebling, et al. 1996). The present study uses a similar approach. The basic theory is the determination of a modified parameter vector p, which is expressed as (Doebling, et al. 1996):

$$\{p\}^{n+1} = \{p\}^n + \{\delta p\}^{n+1}$$

where the parameter perturbation vector $\{\delta p\}^{n+1}$ is computed from a Newton-Raphson iteration problem for minimising an error function:

$$J(\{p\}^n + \{\delta p\}^{n+1}) \approx J(\{p\}^n) + [\frac{\partial J}{\partial p}(\{p\}^n)] \times \{\delta p\}^{n+1} = 0;$$

where $J(\{p\})$, is the error function to be minimised. Typically the error function is selected to be the modal force error.

Friswell, Penny, and Garvey (1998) developed a technique, which is based on combined use of eigensensitivity and genetic algorithms for damage detection location and quantification. They employ a genetic algorithm to minimise a weighted square-value of the frequency error. Structural damage is modelled by a reduction in Young's modulus, while the element number in the finite element model gives damage location.

Thus, the genetic algorithm searches for both the reduction in Young's modulus and element number(s) (corresponding to position on the structure), which are the fittest to have contributed to the frequency error. The technique is applied to the simulated beam example and experimental plate structure and yields very good results. They also demonstrate that the algorithm is robust to systematic errors in the measured data.

Damage is modelled by a dimensionless θ parameter, which represents the contribution of a substructure or element stiffness to the system stiffness matrix. And a damage case is assumed to occur when θ exceeds a certain threshold. They compare the technique to MRP, SEE and DI techniques, and conclude that their technique is superior.

Fritzen, Jennewein and Kiefer (1998) propose a technique for damage detection based on the notion of model updating and is capable of using any type of measured vibration data. The detection scheme relies on the availability of the undamaged system's response data. Then they determine residuals, which are the differences between undamaged and damaged system responses. Structural damage is modelled by dimensionless parameters, which are related to physical system parameters. Changes in dimensionless parameters are related to residuals in a sequentially linearised relation through a sensitivity function. The solution of this equation yields changes in dimensionless parameters, which can be used to detect and quantify structural damage in terms of physical system parameters.

Lam, Ko and Wong (1998) report a damage location method for framed structures based on experimental modal and sensitivity analysis. They use an approximate parameter change (APC) technique to identify the possible damage locations in the structures. They derive relationships between the measured modal parameters and the changed system parameters, in which by means of the least-squares method, the APC values for the i^{th} mode can be estimated for different equation systems. Then they use damage signature matching (DSM) to match the changes in dynamic characteristics between the measured and those predicted by an analytical model for all possible damage cases.

Raich and Liszkai (2003) propose a damage detection technique based on frequency response function data, which uses a genetic algorithm. They model

damage by what they call *damage indices*, which are simply values between 0 and 1. The damage indices are related directly to physical system properties like element stiffness matrices to give more meaning to the measure of structural damage. In the detection scheme, they formulate the damage detection problem as an optimisation problem. The optimisation is performed by genetic algorithm, where the expected number of gene instances is related to the number of possibly damaged elements.

- **Eigenstructure assignment method**: This is based on the design of a fictitious controller which would minimise the modal force error. The controller gains are then interpreted as parameter matrix perturbations to the undamaged structural model (Doebling, et al. 1996).

- **Hybrid matrix update methods and other considerations**: Some researchers have employed methods, which are a combination of the distinct methods given previously.

  Garibaldi, Marchesiello and Bonisoli (2003) use a mixture of techniques including advanced signal processing, FE modelling and updating techniques to identify damage on the Z24-Bridge structure.

1.5.6 ***Nonlinear methods***

These methods are based on the premise that structural damage introduces nonlinearities in the vicinity of the damage location. Thus methods of identifying nonlinearities in structures are developed to detect structural damage at an earliest possible stage.

Much success has been achieved in rotating machinery applications or in structural systems with suspicious joints, where damage is localised and it is fairly easy to detect a nonlinear response at its outset (Doebling, et al. 1996).

Wang, Lin and Lim (1997) propose a damage detection technique, which uses frequency response function data. They assume availability of the undamaged system's response data. The detection scheme employs a non-linear perturbation equation of receptance data to determine the difference between the measured damaged and the analytical undamaged system's response data. Structural damage is modelled by reduction factors applied to each element of the assembled system matrix. A vector containing the reduction factors is called the damage vector. They derive a relation between the damage vector and the differences between the undamaged and damaged system's responses. The damage vector yields both damage location and severity information.

1.5.7 Neural network-based methods

In complex structures where estimation of the structural behaviour during damage is complicated and largely random, neural networks are used. Neural networks have been promoted as universal function approximators for functions of arbitrary complexity (Doebling, et al. 1996).

Zapico, González and Worden (2003) proposed a technique of damage assessment based on neural networks and apply it to the Steel Quake structure. The method is intended to assess the overall damage at each floor in composite frames caused by seismic loading. A neural network is used to calibrate the initial undamaged structure, and another to predict the damage. The natural frequencies of the structure are used as inputs of the neural networks. The data to train the neural networks are obtained from the finite element model.

In order to overcome problems of poor capacity for generalisation encountered in the many previous approaches, a finite element model suitable to the definition of damage is tried. Further work in this paper is concerned with the validation of the method. The damage levels of the structure are obtained through the trained neural networks from available experimental modal data. Then, the stiffness matrices of the structure predicted by the method are compared with those identified from pseudo-dynamic tests. Results are excellent. The new finite element model definition allows the neural networks to have a much better generalisation. The obtained values of the terms of the stiffness matrix of the undamaged structure are almost exact when compared with the experimental ones, while the absolute differences are lower than 8.6% for the damaged structure.

1.5.8 Statistical methods

These methods make use of the statistical (and probability) distribution of data to infer damage. Most available statistical methods are based on outlier and regression analysis. In outlier analysis, the algorithms look for features in freshly acquired vibration response data that cannot be represented by the extrapolation of features from the previously acquired data or from an undamaged structure's response data, while regression analysis involves fitting empirical models to measured data. It also consists of correlating data features with particular types, locations or extents of damage (Bement & Farrar, 2000).

Sohn and Law (1998) propose a damage detection method, which uses experimental load dependent Ritz vectors. They extract Ritz vectors from measured flexibility matrices and utilise a Bayesian probabilistic approach with a branch and bound search scheme to search for the most probable damage cases.

Damage is modelled by a dimensionless θ parameter, which represents the contribution of a substructure or element stiffness to the system stiffness matrix. And a damage case is assumed to occur when θ exceeds a certain threshold. They compare the technique to MRP, SEE and DI techniques, and conclude that their technique is superior.

Bement and Farrar (2000) present damage detection as a problem in statistical pattern recognition. This process is composed of four stages: operational evaluation, data acquisition and cleansing, feature selection, and statistical model development. Contemporary methods regarding supervised learning for statistical model development are discussed and emphasised with the application of this technology to a laboratory structure. Specifically, a comparison is made between a linear discriminant classifier and a general Bayesian classifier for the purpose of determining the existence of damage.

Sohn, Fugate and Farrar (2000) apply process control statistics for continuous structural health monitoring. They firstly derive an AR model of the undamaged structure. They use the residuals between some chosen number (p) of past samples predicted by the model and those measured as damage sensitive feature. The means and variability of the residuals are monitored by using x-bar and control charts. The x-bar charts are used to determine the differences among different subgroups of p samples while the control charts are used to detect the differences within individual samples.

They apply their technique successfully to detect damage in a laboratory bridge column. The technique is shown to be robust against false-positive warnings of damage. It is also capable of detecting low levels of damage.

Worden, Manson and Allman (2000) apply multivariate outlier analysis to transmissibility functions for detection of faults in structural systems. A Mahalanobis squared distance discordancy value is compared to a threshold value determined by the Monte Carlo method. The technique is applied successfully to a simulated three-degree-of-freedom system, two pseudo-experimental cases and one experimental case.

Sohn and Farrar (2001) present a technique based solely on statistical analysis of time series vibration data. They employ a combined AR-ARX model to estimate an undamaged structural response. The residual error between measured response and estimated response from the undamaged model is used as damage sensitive parameter. They show

that a marked increase in the residual error standard deviation occur near the damage locations.

Bodeux and Golinval (2003) use the ARMA and data-driven stochastic subspace methods to perform modal identification and damage detection on the Steel Quake structure by detecting changes in frequencies. The methods work directly with the recorded time signals and allow analysing linear systems, where only the system output is measured, while the input is unknown and produced by uncorrelated random signals. The techniques can also be used directly to analyse data obtained from the free response of linear systems.

Kullaa (2003) uses the univariate and multivariate Shewhart, x, CUSUM, and EWMA control charts for structural health monitoring on Z24-Bridge in Switzerland. The identification of the modal parameters from the response data is automated using the stochastic subspace identification technique and the stabilisation diagram.

Worden et al. (2003) present an analysis approach, which uses novelty detection based on measured transmissibilities from the structure. Three different novelty detection algorithms are considered: outlier analysis, density estimation and auto-associative neural network technique. All three methods are shown to be successful to an extent, although a critical comparison reveals serious faults with the density estimation approach when used on sparse data sets.

Yoon, Heider, Gillespie Jr., Ratcliffe and Crane (2003) develop a two-dimensional gapped smoothing damage detection method. It is applied to homogeneous structures and, therefore, does not require the use of baseline vibration data for damage identification. They use structural irregularity indices to measure damage severity. Structural irregularity indices are calculated from the difference between the measured mode shape or operation deflection shape curvature and the smoothed curvature shape determined by cubic polynomial fitting curve. The calculated structural irregularity indices are averaged and treated statistically using outlier analysis. If normality is not obtained, the Tchebychev inequality approach is used to detect the outliers. The technique is applied successfully to a finite element plate structure and experimental composite plates.

The statistical methods seem to be well-suited for implementation of continuous structural health monitoring systems because they can be applied to time response data.

1.5.9 Comparative studies

Comparative studies of the different vibration-based damage detection methods have been presented in literature. The studies have shown that when damage is severe, most of these methods accurately locate the damage. For less severe damage cases, some of the methods fail to accurately locate the damage. Some studies have also shown that most of these methods give false-positive indications of damage. However, methods that are based on the changes in modal strain energy yield more accurate results and do not give false-positive results (Doebling, et al. 1996).

Fritzen and Bohle (2003) apply four different model-based approaches to identify three cracks on the Steel Quake structure. The measured changes of the modal quantities and the physical structural changes are linked by means of a computational model.

1.5.10 Final remarks on the review

There are two observations made on development of the current techniques for damage detection:

- **Improvement of the efficiency of detection algorithms:** Most of the newly developed modal property extraction- and frequency response-based methods have dwelt on refining the detection algorithms. The motivation for more efficient methods has even resulted in an increased number of algorithms for damage detection and localisation.
- **Development of a structural health monitoring scheme:** Under time response-based methods, there seems to be a general trend towards developing detection systems, which would supply the operator or the structural analyst with information regarding the status of the structure during operation. This is the approach adopted and developed further by this work.

1.6 Scope of the work

This work covers relevant aspects of structural modelling and updating, force identification, dynamic sensitivity analysis, and linear elastic fracture mechanics analysis. Rather than the traditional approach of modal parameter extraction and monitoring

their shifts to identify damage, this work identifies damage by way of monitoring operational responses.

Test statistic values, which correspond to different levels of fatigue damage, are derived from these time histories and matched with those emanating from the measured time histories during fatigue damage. Sensitivity analysis is used to predict responses from a finite element model in their varying degrees of fatigue damage.

The use of crack ratios, however, limits damage quantification to be carried out only during the crack propagation phase. Thus any damage state prior to crack initiation corresponds to zero crack ratio (to represent cases where there is no initial notch). Establishing an initial crack ratio value is a crucial part in the analysis because it influences the accuracy of the resulting service life calculations. In virgin structures it is easy to assume initial crack ratio values corresponding to fatigue threshold values, which are given as 5.5 MPa$\sqrt{m}$ for steels and 3 MPa$\sqrt{m}$ for aluminum. In welded or used structures, determination of an initial crack ratio is dependent on the existing cracks and prevailing mechanical properties.

The uniqueness of the technique lies in the integration of the vibration analysis and linear elastic fracture mechanics analysis into one coherent package.

1.7 *Document Overview*

The document is organised into five chapters, each of which consists of sections and subsections. A brief description of the contents of each chapter is given below.

The first chapter contains a brief introduction to the field of structural damage detection and the current methods and trends in damage detection are presented. The challenges encountered in the application of widely used pure modal-based methods are presented. The proposed technique is also presented.

The second chapter develops the underlying theory for the development of the technique. Firstly, the structural damage problem is presented as a structural dynamic problem mainly in time domain. Secondly, relevant linear-elastic fracture mechanics aspects are discussed and integrated into the structural damage problem through FEM and dynamic sensitivity analysis.

A detailed description of the technique is presented in chapter 3. The chapter also shows by way of charts how the proposed technique is put together for computer

implementation. The advantages and disadvantages of the technique are also presented.

The fourth and fifth chapters verify the technique through numerical and experimental results. Discussions of the performance of the technique are performed. A brief comparative study with the classical modal property based technique is performed in the numerical case study.

Chapter six concludes and highlights areas that need further work in the field.

2. MODELLING THE STRUCTURAL DAMAGE PROBLEM

2.1 Introduction

This chapter presents relevant theory for the development of the proposed damage detection technique. The developed theory mainly considers structural damage in the form of surface cracks. The chapter is organised into four main sections as outlined here.

Section 2.2 formulates the structural damage problem as a problem in structural modification. Then, linear elastic fracture mechanics analysis follows in section 2.4. Crack propagation is described by the Paris relationship. Then, remaining service life may be determined from the propagation life.

Sensitivity analysis is presented in section 2.5, where the necessary link between changes in crack length and changes in time responses is derived. Finally, a statistical model which is based on hypothetical testing of variances is presented in section 2.6.

2.2 Equations of motion

The dynamics of a discrete mechanical system is governed by equation 2.1 (Heyns, 2002),

$$[M]\{\ddot{x}(t)\} + [C]\{\dot{x}(t)\} + [K]\{x(t)\} = \{f(t)\} \tag{2.1}$$

where $[M]$, $[C]$ and $[K]$ are the $N \times N$ mass, viscous damping and stiffness matrices, respectively; $\{f(t)\}$ and $\{x(t)\}$ are the $N \times 1$ forcing and response vectors, respectively.

In case of structural damping, the system equation takes the following form:

$$[M]\{\ddot{x}(t)\} + ([K] + i[H])\{x(t)\} = \{f(t)\}e^{i\omega t} \tag{2.2}$$

where $[H]$ is the structural damping matrix and the forcing function is harmonic. Since the present study focuses on structural systems, it is deemed proper to work with equation 2.2.

In the frequency domain, a direct solution to equation 2.2 may be obtained, (Heyns, 2002):

$$\{X\} = \left[[K] + i[H] - \omega^2[M]\right]^{-1}\{f\} = [\alpha(i\omega)]\{f\} \tag{2.3}$$

In the time domain, equation 2.2 is represented in state space form so that equation 2.4 results (Heyns, 2002):

$$\{\dot{\chi}\} = [E]\{\chi\} + \{D\} \tag{2.4}$$

where,

$$\{\chi\} = \left\{ \begin{array}{c} \{x\} \\ \{\dot{x}\} \end{array} \right\};$$

$$[E] = \left[\begin{array}{cc} [0] & [I] \\ -[M]^{-1}\left([K] + i[H]\right) & [0] \end{array} \right]$$

and,

$$\{D\} = \left\{ \begin{array}{c} \{0\} \\ +[M]^{-1}\{f(t)\} \end{array} \right\}$$

A numerical integration scheme can be used to solve equation 2.4.

2.2.1 *Model of damaged structure*

Structural damage is presumed to change system mass, stiffness and damping matrices. However, for a surface cracked structure, where disintegration (resulting in mass loss) is not likely and change in system damping is insignificant, damage can be assumed to affect the system stiffness matrix only. The influence of the crack to the system stiffness matrix is localised in the elements, which are located where the cracks occur.

Therefore the most common approach to modelling structural damage is by applying a reduction factor, d_{Ks}, to the element stiffness matrix $[K]^e$. In this way the change of the system stiffness matrix due to damage could be represented as a sum of each element matrix multiplied by a reduction factor (Wang, Lin & Lim, 1997).

$$[\Delta K_d] = \sum_{s=1}^{L} d_{Ks}[K_s]^e \tag{2.5}$$

where L is the total number of elements, and d_{Ks} is the stiffness reduction factor of the s^{th} element. Wang et al. (1997) further noted that if the element is undamaged, it has a value of 0, on the other hand, if it is completely removed, it has a value of -1. When the element is partially damaged, it takes values in between the two limits. There are other variations to the reduction factor where it is 1 when the element is not damaged and 0 when the element is damaged (Messina, Williams & Contursi, 1998). This modelling approach has the main advantage that the connectivity of the system matrix is preserved.

The other approach is by separating adjacent elements along their shared boundaries. Although this does not change the total number of elements, it changes the total number of nodes. This affects node numbering beyond the damage location, hence disturbing element connectivity. It also yields infinite values of stresses at the singular

point. However, it can be used for modelling cracks across thicker sections of material and it also provides for crack closure, which might be suitable for nonlinear response. Appendix A provides a comprehensive description of this modelling.

Structural damage is also modelled by using specialised cracked elements. In this approach, a special cracked element is introduced into the location of damage. It is required that a single element be placed in the damage location, thus spanning the entire thickness through which damage is assumed to occur. This damage modelling has been adopted in this work. An open cracked beam element has been used to model the damaged part of the structure. Its element stiffness matrix was derived from the theory of linear elastic fracture mechanics where it is assumed that a small plastic zone develops at the crack tip (Krawczuk, et al. 2000). The existence of the plastic zone at the crack tip increases the local flexibility of the element which consequently affects the stiffness of the system matrix. The underlying theory for the formulation of this element is given in Appendix C. A better derivation can be found in the source work (Krawczuk, et al. 2000).

2.3 ***Plane stress and plane strain states***

In the analysis of stress in loaded structures, two states of stress are encountered namely, plane stress and plane strain. The state of plane stress is said to occur when one of the principal stresses is zero, while the state of plane strain occurs when one of the principal strains is zero. As an illustration consider a cylindrical material near the tip of the crack in Figure 2.1a. The action of the forces causes a contraction of the faces of the cyclinder at the free surfaces. As a result there are no stresses on the free surfaces and since there is no shear as well, it is a principal plane with the principal stress of zero.

On the other hand, Figure 2.1b the action of the surrounding material constrains the free surface of the cylinder from contraction. Thus it results into a principal plane with the principal strain of zero. It can be noted that the principal stresses are not equal to zero in this state.

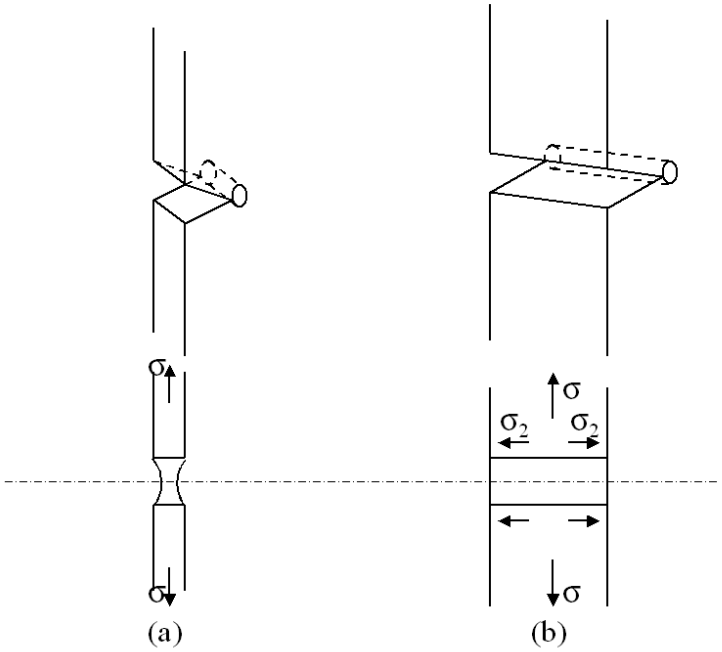

Fig. 2.1: Plane stress vs plane strain states in loaded structures

2.4 *Linear-elastic fracture mechanics analysis*

Linear elastic fracture mechanics (LEFM) upholds the theory of elasticity with regard to the relationship between stress and strain, and also, the assumption of small displacements for application to cracking bodies. The plastic zone size $2r_y$ at the crack tip is small because it is restricted by the surrounding elastic body, (figure 2.2). This assumption is more applicable to cyclic loading cases, where it is shown that the plastic zone size is four times less than the comparable monotonic value, (Bannantine, Comer & Handrock, 1990):

$$r_y = \begin{cases} \frac{1}{8\pi}\left(\frac{K}{\sigma_y}\right)^2 & \text{plane stress} \\ \frac{1}{24\pi}\left(\frac{K}{\sigma_y}\right)^2 & \text{plane strain} \end{cases} \tag{2.6}$$

Compare with the expressions for the monotonic case:

$$r_y = \begin{cases} \frac{1}{2\pi}\left(\frac{K}{\sigma_y}\right)^2 & \text{plane stress} \\ \frac{1}{6\pi}\left(\frac{K}{\sigma_y}\right)^2 & \text{plane strain} \end{cases} \tag{2.7}$$

where, K is the stress intensity factor and σ_y is the yield strength of the material.

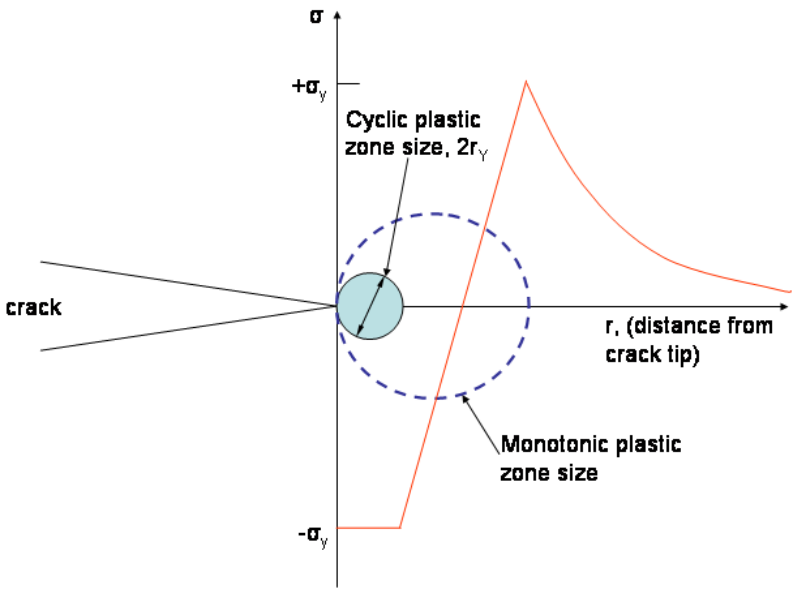

Fig. 2.2: Reversed plastic zone size

In LEFM, structural damage is specified by crack length. For a given crack length and geometry, plus a magnitude of applied stress, σ, it is possible to determine the stress intensity factor by equation 2.8, (Bannantine, et al. 1990).

$$K = f(g)\sigma\sqrt{\pi a} \tag{2.8}$$

where $f(g)$, is the correction factor that depends on the specimen and the crack geometry. For a beam in bending, the correction factor is given by (Bannantine, et al. 1990):

$$f(g) = 1.122 - 1.40\left(\frac{a}{b}\right) + 7.33\left(\frac{a}{b}\right)^2 - 13.08\left(\frac{a}{b}\right)^3 + 14.0\left(\frac{a}{b}\right)^4 \tag{2.9}$$

where the values of $f(g)$ for many engineering situations lie between 1 and 1.2.

The application of LEFM theory however, assumes that the plastic zone size must be small compared to the distance from the crack tip to any boundary of the member, such as distances a, $(b-a)$ and h for a cracked plate. A distance of $8r_y$ is generally considered sufficient (Dowling, 1999). Thus an overall limit on the use of LEFM is:

$$a, (b-a), h \geq \frac{4}{\pi}\left(\frac{K}{\sigma_y}\right) \tag{2.10}$$

Equation 2.10 must be satisfied for all three of a, $(b-a)$ and h. Figure 2.3 shows the distances.

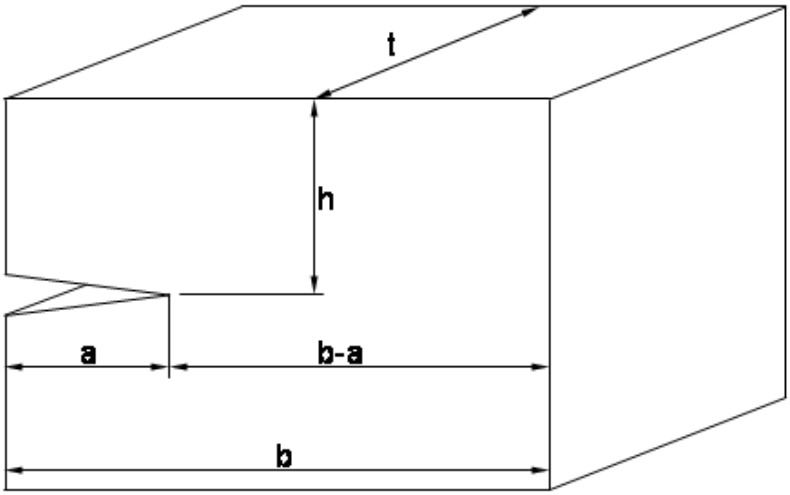

Fig. 2.3: Distances from the crack tip to material boundaries

For thick members, a transition from plane strain into plane stress occurs during crack growth. The overall requirement for plane strain is:

$$t, a, (b-a), h \geq 2.5\left(\frac{K}{\sigma_y}\right) \tag{2.11}$$

where t is the material thickness shown in figure 2.3.

2.4.1 ***Crack growth***

Fatigue life consists of two main phases: crack initiation and crack propagation. During crack propagation it is found that a structure spends more of its life in the earliest stages of crack growth. This behaviour is best described by the crack propagation curve shown in figure 2.4b (Bannantine, et al. 1990). During crack propagation, the structure goes through three main crack growth regions. Figure 2.4a shows these regions and a brief discussion of what happens in each region follows.

Region I

This region is associated with threshold effects. The crack is usually of microscopic order when it just initiates, but its approximate value a_o, may be determined from equation 2.12:

$$a_o = \frac{1}{\pi}\left[\frac{1}{f(g)}\left(\frac{\Delta K_{TH}}{\sigma_y}\right)\right]^2 \tag{2.12}$$

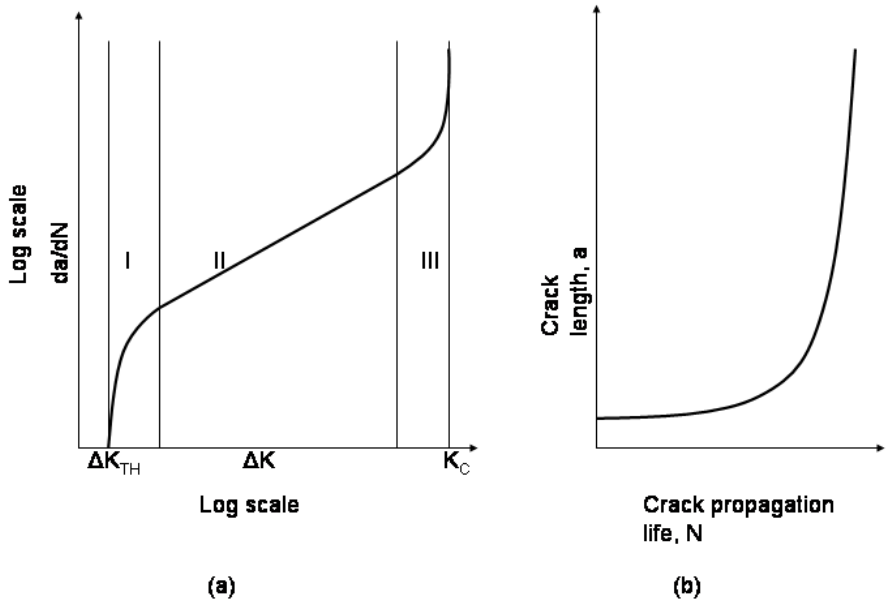

Fig. 2.4: Illustration of crack growth regions (a) and crack propagation curve (b)

where the values of ΔK_{TH} can be obtained from material handbooks. Figure 2.4a shows that crack growth in this region is extremely slow. This means that establishing the size of the initial crack is very important in life calculation, because for a very small error in millimetres of initial crack size, the corresponding discrepancy in life prediction may be of the order of thousands of cycles.

Region II

Linear effects and stable crack growth characterise this region as shown in figure 2.4a. Life calculations can be made with reasonable accuracy by applying the Paris law in region II. The rate of crack growth also renders itself amenable for taking good measurements.

Region III

This region is characterised by unstable crack growth. In fact, beyond the fracture toughness of the material K_c, it is hard to acquire reliable measurement data. The final crack size a_f can be calculated from equation 2.13 by using K_c:

$$a_f = \frac{1}{\pi}\left[\frac{1}{f(g)}\left(\frac{K_c}{\sigma}\right)\right]^2 \tag{2.13}$$

2.4.2 Life calculation

As noted in section 2.4.1, life predictions can be made more reliably in region II. The relationship which most suitably describes crack growth behaviour is given by the Paris law in equation 2.14:

$$\frac{da}{dN} = C\,(\Delta K)^m \tag{2.14}$$

where C and m are the crack growth coefficient and exponent respectively, and are material constants.

Equation 2.14 can be integrated and solved for N to give an expression for crack propagation life N_f (in cycles):

$$N_f = \int_{a_i}^{a_f} \frac{da}{C\,(\Delta K)^m} \tag{2.15}$$

The integration in equation 2.15 is often solved numerically because ΔK is dependent on a and $f(g)$ (see equation 2.8). In order to account for mean stress effects, the Forman's equation is used and equation 2.15 can be rewritten as:

$$N_f = \int_{a_i}^{a_f} \left((1-R)K_c - \Delta K\right) \frac{da}{C\,(\Delta K)^m} \tag{2.16}$$

where R is the stress ratio which must be greater than zero and K_c is the critical stress intensity factor. Test observations show that as R increases the crack growth rate increases.

2.5 Linking by sensitivity analysis

In order to infer damage by observing changes in structural time responses, it is important to establish how structural damage (i.e. crack length) influences the time responses. In this section, a sensitivity function which relates the change of time responses with respect to the change in crack length is derived. Thus equation 2.4 is differentiated with respect to crack length, a:

$$\frac{\partial\{\dot{\chi}\}}{\partial a} = \frac{\partial\left([E]\{\chi\}\right)}{\partial a} + \frac{\partial[D]}{\partial a} \tag{2.17}$$

Since the mass matrix, damping matrix and force vector are assumed independent of crack length changes, equation 2.17 yields equation 2.18.

$$\frac{\partial\{\dot{\chi}\}}{\partial a} = [E]\frac{\partial\{\chi\}}{\partial a} + [\acute{E}]\{\chi\} \tag{2.18}$$

where,

$$[\acute{E}] = \begin{bmatrix} [0] & [0] \\ -[M]^{-1}\frac{\partial[K]}{\partial a} & [0] \end{bmatrix}$$

and the sensitivity function $[S]$, is given by:

$$\{S\} = \frac{\partial\{\chi\}}{\partial a} \tag{2.19}$$

The forward finite difference method (Rao, 1995) may be used to compute $\frac{\partial[K]}{\partial a}$ thus:

$$\frac{\partial[K]}{\partial a} = \frac{[K(a_j)] - [K(a_0)]}{a_j - a_0} \tag{2.20}$$

It is worth noting that if the crack is modelled by the procedure outlined in Appendix A, the two system stiffness matrices are of unequal sizes, thus a normal subtraction operation cannot be used. This difficulty may be circumvented by using a modal reduction procedure (Haftka, G*ü*rdal & Kamat, 1990), where the system matrices are reduced by using m basis functions where m is less than the total number of degrees of freedom N of the structure. Thus, equation 2.20 may now be written as:

$$\frac{\partial[\bar{K}]}{\partial a} = \frac{[\bar{K}(a_j)] - [\bar{K}(a_0)]}{a_j - a_0} \tag{2.21}$$

where,

$$[\bar{K}] = [U]^T[K][U]$$

$[U]$ is a matrix whose columns are made up of $u^i \rightarrow \ i = 1, 2, ..., m$ basis functions (Haftka, et al. 1990). The reductions are also performed on $[M]$, $[H]$, $\{\chi\}$ and $\{f\}$ to yield $[\bar{M}]$, $[\bar{H}]$, $\{\bar{\chi}\}$ and $\{\bar{f}\}$, respectively. Thus equation 2.18, can be re-written as:

$$\frac{\partial\{\dot{\bar{\chi}}\}}{\partial a} = [\bar{E}]\frac{\partial\{\bar{\chi}\}}{\partial a} + [\acute{\bar{E}}]\{\bar{\chi}\} \tag{2.22}$$

where,

$$[\bar{E}] = \begin{bmatrix} [0] & [I] \\ -[\bar{M}]^{-1}\left([\bar{K}] + i[\bar{H}]\right) & [0] \end{bmatrix}$$

and,

$$[\acute{\bar{E}}] = \begin{bmatrix} [0] & [0] \\ -[\bar{M}]^{-1}\frac{\partial[\bar{K}]}{\partial a} & [0] \end{bmatrix}$$

The sensitivity function is now re-defined as:

$$\{\bar{S}\} = \frac{\partial\{\bar{\chi}\}}{\partial a} \tag{2.23}$$

from which time responses may be predicted by equation 2.24:

$$\{\bar{\chi}\}_{a_j} = \{\bar{\chi}\}_{a_0} + \{\bar{S}\}\Delta a \tag{2.24}$$

where $\Delta a = a_j - a_0$.

2.6 Statistical damage detection

Given a set of data sequences, $x(k)^1, x(k)^2, ..., x(k)^n$, the following two hypotheses may be used to test the sequences' equality.

2.6.1 Test of equality of means

This constitutes a hypothesis statement, which tests whether the individual means for the data sequences are equal. This is done by comparing the variability of data within any single sequence, x^j with the variability among all the concerned sequences $x(k)^1, x(k)^2, ..., x(k)^n$. The statement is given by equation 2.25 (Montgomery, 1996):

$$\begin{aligned} H_0^1 &: \mu_1 = \mu_2 = ... = \mu_n \\ H_1^1 &: \mu_j \neq \mu_k \text{ for at least one pair}(j,k) \end{aligned} \tag{2.25}$$

where μ_j and μ_k are statistical means for the j^{th} and k^{th} data sequences, respectively.

The variability within the single data sequence is measured by a mean square value of the internal deviations of data from the sequence mean, which is denoted by MS_E. While the variability among the different data sequences is obtained from the mean square value of the deviations of sequence averages from the overall average, and it is denoted by MS_{DS}. The ratio F_0 is computed by equation 2.26:

$$F_0 = \frac{MS_{DS}}{MS_E} \tag{2.26}$$

The value of F_0 is the test statistic, and is compared to the threshold value, F_α to establish whether the given data sequences are equal or not. The value of α (called the significance level of the test) may be established from the knowledge of the influence of prevailing noise and/or other disturbances during data acquisition. Thus, if $|F_0| > |F_\alpha|$, it can be established with $(1-\alpha) \times 100\%$ confidence that the data sequences are not equal, therefore, the null hypothesis, H_0^1, can be rejected. Otherwise, the null hypothesis is true and the data sequences are equal. However, when testing equality of means on cyclic data sequences, it is problematic to detect any differences because their means tend to be cluster closely around zero. In this regard, a test of equality of variances seems more appropriate.

2.6.2 Test of equality of variance

This involves a hypothesis statement, which tests whether individual variances for the given data sequences, $x(k)^1, x(k)^2, ..., x(k)^n$, are equal. This is written as in equa-

tion 2.27 (Montgomery, 1996):

$$\begin{aligned} H_0^2 &: \sigma_1^2 = \sigma_2^2 = ... = \sigma_n^2 \\ H_1^2 &: \sigma_j^2 \neq \sigma_k^2 \text{ for at least one pair}(j,k) \end{aligned} \tag{2.27}$$

where σ_j^2 and σ_k^2 are statistical variances for the j^{th} and k^{th} data sequences, respectively.

The Bartlett's test provides a test procedure for the variability of variances among different data sequences. The test statistic is computed from equation 2.28:

$$\chi_0^2 = 2.3026\frac{q}{c} \tag{2.28}$$

where,

$$q = (N-a)\log_{10} S_p^2 - \sum_{j=1}^{a}(n_j - 1)\log_{10} S_j^2;$$

$$c = 1 + \frac{1}{3(a-1)}\left(\sum_{j=1}^{a}(n_j-1)^{-1} - (N-a)^{-1}\right)$$

$$S_p^2 = \frac{\sum_{j=1}^{a}(n_j-1)S_j^2}{N-a}$$

and S_j^2 is the sample variance of the j^{th} data sequence.

Similarly, the test statistic value χ_0^2, is compared with a threshold value χ_α^2. If $|\chi_0^2| > |\chi_\alpha^2|$, the null hypothesis is rejected and it may be declared with $(1-\alpha)\times 100\%$ confidence that the concerned sequences are not equal.

2.7 Summary

In this chapter, the underlying theory for the proposed damage detection technique has been presented. Structural damage has been modelled by using a special cracked beam element with a plastic region around its crack tip.

Crack propagation and life prediction has been assumed to follow the Paris law. Thus, analysis has been restricted to region II, which is associated with stable crack growth. It has been shown that both in region I and III, it is relatively hard to make reliable measurements.

Finally, the statistical procedure upon which the damage detection procedure is based has been presented. It involves the hypothetical testing of equality of data means and variances. Hypothetical testing of variances has been shown to be more promising in detecting data variability where cyclic data sequences are involved.

3. SYSTEM DEVELOPMENT AND IMPLEMENTATION

3.1 Introduction

In chapter 1, the proposed technique was introduced and its operation was described in terms of four main functions. This chapter presents a more detailed discussion of the proposed technique. The chapter identifies the building blocks of the technique and shows how each block does fit into the identification process. Flowcharts have been used to illustrate certain aspects for practical implementation.

3.2 Finite element modelling

It was pointed out in chapter 1 that the derivation of an accurate finite element model is central to the development of the entire technique. This section discusses the process of deriving and updating the finite element model. The important factors to be considered in both the derivation and updating processes are presented.

3.2.1 Derivation of a finite element model

The derivation of an accurate finite element model is usually marred by five main factors. Therefore, to arrive at a reasonably accurate FEM, the following factors must be properly addressed.

- Boundary conditions cannot be modelled accurately
- Modelling of distributed parameter systems as discrete is only approximate
- Physical properties of different structural materials are only estimates
- Damping is very difficult to model
- Joints and couplings are very difficult to model accurately

The approximation of a solution by shape functions dictates that an optimal number of finite elements be used to model the structure in order to obtain a closer estimate. Friswell and Mottershead (1995) present a case study of a cantilever beam where prediction of the first five vibration modes are made more accurate by increasing the number of degrees of freedom in the finite element model. Often, the problem of discretisation is dealt with by mesh refinement on the whole structural model or in some critical areas of the model.

For reliable estimates of physical properties, it is considered good practice to obtain them from material tests conducted under real environmental and operating conditions. These values are considered to yield more accurate results than those available in most material handbooks.

In the modelling of vibrating structures, damping is one of the most notorious structural properties to estimate. Basically, this is due to the fact that the actual mechanism which causes it in structural systems is not very clear. Therefore, in practice, damping ratios and loss factors are determined experimentally by conducting a modal analysis (Ewins, 1984; Heyns, 2002).

The problems of modelling joints, couplings and boundary constraints are best dealt with by a proper model updating procedure. These joints and boundary constraints possess physical properties of their own which must be available for improvements (Friswell & Mottershead, 1995).

Finite element modelling in the present study has been performed in MATLAB. Euler-Bernoulli beam elements have been used to model undamaged parts of the structure. The damaged part has been modelled by an open cracked beam element.

A summary of the finite element analysis process is given in figure 3.1. Note that the short forms *PRBS* and *upd.* in the figure represent *pseudo-random binary sequence* and *updated*, respectively.

3.2.2 Finite element model updating

The objective of model updating here, is to have a finite element model that accurately predicts the measured time responses both during undamaged and damaged states. This is coupled with the necessity that the updated model is used for damage detection. Thus, there is need for the model parameters used in updating to be correct. If the wrong parameters are updated, it may affect the subsequent identification of damage.

The present study uses a response function method (RFM), which is based on measured frequency response function data. Because this approach uses raw measured data directly, it avoids lengthy modal analysis procedures, which are necessary when modal data are used. Furthermore, extracting natural frequencies and mode shapes for structures with close modes or a high modal density can be difficult (Friswell & Mottershead, 1995).

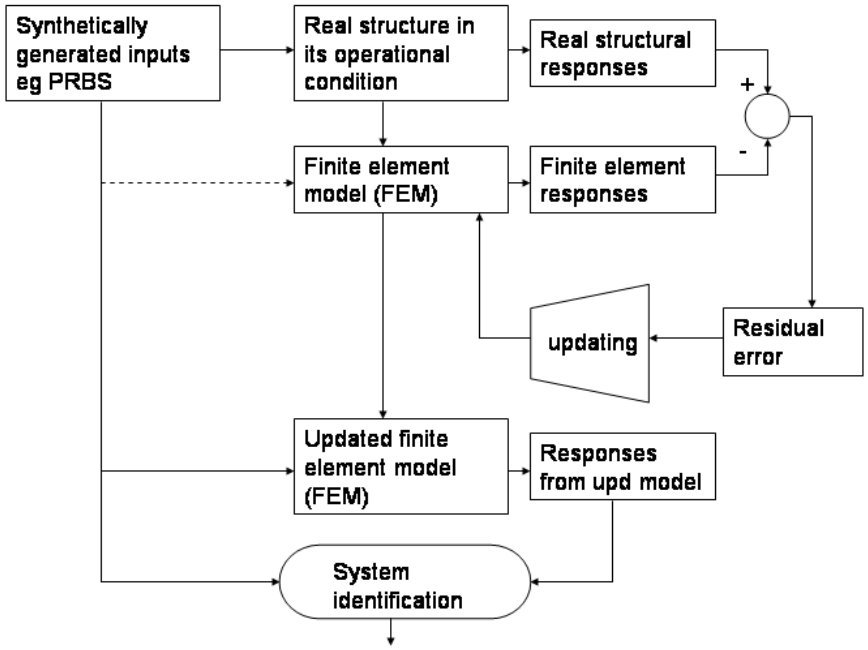

Fig. 3.1: Finite element model updating leading to system identification

The RFM updating algorithm is based on the identity (Ziaei-Rad & Imregun, 1996):

$$[I] - [D_A(i\omega)][\alpha_X(i\omega)] = [\Delta D(i\omega)][\alpha_X(i\omega)] \tag{3.1}$$

where $[I]$, $[D_A(i\omega)]$, and $[\alpha_X(i\omega)]$ are the identity, analytical dynamic stiffness and experimental receptance matrices respectively, $[\Delta D(i\omega)]$ being the unknown dynamic stiffness correction matrix. Further manipulation of equation 3.1 yields (Heyns, 2002):

$$\{\alpha_A(i\omega)\}_i^T - \{\alpha_X(i\omega)\}_i^T = \{\alpha_X(i\omega)\}_i^T[\Delta D(i\omega)][\alpha_A(i\omega)] \tag{3.2}$$

where $[\alpha]$ and $\{\alpha\}_i$ represent the receptance FRF matrix and i^{th} column of the matrix, respectively. $[\Delta D]$ is the difference between the measured (subscripted by X) and analytical dynamic stiffness matrices (subscripted by A).

Equation 3.2 is an under-determined set in which there are often twice as much unknowns as the system of independent equations. To deal with this problem, a set of over-determined equations is formed by writing equation 3.2 at a number of selected optimal frequency points. The resulting equation can be presented in its compact form as (Heyns, 2002):

$$[C(i\omega)]\{\Delta p\} = \{B(i\omega)\} \tag{3.3}$$

where matrix $[C(i\omega)]$ and vector $\{B(i\omega)\}$ are known in terms of measured and predicted response properties or both, and the elements of vector $\{\Delta p\}$ indicate the position of the error in the original system matrices.

It is shown (Ziaei-Rad & Imregun, 1996) that the level of noise pollution in the experimental data is a crucial factor in the efficiency of this updating procedure. In order for the updating algorithm to work efficiently, the noise must be kept within at least a tenth of the modelling error level (1-10 percent error).

Model quality assessment

The assessment of model quality is performed by measuring its speed of convergence, improvement of the model output and ability to predict output not used for the updating of the model. The number of iterations and time the updating algorithm takes to converge to a solution is considered as a measure for its speed. The fit which is determined from the Frobenius norm of the error between the model output and the measured data is used to indicate how much improvement has been carried out on the model. In this study, the accuracy of the derived models has been illustrated by plotting the models' outputs over the measured outputs.

The entire RFM updating procedure is illustrated in figure 3.2.

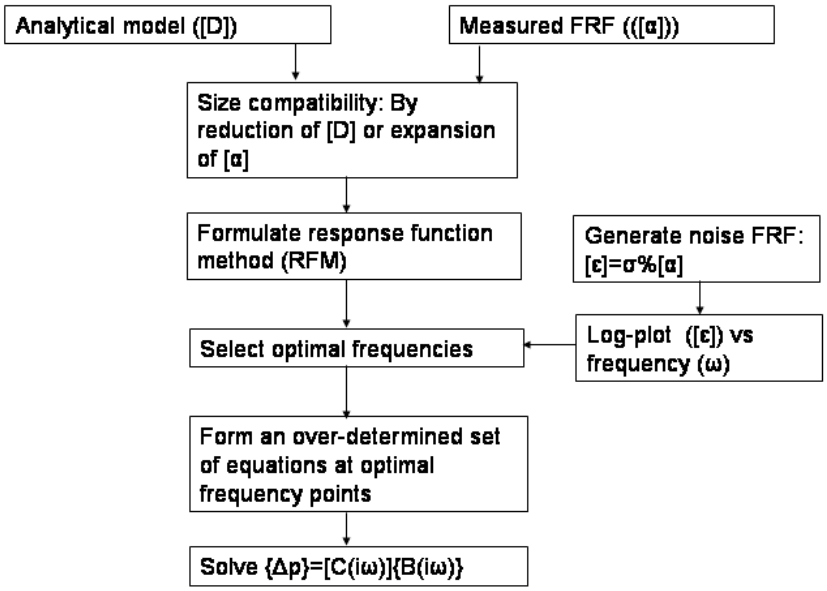

Fig. 3.2: Response function updating procedure

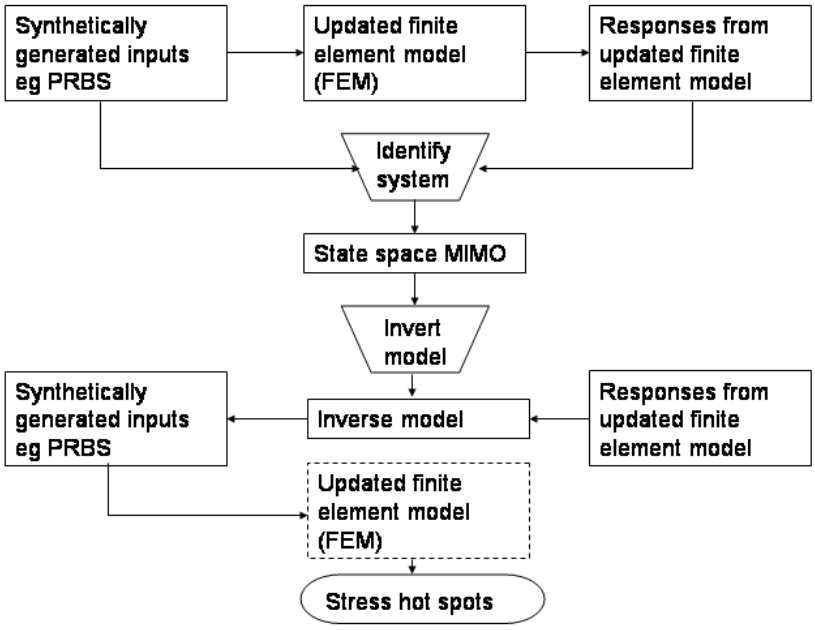

Fig. 3.3: Flowchart showing process of force and 'hot spots' identification

3.3 *Force identification*

Synthetically generated inputs are applied to the updated finite element model. Several sets of (ARX) models are identified from the input-output data. These are converted into multiple input single output (MISO) state-space models, which are subsequently combined into a multiple input multiple output (MIMO) state-space model of the structural system. The resulting state-space model is inverted. Then the operational responses are applied to the inverse model to calculate corresponding operational forces. Figure 3.3 illustrates the force identification procedure recommended for this work.

The general concept of the force identification procedure was introduced in chapter 1. In the present chapter, its relevance to the present study is discussed with emphasis placed on how it can be implemented in the proposed structural damage detection technique. It should be noted that this is only applicable where the structural system makes it hard to measure back the excitation forces, like in the case of a vehicle structure.

3.3.1 Generation of the synthetic excitation signals

Firstly, a proper choice of the excitation signals is necessary. The excitation signals should be chosen so that the identified model can reproduce responses of the real system in the frequency bandwidth of the measured operational responses. Thus, the frequency content of the operational responses dictates the choice of the exciting inputs. It might therefore, be desired that the chosen exciting inputs excite all the modes of the dynamic system within the desired frequency bandwidth.

3.3.2 Estimation of model structure

There are two main stages in identifying an inverse model of the dynamic system. At the initial stage, parameter indices of either a direct inverse or normal model for each output are estimated using short sequences of input-output data. The parameter indices contain numbers of model orders and delays for each output. Residual and stability analyses are performed on each identified MISO model.

At the second stage, the full length of input-output data sequences and the parameter indices from initial stage are used to identify initial ARX parameters for each output. Then, stochastic ARMAX models are identified using the ARX model parameters from above, so that noise effects are taken into account. Finally, more accurate deterministic ARX models are determined using the updated parameters from the ARMAX models. These are subsequently converted into a multivariable state space model which might be inverted or not, depending on whether the MISO ARX models are normal ARX models or direct inverse ARX models.

Raath (1992) noted that there were some dynamic systems which exhibited unstable inverses for all the inversion techniques that he developed. In such cases, he recommended use of a linear quadratic optimal controller (LQOC). The LQOC method is based on servo-controller theory where the plant output is controlled through a feedback loop to follow a prescribed desired path. The servo-controller outputs are estimates of the desired operational inputs. Appendix B outlines some of the important ideas on model inversion.

3.3.3 Force determination

The operational forces are determined by simulating the identified inverse multivariable state space model by the operational responses. The inputs calculated in this manner are termed *the linear solution*, and represent an initial attempt at the system inputs. In the case of the LQOC, a number of iterative corrections may be required for systems which exhibit a poor step response (Raath, 1992).

3.4 Damage location

In this technique, structural damage is located by using FEM. Critical points on the structural system are obtained from the location of high stress points on the finite element model. The operational forcing inputs determined in section 3.3 are applied to the updated finite element model. The stress *hot spots* on the finite element model are used as damage candidates on the structure. This approach is straightforward and can be considered more conservative for complex structural systems than most of the other methods. Once an accurate finite element model is calculated, one is assured of obtaining reliable likely damage locations.

3.5 Damage scenarios

It is inherently assumed that isotropic homogeneous materials under fatigue loading in pure bending do crack in a near straight line without much branching. Thus, when conceiving different damage scenarios in this work, the crack is assumed to propagate through the thickness of the structural member at the critical location in a straight path. Therefore, the damage scenarios are represented by crack extensions at critical locations.

In the present work, the use of the cracked beam element makes this possible by assigning values between 0.0 and 0.6 for the crack ratio in its stiffness matrix. However, the chosen crack ratios are influenced among other things, by the geometry of the structure at the location of the critical point. In a case where this is located at the tip of a notch for example, the initial crack ratio cannot be zero. Therefore, it is more convenient to firstly establish crack lengths on the finite element model, and compute their corresponding crack ratios later.

3.6 Determining remaining service life

Knowing the crack length a, at each damage scenario, remaining service life is calculated using linear elastic fracture mechanics. The calculation requires the specification of loading conditions, crack geometry factor, and material properties of the structure. The loading conditions are governed by the actual operational conditions while crack geometry factor is determined from the shape and extent of the crack. In the present study, an assumption has been made for a surface crack under a pure bending moment. The required material properties are obtained from standard design textbooks (Shigley, Mishke & Budynas, 2003). In practice, it is recommended that the properties be obtained experimentally.

In order to determine the remaining service life, the crack propagation life curve is obtained from the Paris law:

$$N_f = \int_{a_i}^{a_f} \frac{da}{C(\Delta K)^m} \tag{3.4}$$

Then, subtracting propagation life at each crack length N_a from the expected life at fracture N_f, yields the remaining service life at each crack length, written as:

$$RSL_a = N_f - N_a \tag{3.5}$$

Therefore, each damage scenario, as conceptualised in section 3.5, has a corresponding remaining service life. Once this curve is obtained, it is used in conjunction with the statistical parameters calculated in the next section to predict the remaining service life of the structure.

3.7 Predicting dynamic displacement responses

Dynamic responses are predicted in two stages. Initially, they are calculated at each damage scenario for a few critical points on the structure using FEM. These responses are benchmarked against measured ones and are used in a statistical model to obtain rough estimates of the crack length.

After this stage, a closer estimate is desired. This is performed by minimising the error between the measured response and the predicted response. The error is expressed as the Frobenius norm of the difference between the responses. Sensitivity analysis is used in predicting the responses. The sensitivity function is re-written here from chapter 2:

$$\{\bar{S}\} = \frac{\partial\{\bar{\chi}\}}{\partial a} \tag{3.6}$$

Therefore, the predicted response is given by equation 3.7, which is in the form of the first order Taylor series expansion.

$$\{\bar{\chi}\}_{a_j} = \{\bar{\chi}\}_{a_0} + \{\bar{S}\}\Delta a \tag{3.7}$$

3.8 Statistical model

The developed statistical model employs a hypothetical test of equality of means and variances between different data sequences. Firstly, a test of equality of means may be performed. The problem with this test is that it is difficult to detect any significant differences, because the effect of localised damage on the sequence mean is very small. The small difference tends to be distributed over the length of the sequence, hence almost always undetectable unless the damage is quite substantial.

The second test involves comparison of internal data variability. The Bartlett's test for equality of variance is performed on the root square values of the calculated response residuals. This test exhibits better discriminating ability. The noise effects can be accommodated into the model by establishing a threshold test statistic value $\chi^2_{0,TH}$.

3.8.1 Determining the test statistics

This section presents the procedure for determining both the threshold value and the general test statistic values. The changes in the structural time responses during lower levels of damage are extremely small, therefore, the threshold value was established by assessing the effectiveness of the technique during those early stages of damage. Thus the effectiveness of the technique at several system disturbance levels were assessed. The disturbance levels were expressed as percentages ranging from 0.1 % to 10 % of the undamaged structure's time response levels. It was noted that the technique was effective up to a disturbance level of 1 %. Therefore, 1 % was recommended as the allowable level of disturbances which implies that the threshold residual might be expressed as:

$$\epsilon_{TH}(t) = 0.01 x_u(t) \tag{3.8}$$

The root square values $RS(\epsilon)_{TH}$ of the residuals are calculated. In order to perform the tests on $RS(\epsilon)_{TH}$, there has to be another data sequence that represents a zero change of response. Ideally, a null vector may be used. But to avoid some numerical problems in the calculations, a much smaller percentage $\tau = 0.1\%$ of the operational

response level is recommended. Likewise, the root square values of this sequence are computed and denoted as $RS(\epsilon)_\tau$.

Test on means equality

The analysis of variance is done on $RS(\epsilon)_{TH}$ and $RS(\epsilon)_\tau$. This yields, $F_{0,TH}$ which is the threshold test statistic value for the hypothesis test of no differences in sequence means. Although it has been discussed that this test is insensitive to the effects of damage on structural responses, it can be used to monitor unexpected force level fluctuations.

Test on variances equality

The Bartlett's test is performed on the two sequences ($RS(\epsilon)_{TH}$ and $RS(\epsilon)_\tau$). The result is a $\chi^2_{0,TH}$ value, which is a threshold test statistic value for the test of variances equality. It is noted that the localised effects of damage on vibration time response data seems to be better picked up by this hypothesis test than the test of equality of means.

Thus given a freshly predicted or measured data sequence $x(t)$, the residual in response is calculated by:

$$\epsilon(t) = x(t) - x_u(t) \tag{3.9}$$

The root square values $RS(\epsilon)$ are computed as before. The test statistics are determined by using $RS(\epsilon)_\tau$ sequence already determined above.

3.9 Damage detection

In this section, it is shown how damage identification and quantification are performed in the proposed technique.

3.9.1 Identifying the presence of damage

The measured operational responses are treated in the same manner as the predicted responses in section 3.8 to obtain χ^2_{0m} values. The mere identification of the presence of damage is performed by comparing the test statistic values calculated from a measured response with the threshold $\chi^2_{0,TH}$ value. The threshold value is established by the prevailing levels of noise and other uncontrollable factors in the test. When a χ^2_{0m} value exceeds the threshold value, it is expected to give a damage warning alarm.

3.9.2 Quantifying the damage

The responses calculated using FEM at each damage scenario are used to determine χ^2_{0p} values. Thus, initial estimates of damage extent are obtained by matching these values with those obtained from measured data . The damage scenario whose χ^2_{0p} value closely matches the χ^2_{0m} value from the measured data, is considered close to the actual structural damage and its crack length is given as the damage extent at that measured response. Then better estimates are determined by performing sensitivity-based calculations.

3.10 Technique summary

A summary of the technique is necessary. Firstly, a representative finite element model of the structure is developed. The developed finite element model is used to calculate operational forces and locate likely damage zones on the structure.

Different damage scenarios are conceived by assuming linear crack growth represented by the Paris law. Structural time responses are predicted from which the statistical model computes test statistics values for each damage scenario. These are used as damage sensitive features, which are matched with those calculated from measured responses to help in initial estimates of structural damage. Then a sensitivity based search is initialised at the closest matching predicted response by minimising its error from the measured response. This yields more refined estimates.

The whole procedure is summarised in 3.4 while the statistical based damage identification scheme is illustrated by figure 3.5.

3.11 Comparison with other approaches

There are two main points from which this approach draws its advantages. Firstly, it treats fracture mechanics analysis as an integral part of the identification process. Secondly, it employs time domain data for the identification, which affords it suitability for use in continuous health monitoring systems.

Here are some of the advantages of the approach over the widely used modal property based techniques:

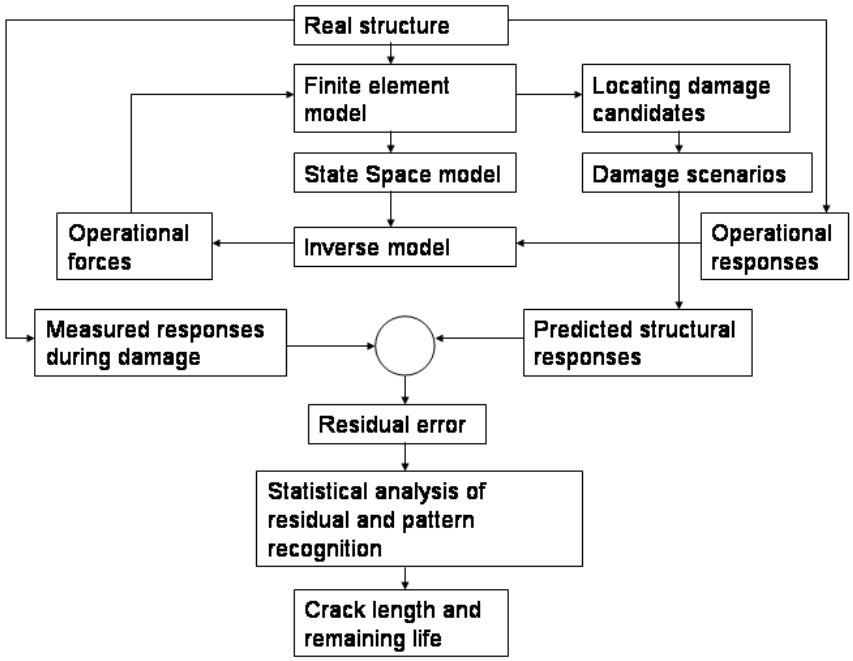

Fig. 3.4: Flowchart summarising the whole damage detection technique

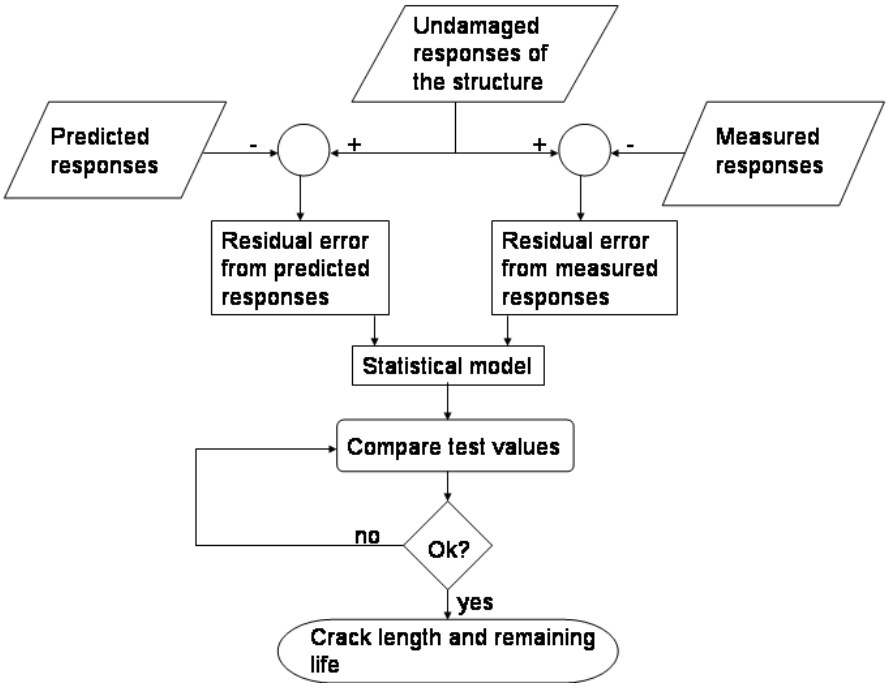

Fig. 3.5: Illustration of the damage identification scheme

- It facilitates the determination of severity of damage by expressing it as physical quantity (crack length).
- It facilitates the determination of the remaining service life by using the Paris law.
- It avoids the modal analysis and its associated problems of data compression, frequency resolution and high user-test interaction.
- It is more efficient in situations where only a few operational conditions are of interest, (which is typical of most structures).
- It is more reliable where the operational forces are difficult to measure, or analytically indeterminable, but expected to remain unchanging.

The disadvantages of the approach are:

- The finite element modelling can make the technique more computationally expensive especially when it is applied to complex structures.
- The force identification in time domain requires some technical skills.

4. TECHNIQUE VERIFICATION: NUMERICAL STUDY

4.1 Introduction

The previous three chapters were mainly concerned with introducing and describing the proposed damage detection technique. Chapter 1 reviewed the existing techniques and highlighted the particular shortfall of not being able to realise all four damage detection levels, which the present study attempts to address. This was followed by the underlying theory for the development of the technique in chapter 2. Chapter 3 presented a detailed description of the technique in the form of its building blocks.

The present chapter deals with verification and application of the technique. This is done by solving the damage detection problem for a numerically simulated beam structure. It is assumed that operational time responses are measured from a beam structure under fatigue cracking. The responses are measured at different states of damage, and it is desired to determine the amount of damage, in terms of crack length, and the remaining service life. Finally, section 4.6 provides a brief comparison of sensitivity with the frequency monitoring technique.

4.2 The beam structure

In this case study, a numerical simulation of a steel cantilever beam is presented. The beam measures 800 mm × 40 mm × 10 mm and its Young's modulus E and material mass density ρ are estimated to be 207×10^9 N/m^2 and 7810 kg/m^3, respectively. Figure 4.1 is a diagrammatic representation of the structure. The load application and response points are also shown in the figure. The relevance of their location with respect to displacements in the mode shape vectors is illustrated by figure 4.2.

For demonstration purposes the structure is assumed to be excited by a force of 1.3 kN at a frequency of 5 Hz. Then the operational responses were generated using a finer mesh, which approximated quite closely the natural mode shapes and frequencies calculated by using exact equations of beams in transverse vibrations (Rao, 1995). It is shown in figure 4.3 that an 80-element finite element model satisfies this requirement reasonably well. As a result, it has been used to simulate measured operational responses (referred to as *pseudo-measured*) at six different states of structural damage: 0.0 mm, 0.2 mm, 1.4 mm, 3.3 mm, 4.2 mm and 5.7 mm crack lengths.

Thus, an effort is made to identify damage completely using the given *pseudo-measured* operational responses. To achieve this, a working finite element model of the structural beam is developed. The density of its mesh is decided upon by the accuracy required

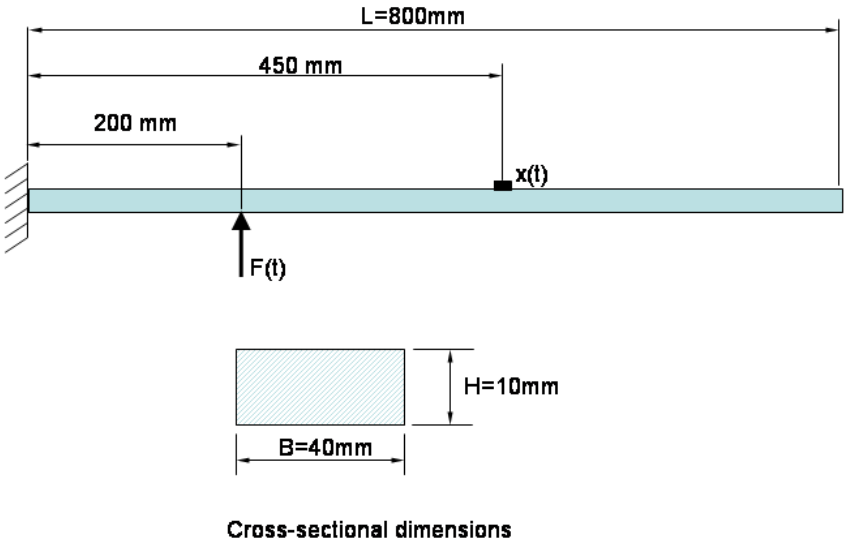

Fig. 4.1: Cantilever beam structure: dimensions and excitation point

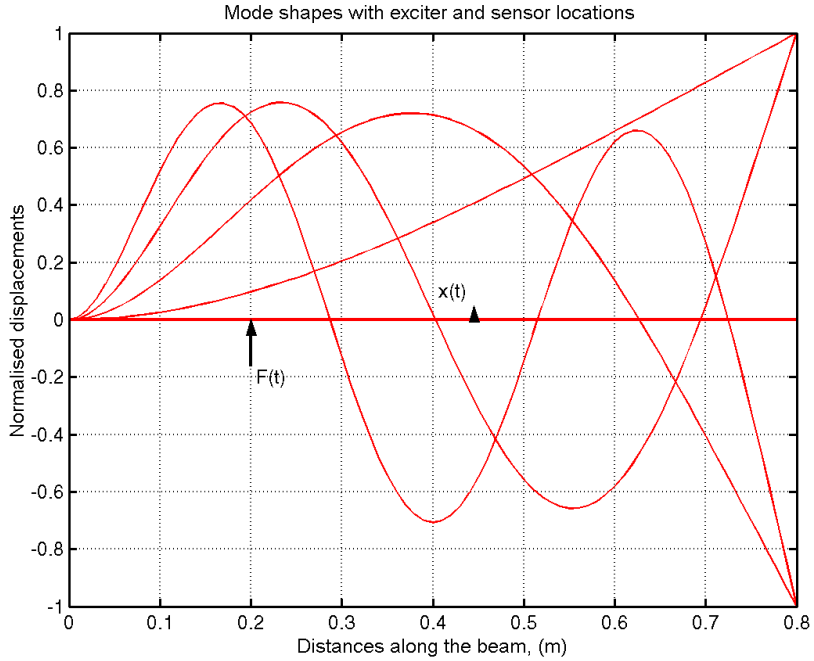

Fig. 4.2: Suitability of the excitation and response points with respect to mode shape displacements

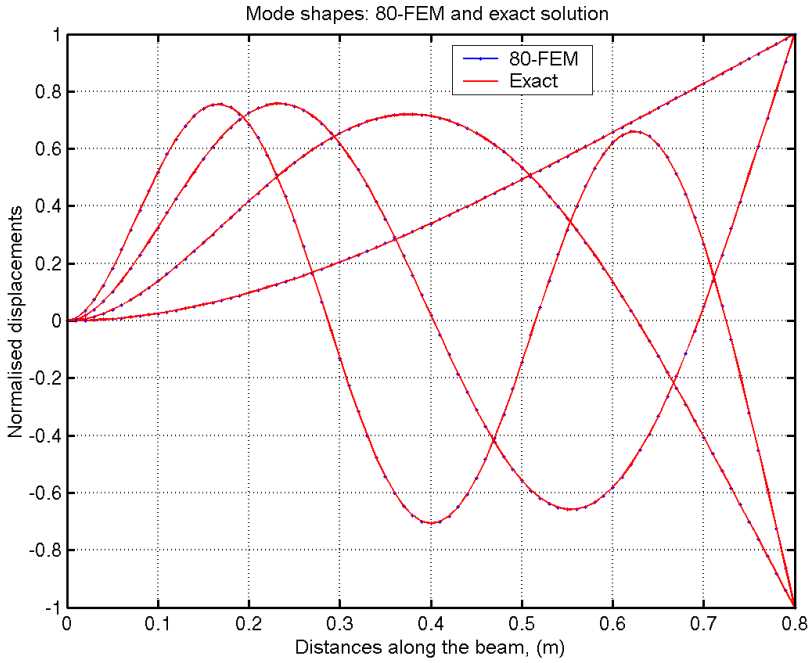

Fig. 4.3: Mode shape fit between 80-element FEM and exact equations

to predict the given *pseudo-measured* responses. It is important to note that the influence of the volume effect on fatigue plus the amplitude-frequency relationship of most actuators, make the first mode the most dominant during fatigue. In this way, the desired working finite element model must approximate the first mode accurately.

4.3 *Modelling the beam*

The beam was modelled in MATLAB 6.1 on a Pentium 4 with 1.7 GHz and 256 MB of random access memory (RAM). The Euler-Bernoulli beam elements have been used to model all undamaged parts of the structure, while the damaged part has been modelled by a special cracked beam element (Krawczuk, et al. 2000). It was noted that when only the first two natural frequencies were of interest, the beam could be modelled accurately by twenty elements. Figure 4.4 and table 4.1 show that the approximation errors with respect to the exact solution are less than 1 percent for the first four natural frequencies. Similarly, the calculated frequency response functions in figure 4.5 show a very close correspondence between the two finite element models.

The correspondence between the accelerations calculated using the 80- and 20-element FEMs was also checked. The force of 1.3 kN at $5Hz$ was applied to both models in

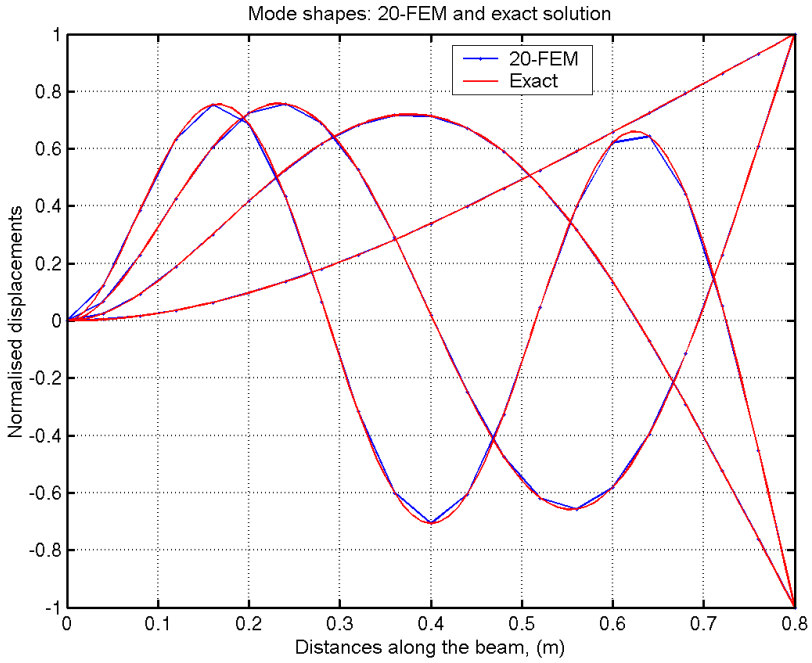

Fig. 4.4: Mode shapes for 20-element FEM and exact equations

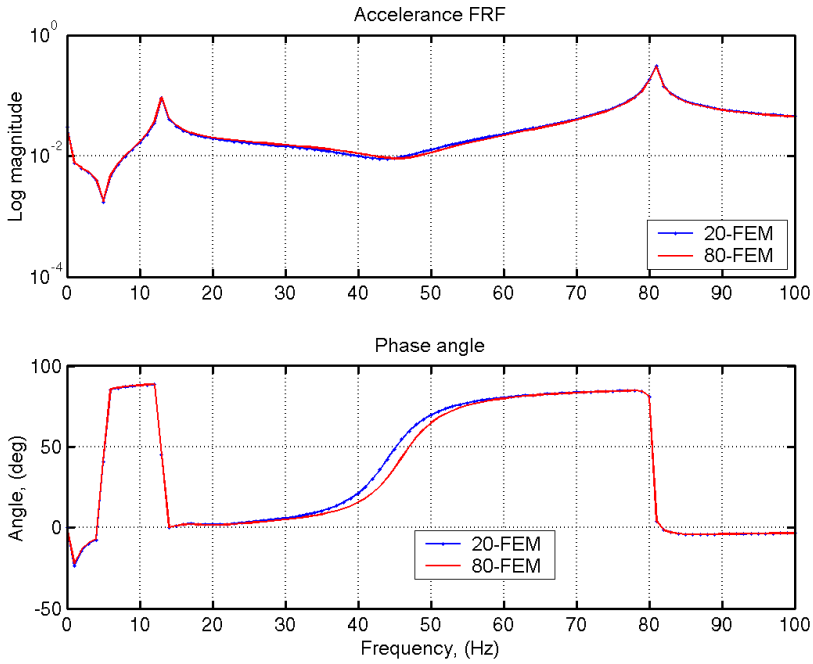

Fig. 4.5: Mode shape correlation between a 20- and 80-Element FEMs

Tab. 4.1: Comparison of the predicted first four natural frequencies

Exact (Hz)	**Eighty-FEM (Hz)**	**% Error**	**Twenty-FEM (Hz)**	**% Error**
12.9945	12.9945	0.0	12.9945	0.0
81.4352	81.4352	0.0	81.4354	0.00025
228.0209	228.0210	0.000044	228.0247	0.0017
446.8301	446.8302	0.000022	446.8580	0.0062

their undamaged states to obtain the accelerations. Since the first two modes were of interest in this case study, the interest band width was 10 Hz to 90 Hz. Thus the accelerations were filtered in the following manner:

- Between 10 Hz and 90 Hz: This was done to show a general correspondence of the two models in the accelerations within the interest frequency band width (Figure 4.6).
- Around 13 Hz and 81 Hz: This was meant to show the correspondences of the models in the accelerations around the first and second natural frequencies separately (Figures 4.7 and 4.8).

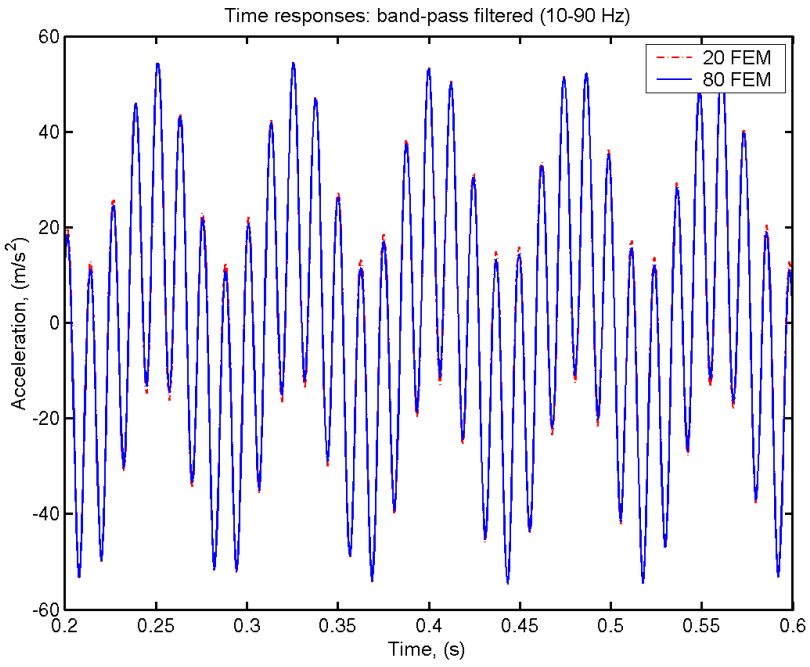

Fig. 4.6: Acceleration responses plotted over each other

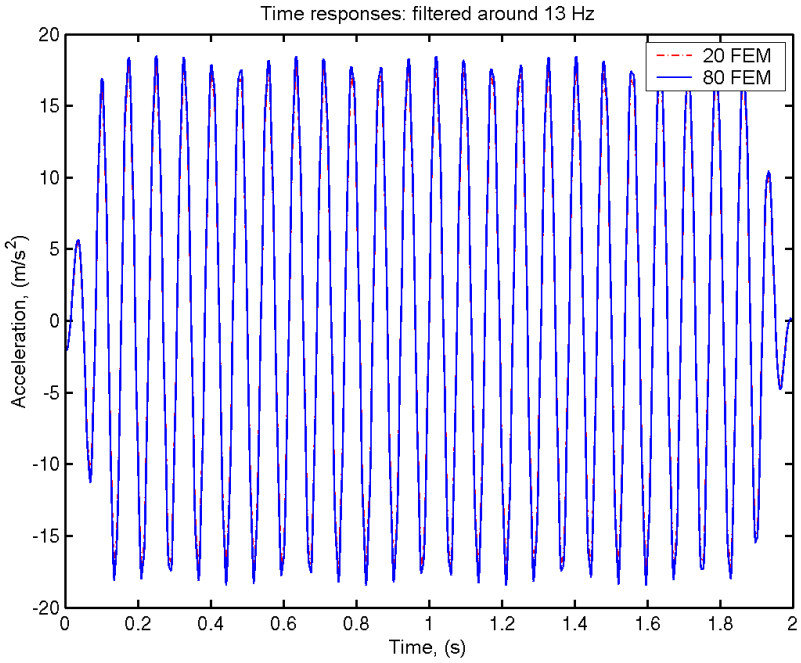

Fig. 4.7: Acceleration responses filtered around 13 Hz plotted over each other

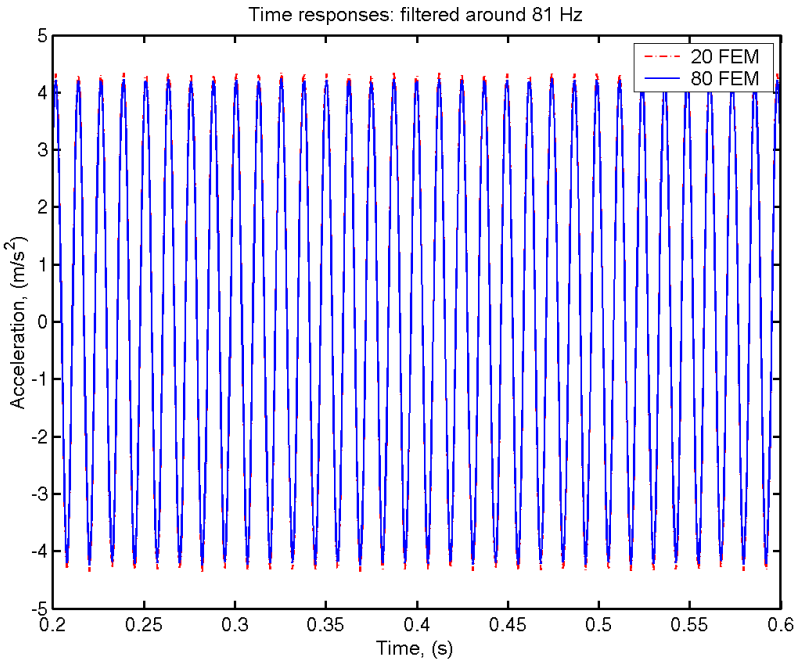

Fig. 4.8: Acceleration responses filtered around 81 Hz plotted over each other

The results in figures 4.6, 4.7 and 4.8 show very good correlation between the accelerations calculated by the two models. Therefore, the 20-element FEM was chosen as the working model and has been used in the rest of the analysis.

4.4 *Damage scenarios*

For the uniform cross-section cantilever beam, the fixed end is the most likely damage location because the stresses are the highest there. Hence, the cracked beam finite element model is located on the first element of the structural FEM. Since the crack is located in the middle of this element, it is geometrically 20 mm from the fixed end of the beam.

The formulation of this element allows for a direct manipulation of the stiffness matrix through the crack ratio. Thus, in this example damage scenarios have been classified by the following crack ratios: 0, 0.1, 0.15, 0.2, 0.25, 0.3, 0.35, 0.4, 0.45, 0.5, 0.55, and 0.6. Since the beam thickness is 10 mm, these crack ratios convert into crack lengths of: 0.0 mm, 1 mm, 1.5 mm, 2 mm, 2.5 mm, 3.0 mm, 3.5 mm, 4.0 mm, 4.5 mm, 5.0 mm, 5.5 mm and 6.0 mm deep.

Having established the damage scenarios, the corresponding time responses were calculated for each crack ratio. The calculated acceleration responses were band-pass filtered around the first and second natural frequencies. The root square values of the filtered responses were computed and sorted in an ascending order to provide a rough check for data variation. These values are plotted in figures 4.9 and 4.10.

The figures show that changes in crack length affects the amplitude values of the acceleration signals. The decline in the values of the acceleration signals as crack length changes is due to the shift in natural frequencies caused by damage. It is noted that this decline becomes more significant at larger crack sizes. This is not always the case, because when the frequency bandwidth of interest is far away from any natural frequency during the entire cracking period, the acceleration signal is observed to increase with damage. The sudden diversions towards the end are due to the tapering operation which was necessary during filtering.

The Bartlett's test was applied to the acceleration amplitude values calculated above to yield corresponding χ^2_{0p} values. It might be recalled from chapter 3 that the subscript p denotes predicted values. Thus each damage scenario has a corresponding χ^2_{0p} value. Figures 4.11 and 4.12 show graphs of these values plotted against crack lengths for the

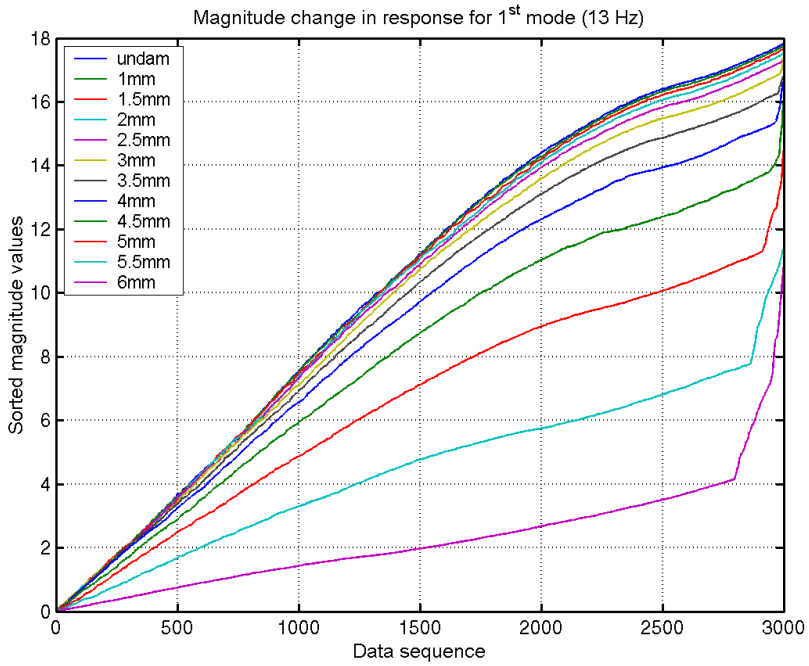

Fig. 4.9: The variation of acceleration response signal due to crack growth at 13 Hz.

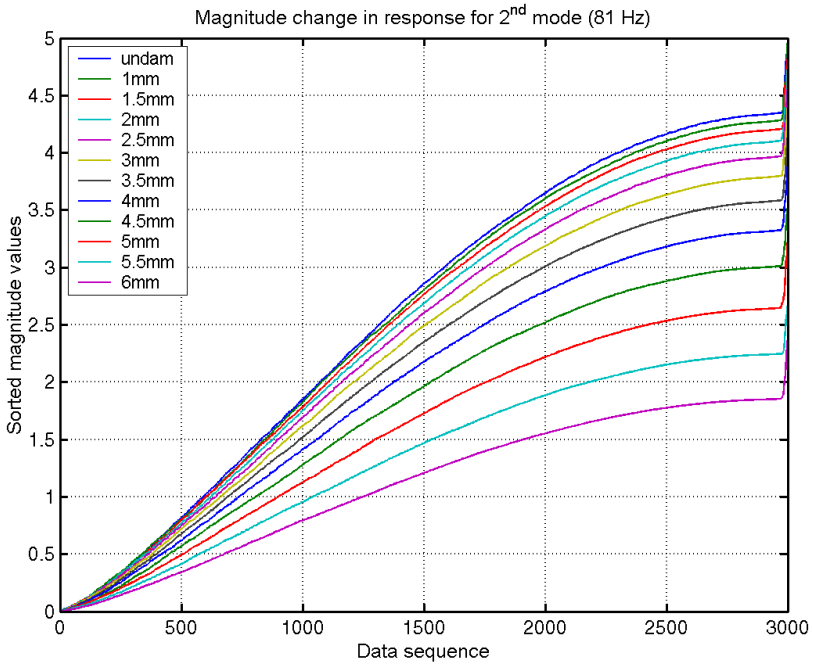

Fig. 4.10: The variation of acceleration response signal due to crack growth at 81 Hz.

first and second natural frequencies.

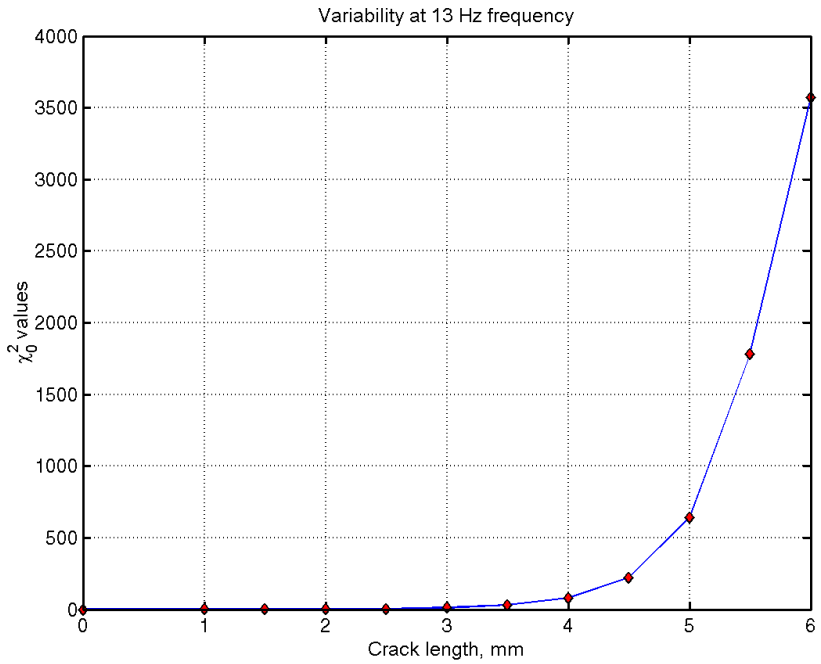

Fig. 4.11: Data variability at first natural frequency

Both plots depict a trend which is typical of crack propagation behaviour. Thus, the parameters quite ably capture the crack propagation behaviour.

As mentioned in chapter 3, the remaining service lives are also predicted for each damage scenario. Thus, the remaining service lives are computed from the crack propagation lives and the relevant curves are plotted in figure 4.13.

It is noted that when the crack length reaches the crack ratio of 0.6, the remaining life (to crack through the remaining 0.4) is half as much as that required for the material to crack from 0.5 to 0.6 (which is just 0.1). This strengthens the decision to use the final crack ratio of 0.6 because the LEFM assumption is violated. Table 4.2 presents the results (*Rem.* denotes *Remaining*).

4.5 *Damage detection*

It is now desired to identify structural damage using the previous *pseudo-measured* time responses. The detection scheme computes χ^2_{0m} value of the measured signal and

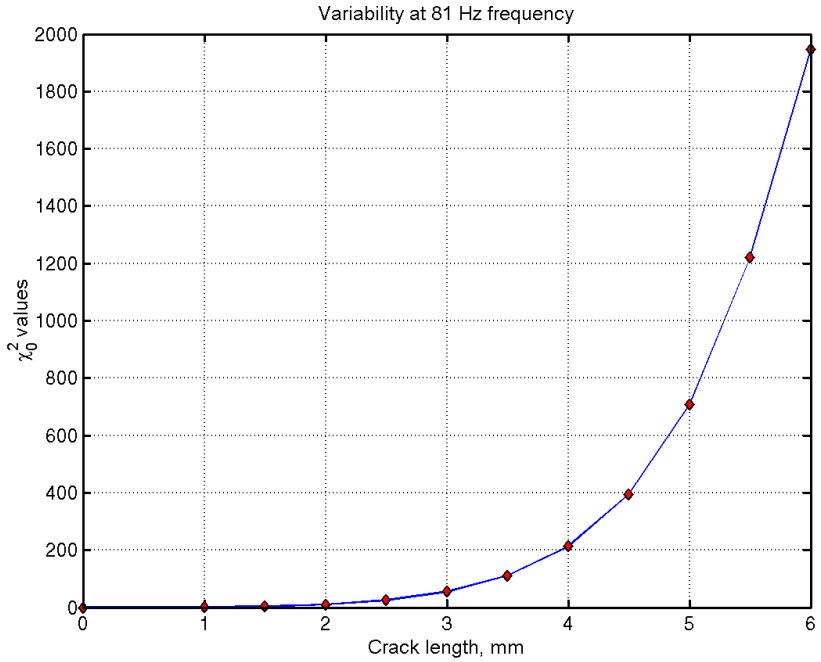

Fig. 4.12: Data variability at second natural frequency

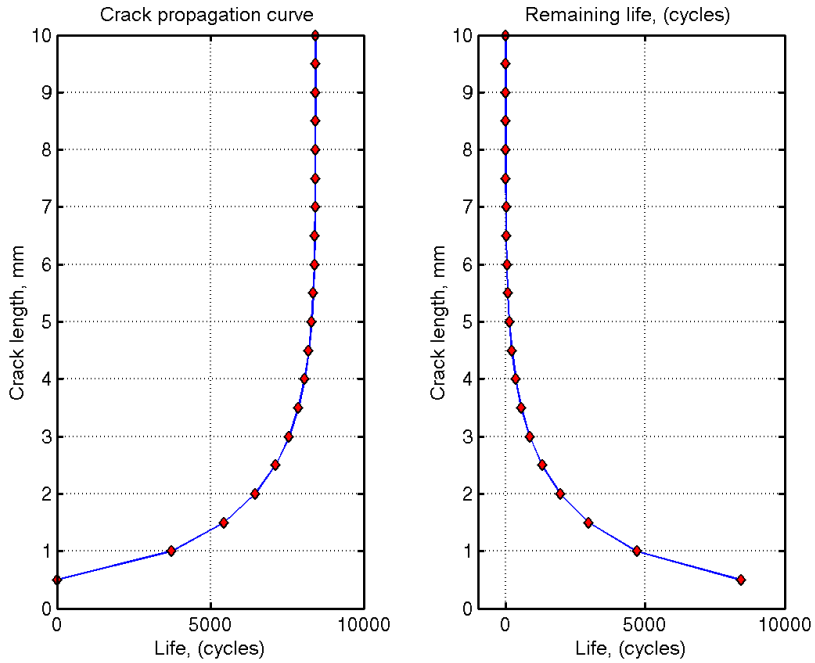

Fig. 4.13: Propagation and remaining service lives calculated at each crack length

Tab. 4.2: Test statistics values for different crack lengths

Crack ratio	**Crack (mm)**	**Rem. Life (cycles)**	$\chi_0^2 : 13Hz$	$\chi_0^2 : 81Hz$
0.05	0.50	8438	–	–
0.10	1.00	4710	0.10	0.80
0.15	1.50	2981	0.50	3.20
0.20	2.00	1963	1.40	10.30
0.25	2.50	1307	4.00	25.30
0.30	3.00	867	11.30	55.30
0.35	3.50	566	30.50	111.30
0.40	4.00	361	80.80	213.80
0.45	4.50	224	222.20	394.00
0.50	5.00	134	641.50	708.00
0.55	5.50	78	1779.10	1220.00
0.60	6.00	43	3568.90	1947.30

matches it to the predicted χ_{0p}^2 values. It yields the crack length whose χ_{0p}^2 value is closest to the computed χ_{0m}^2 value. Therefore, the *pseudo-measured* responses were applied to the detection scheme and yielded the results given in table 4.3 (*Rem.* denotes *Remaining*). These were considered initial estimates of the actual damage level.

Tab. 4.3: The initial estimates of crack length

Actual			**Estimates**			**Rem. Life**
Crack	$\chi_0^2 : 13Hz$	$\chi_0^2 : 81Hz$	**Crack**	$\chi_0^2 : 13Hz$	$\chi_0^2 : 81Hz$	
0.2	0.00	0.00	0.0	0.00	0.00	8438
1.4	0.40	2.40	1.5	0.50	3.20	2981
3.3	19.00	84.30	3.0	11.30	55.30	867
4.2	115.50	273.40	4.0	80.80	213.80	361
5.7	2380.30	1485.70	5.5	1779.1	1220.00	78

The resulting initial estimates provided a basis for a more refined estimation of crack length in a sensitivity-based algorithm. The search was initialised from the time responses which corresponded to the predicted crack lengths given in table 4.3. The second order Taylor series expansion was used with a step size of 0.001 for the crack ratio. The first and second derivatives were calculated numerically using a central difference scheme. As expected, the truncation of higher order derivatives in the central difference scheme affected the accuracy of the solution especially at the end of the time span. In this case, it was noted that for crack ratios of up to 0.45, over a third of

the data length closely matched the actual responses. Beyond the crack ratio of 0.45, higher orders both of the Taylor series expansion and central difference scheme might be required for accurate prediction of the time responses.

In figures 4.14, 4.15, 4.16, 4.17 and 4.18, the top graphs show the correspondence between the acceleration for the initial estimates and the actual damage, while the bottom graphs show the correspondence after the refined estimation.

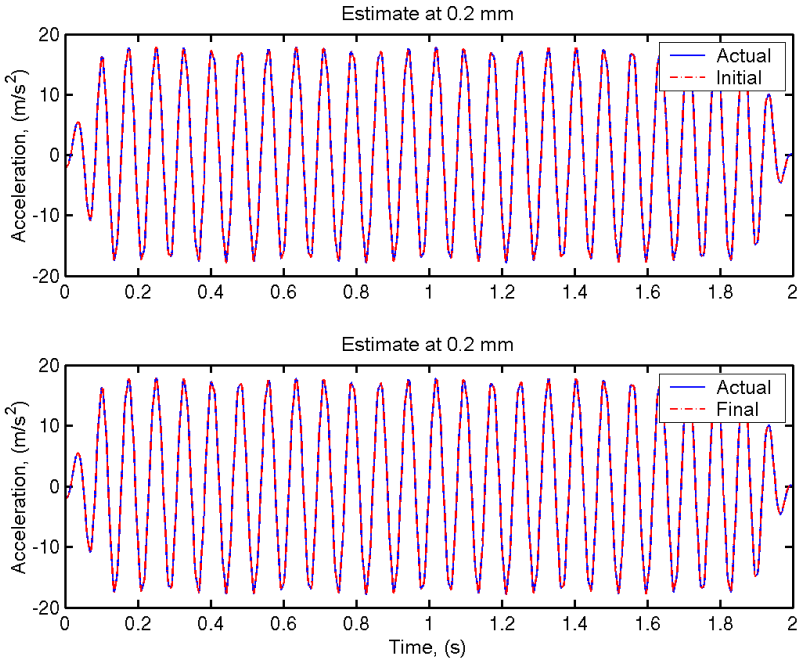

Fig. 4.14: Estimates for crack length of 0.2 mm

It was noted that for 0.2 *mm*, 4.2 *mm* and 5.7 *mm*, the scheme converged after 20 iterations. For 1.4 *mm* and 3.3 *mm*, convergence occurred after 10 backward and 30 forward iterations, respectively. When the products of the number of iterations and step size were added to the initial estimates, it was found that convergence took place at exact crack lengths. Thus the crack lengths were identified very accurately. The corresponding remaining service lives can be easily read off from the remaining service life curves. However, such accurate estimation of remaining life would be unnecessary in a real test because remaining life estimates are quite wild especially at larger crack sizes ($>$ 0.5 crack ratio).

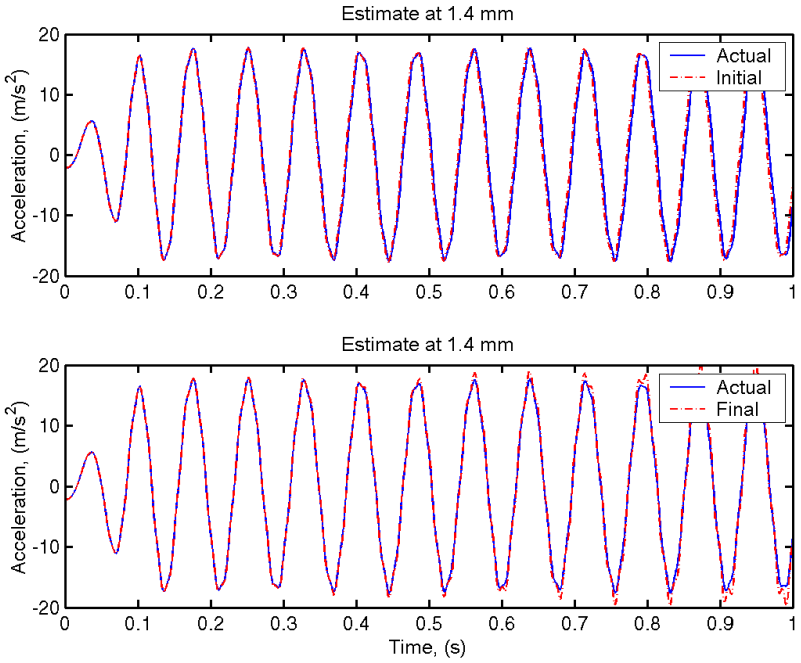

Fig. 4.15: Estimates for crack length of 1.4 mm

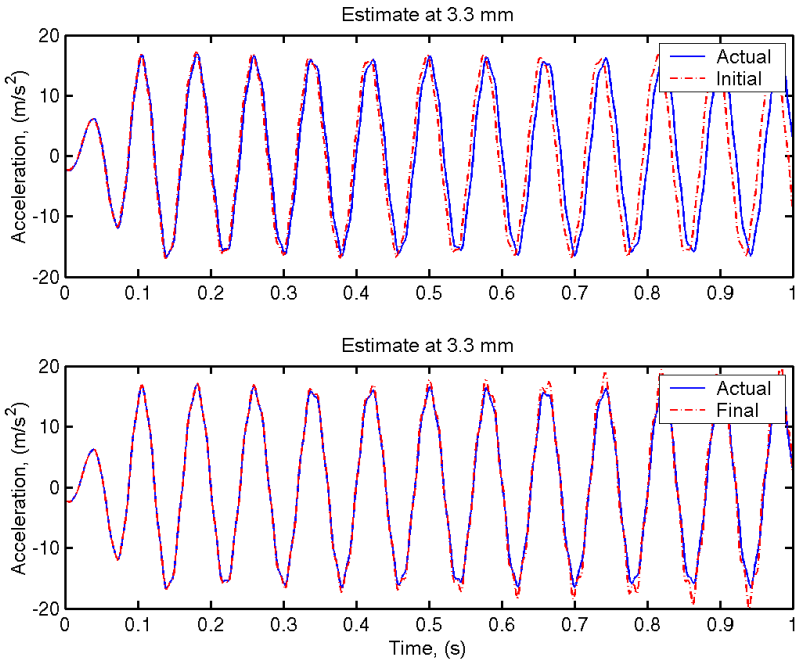

Fig. 4.16: Estimates for crack length of 3.3 mm

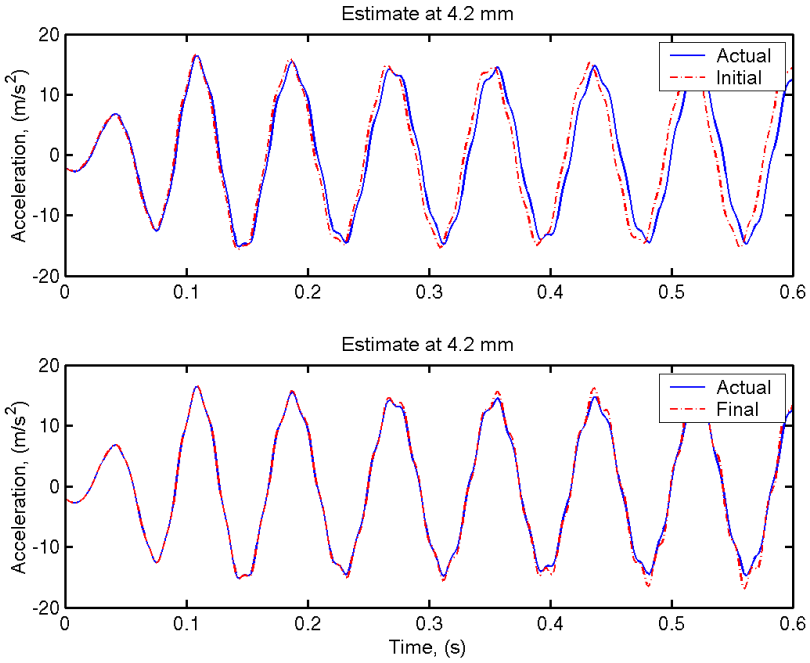

Fig. 4.17: Estimates for crack length of 4.2 mm

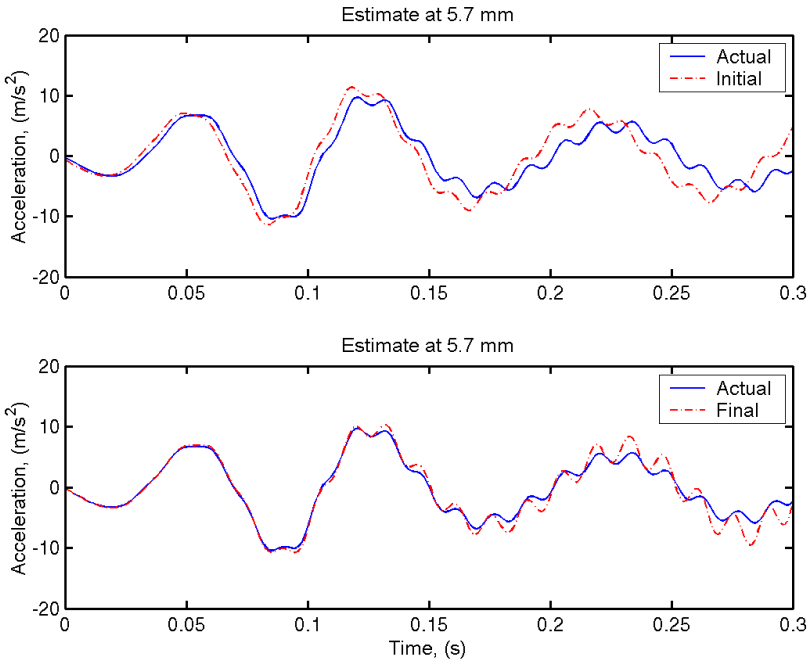

Fig. 4.18: Estimates for crack length of 5.7 mm

4.6 *Comparison with the natural frequency changes*

In this section, a comparison is made between the proposed technique and the change in natural frequencies. The changes in the first two natural frequencies are presented in table 4.4 and figure 4.19.

Tab. 4.4: Natural frequency changes with crack length

Crack (mm)	**Natural frequency (Hz)**		**Relative frequency**	
	First	Second	First	Second
0.5	12.9832	81.3764	0.9991	0.9993
1.0	12.9519	81.2145	0.9967	0.9973
1.5	12.9013	80.9553	0.9928	0.9941
2.0	12.8287	80.5885	0.9872	0.9896
2.5	12.7283	80.0922	0.9795	0.9835
3.0	12.5910	79.4323	0.9689	0.9754
3.5	12.4019	78.5590	0.9544	0.9647
4.0	12.1370	77.3993	0.9340	0.9504
4.5	11.7554	75.8502	0.9046	0.9314
5.0	11.1878	73.7828	0.8610	0.9060
5.5	10.3227	71.0940	0.7944	0.8730
6.0	9.0150	67.8685	0.6938	0.8334

Table 4.5 compares the absolute changes in natural frequencies and the absolute changes in χ_0^2 values per millimetre of crack length change at each damage scenario (from 0.5 mm to 6 mm). The results show that the proposed technique is far more sensitive than the frequency shift technique. It is observed that at the first natural frequency, its sensitivity ranges from three times to over a thousand times the sensitivity of the natural frequency shift technique around the first natural frequency. Around the second natural frequency, the sensitivity ranges from four times to over two hundred times that offered by the natural frequency shift technique. Secondly, the proposed technique provides more room between adjacent scenarios for further statistical manipulation.

4.7 *Summary*

The proposed technique has been applied successfully to damage detection problem of a numerical cantilever beam structure.

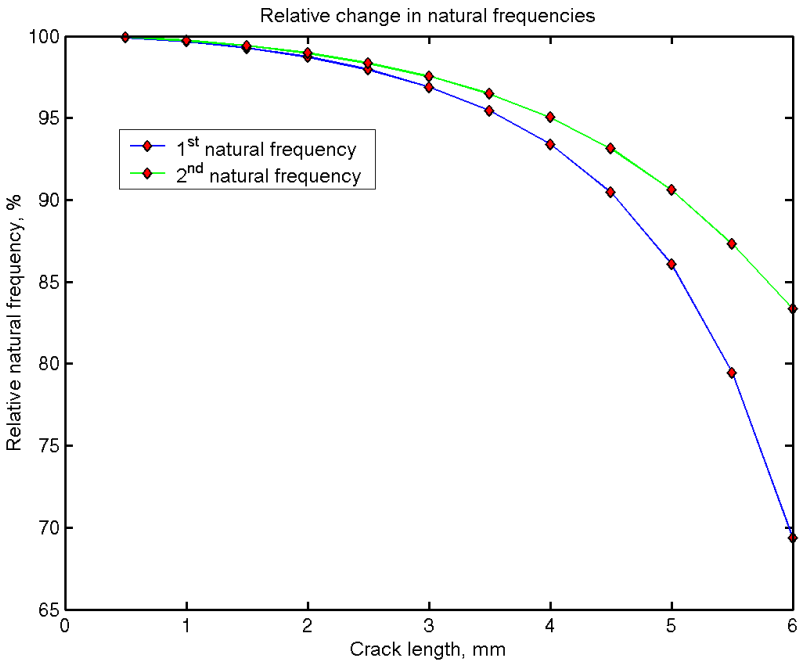

Fig. 4.19: Illustration of relative change in natural frequencies

Tab. 4.5: Comparing natural frequency changes and test statistic value changes

Crack change		**Frequency derivatives**		χ_0^2 **derivatives**	
From (mm)	To (mm)	$\lvert\Delta f_n/\Delta a\rvert_{13Hz}$	$\lvert\Delta f_n/\Delta a\rvert_{81Hz}$	$\lvert\Delta\chi_0^2/\Delta a\rvert_{13Hz}$	$\lvert\Delta\chi_0^2/\Delta a\rvert_{81Hz}$
0.5	1.0	0.0626	0.3238	0.20	1.60
1.0	1.5	0.1012	0.5184	0.80	4.80
1.5	2.0	0.1452	0.7336	1.80	14.20
2.0	2.5	0.2008	0.9926	5.20	30.00
2.5	3.0	0.2746	1.3198	14.60	60.00
3.0	3.5	0.3782	1.7466	38.40	112.00
3.5	4.0	0.5298	2.3194	100.60	205.00
4.0	4.5	0.7632	3.0982	282.80	360.40
4.5	5.0	1.1352	4.1348	838.60	628.00
5.0	5.5	1.7302	5.3776	2275.20	1024.00
5.5	6.0	2.6154	6.4510	3579.60	1454.60

The results of the numerical study show the proposed technique being more sensitive to structural damage at all damage scenarios. It is also shown that the spacing between χ_0^2 values belonging to adjacent crack ratios provides more room for further statistical manipulation.

In the next chapter, the proposed technique is verified by experimental results obtained from laboratory beam structure.

5. TECHNIQUE VERIFICATION: EXPERIMENTAL STUDY

5.1 Introduction

In this case study a mild steel beam of dimensions, 1165 mm long, 50 mm wide and 12 mm thick is clamped at one end over a length of 125 mm leaving a cantilever length of 1040 mm. The beam structure has the following material and fatigue properties : Young's modulus of elasticity E, 207×10^9 N/m^2, mass density ρ, 7810 kg/m^3, yield strength σ_y, 658×10^6 N/m^2, crack growth coefficient C, 6.89×10^{-12} $MPa(\sqrt{m})$ and crack growth exponent m, 3.0 (Shigley, et al. 2003). A 45^o v-notch 2 mm deep is cut at a distance of 40 mm from the fixed point.

Three tests were performed. During tests 1 and 2, the structure was excited by a 1.4 kN force at a frequency of 7 Hz. This resulted in a stress level of 177.0 MPa and a strain amplitude of 856.81 $\mu\epsilon$, which were verified by actual strain gage measurements. The crack measuring sensor was applied at a distance of 1 mm below the notch tip giving a total crack measuring depth of 8.0 mm. The initial crack length was 3.0 mm.

In test 3, the excitation was slightly lowered to 1.25 kN, which resulted in 158 MPA of stress. The crack sensor was applied 2.0 mm below the notch tip giving a total initial crack length of 4.0 mm. This allowed crack length measurements to be taken up to a total depth of 9.0 mm.

In all the three tests the beam was excited at a distance of 465 mm from its fixed end. A pictorial view of the experimental set-up with inserts showing more clearly the location of the crack and excitation is presented in figure 5.1.

The tests were performed in displacement control using a Zonic actuator control unit shown in figure 5.2. The excitation was externally generated through a CDAS system to provide proper control of the actuation period. In all these tests the actuation was performed in durations of 60 s during which measurements were taken for a period of 10 s. The cycles were read from the cycle counter display on the Zonic controller.

5.2 The measurement system

The data was acquired using a spider measurement system through a laboratory desk-top computer shown in figure 5.3. A 10 mV/g accelerometer (with its signal conditioning box), a strain gage and a crack propagation gage were used as sensors in the set-up. A half-bridge Y-series ($1 - LY11 - 6/120A$) strain gage with a gage factor of 2.07, a transverse sensitivity of 0.1% and a temperature coefficient of 104 was used to

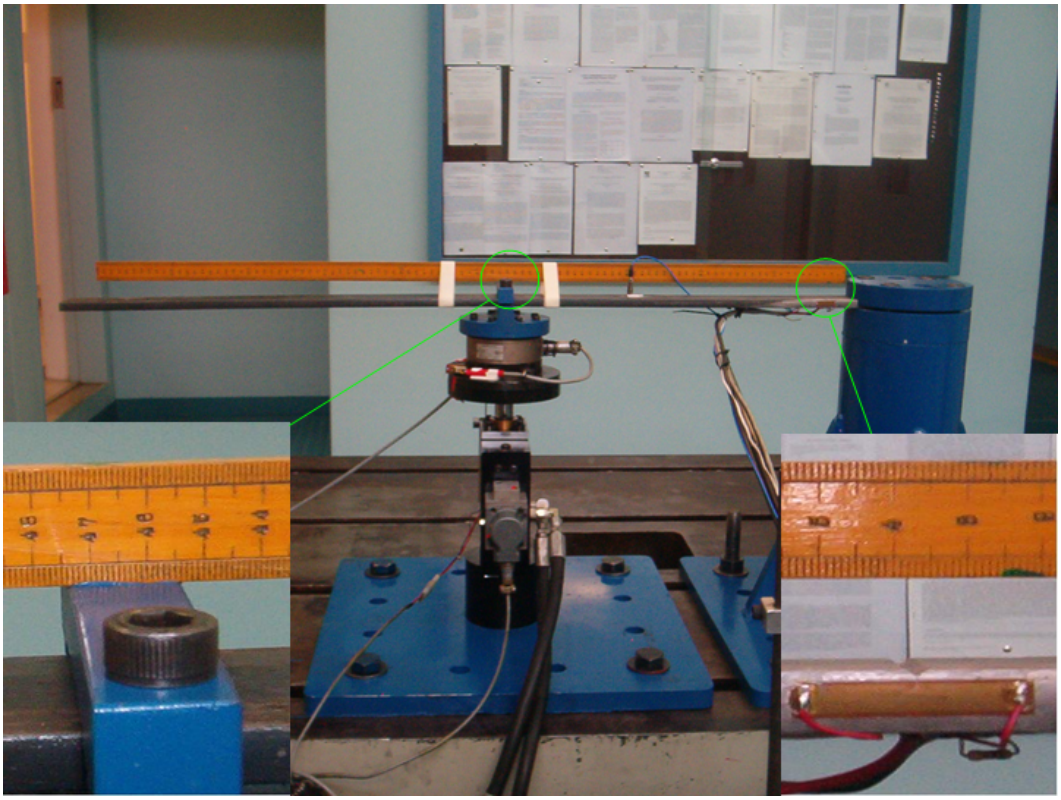

Fig. 5.1: Experimental set up in pictorial form

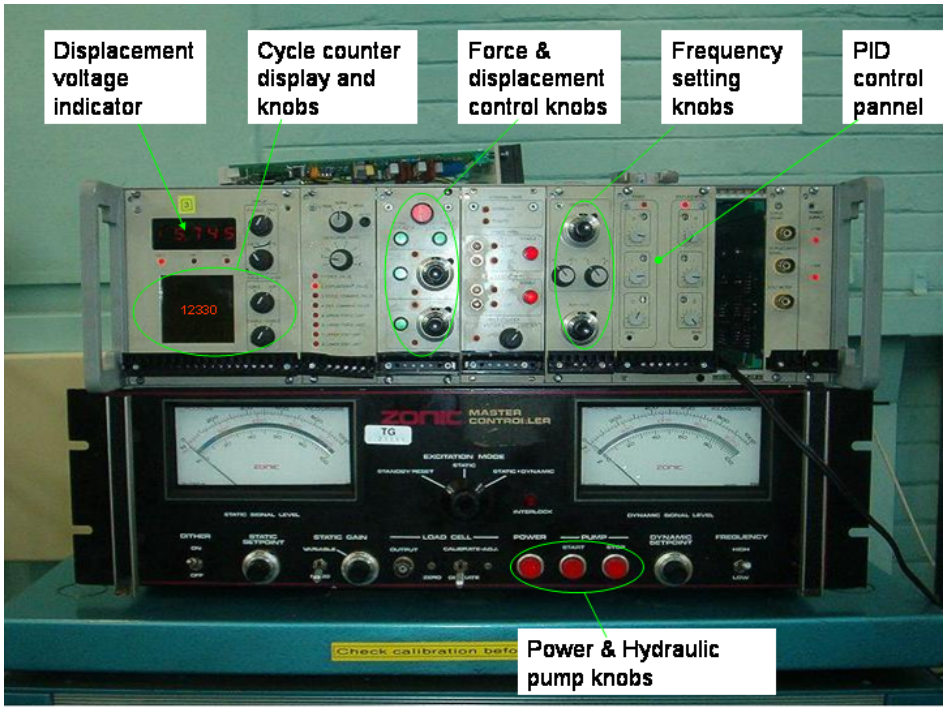

Fig. 5.2: The actuator control unit

Fig. 5.3: A pictorial view of the measurement system

validate the integrity of the calculated stresses (Van Tonder, 2004; Appendix D).

An RDS22 series crack gage with 50 grids of resistance circuits spanning a total width of 5 mm was used to measure crack length as the crack propagated through the material. This gives it a measurement resolution of 0.1 mm per grid. Figure 5.4 shows schematically the crack gage external circuit. The working principle of the crack gage is that its resistance increases as the growing crack breaks the grid. The change in crack length is indicated by the decrease in the voltage measured across the resistor labelled R, in the diagram. Figure 5.5 shows a plot of the voltage vs. crack length, where the voltage was calculated using a supply voltage v_s of 1 V. This supply voltage of 1 V was maintained throughout the three tests. Thus the crack length was determined by adding a_i (from figure 5.4) to the crack length value that corresponded to the measured voltage on the curve in figure 5.5.

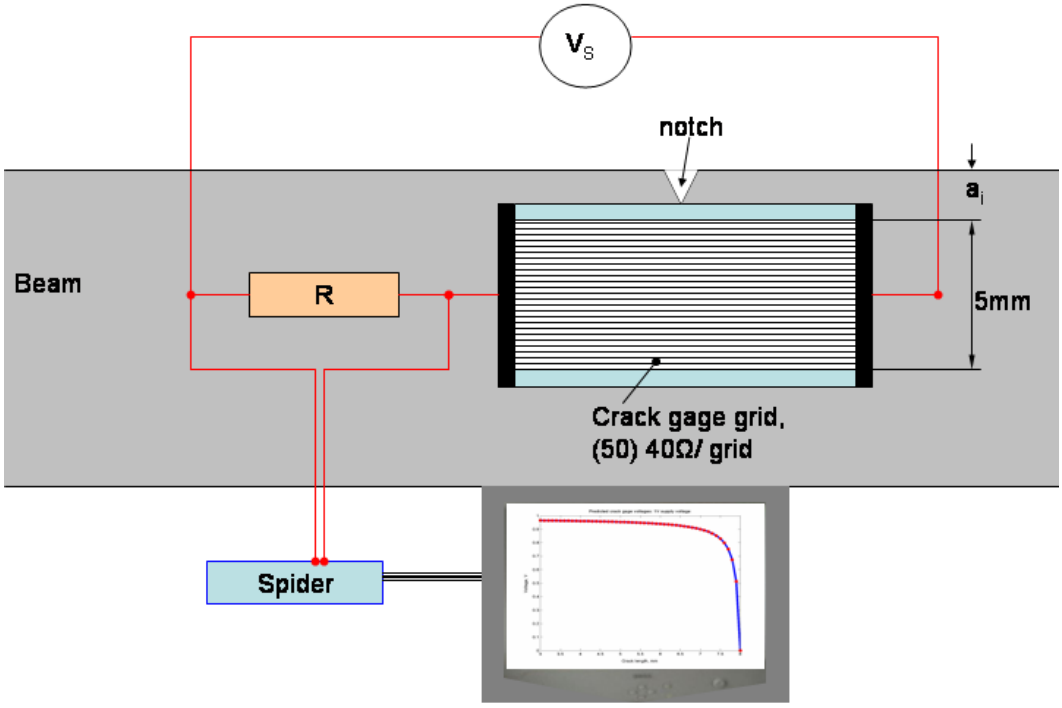

Fig. 5.4: Schematic diagram of the crack gage circuit.

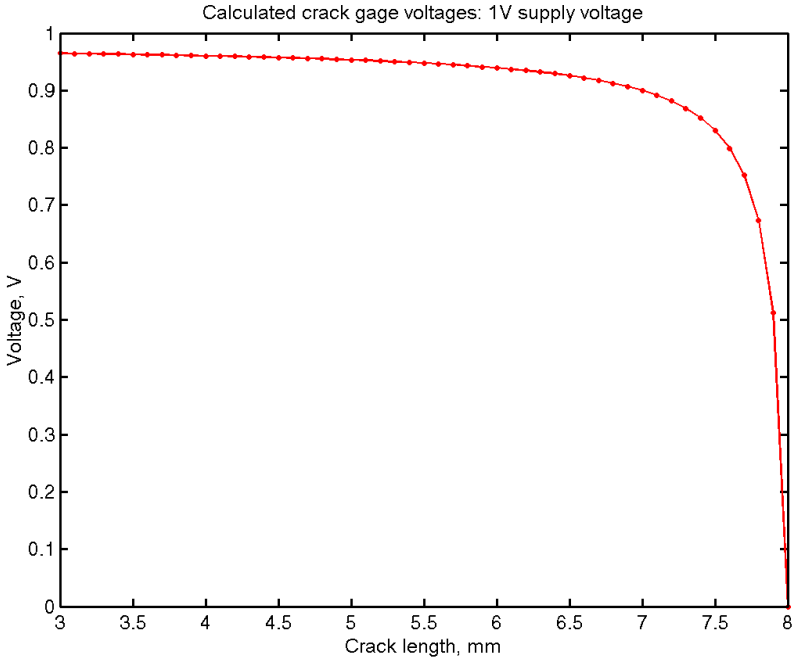

Fig. 5.5: Change of voltage due to change in crack length

5.3 Finite element model

The cantilever beam was modelled in MATLAB using a total number of thirty-eight beam elements on a Pentium 4 platform, with 1.7 GHz and 256 MB of random access memory (RAM). The undamaged parts of the beam were modelled by thirty-seven Euler-Bernoulli beam elements while the damaged part was modelled by the cracked beam element. A schematic diagram of the beam model is shown in figure 5.6. It shows

Element No:	Length (mm)	Element No:	Length (mm)
1	10	17-21	20
2	20	22	25
3(crack)	20	23(Exciter)	40
4-15	20	24	15
16(Sensor)	10	25-38	40

Fig. 5.6: Schematic diagram of the FEM showing element numbering and lengths

the element composition of the beam model. Different lengths were used to capture the locations of the crack and the exciter.

The acceleration response calculated by using this model is plotted over the measured response of the actual structural beam in figure 5.7. The results show a very good fit between test results and the model predicted results. Thus, the model was considered accurate enough for further use in the damage identification procedure.

5.4 Damage scenarios

The finite element model obtained from section 5.3 was used to conceive different damage scenarios. The damage scenarios on the FEM were from an initial notch depth of 2 mm to a final total crack length of 7.2 mm. The initial crack length corresponded to a crack ratio of 0.167, while the final one corresponded to a crack ratio of 0.6. Table 5.1 presents these damage scenarios where $C.L.$ and $C.R.$ denote *crack length* and *crack ratio*, respectively. Crack propagation lives and time responses were calculated for each damage scenario. Then remaining service lives and χ^2_{0p} values were predicted from the crack propagation lives and time responses, respectively. Therefore, each damage

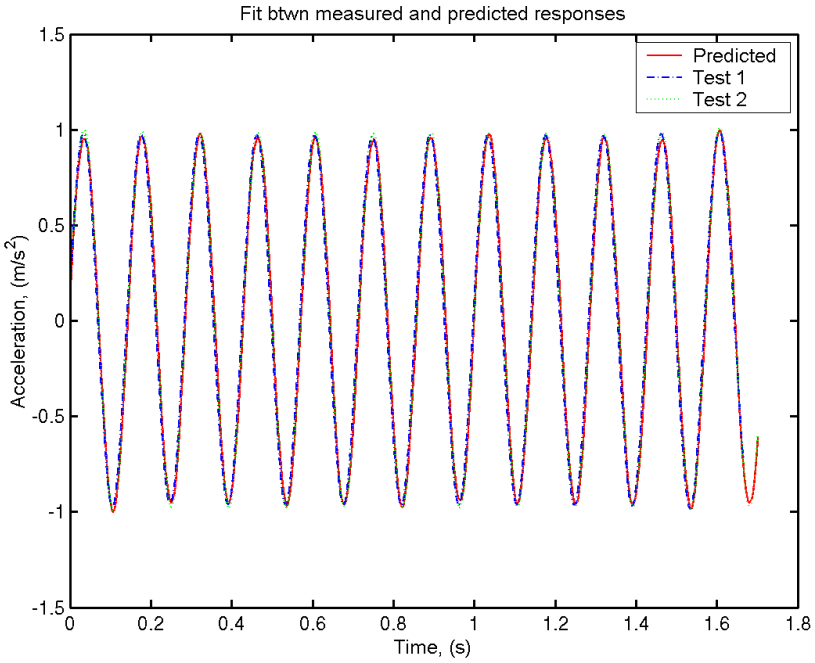

Fig. 5.7: Time response fit for beam with an initial notch of 2 mm.

Tab. 5.1: Damage scenarios from an initial notch of 2 mm

$C.L.\ mm$	2	2.5	3	3.5	4	4.5	5	5.5	6	6.5	7	7.2
$C.R.$	0.167	0.208	0.25	0.292	0.333	0.375	0.417	0.458	0.5	0.542	0.583	0.6

scenario had a corresponding remaining service life and χ^2_{0p} value. These were plotted against crack lengths to obtain predicted curves. In section 5.5, the correspondence between these predicted curves and those obtained from measured data is presented.

The validity of LEFM and plane strain assumptions were also checked for each damage scenario. Equation 2.10 in Chapter 2, states that any of the following parameters, the crack length a, the depth of remaining material $b-a$ and the distance from the crack tip to the boundary along its length h (Figure 2.2) must not exceed an overall plain stress or LEFM limit given by $\frac{4}{\pi}\left(\frac{K}{\sigma_y}\right)$. For plane strain state assumptions to be satisfied, the plain strain limit given by $2.5\left(\frac{K}{\sigma_y}\right)$ must not be exceeded by any of the distances as given above plus the material thickness t (Figure 2.2). However, by the dimensions of the test structure, the material thickness t and the distance h far exceed both limits. Therefore they were ignored.

Figures 5.8 and 5.9 portray the validity of applying LEFM and plain strain theory to

tests 1 and 2, and test 3 respectively. In the figures the blue plots show the changes in crack length a and the remaining material $b-a$ for each damage scenario (crack length). The red curves show the changes in plain strain and LEFM limits for each damage scenario. Figure 5.8 shows that plane strain and LEFM are applicable up to 5.5 mm and 6.7 mm crack lengths respectively in tests 1 and 2. Thus there is a transition from plane strain state into plane stress state at 5.5 mm. For test 3, plane strain and LEFM are valid up to 6.0 mm and 6.8 mm respectively (figure 5.9). Predictions may therefore be expected to be poor beyond the LEFM limits of application.

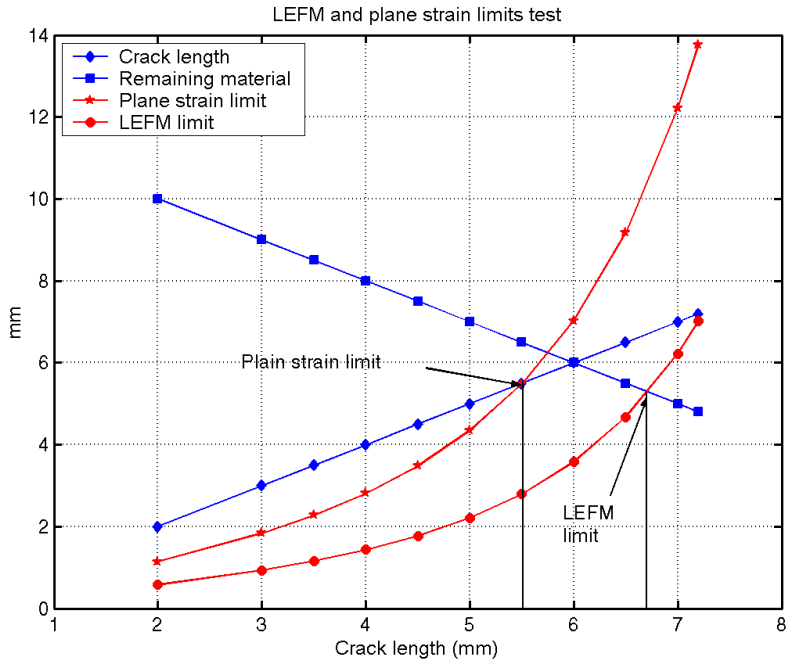

Fig. 5.8: Assessing LEFM and plane strain applicability for tests 1 and 2

5.5 *Results and discussions*

5.5.1 *The crack propagation curve*

The expected crack growth behaviour for constant amplitude loading is represented by the crack propagation curves where most of the life of the structural component is spent during earlier stages of crack growth (Bannantine,et al. 1990). This behaviour is described by the Paris law. In this section, it will be shown that the predicted propagation curves obtained in section 5.4 represent crack growth behaviour in the

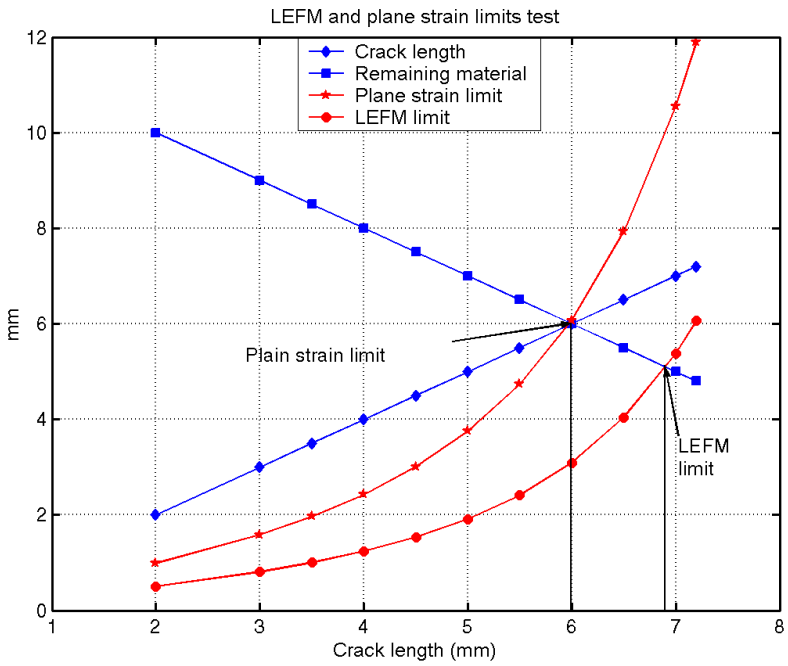

Fig. 5.9: Assessing LEFM and plane strain applicability for test 3

tested beams.

The measured propagation curves from tests 1 and 2 and the predicted propagation curve are shown in figure 5.10. It can be noted that the prediction corresponds fairly well to the measured results. Test 1 had a slightly more accentuated diversion beyond a crack length of 7 mm. This was mainly because LEFM theory was violated figure 5.8. Besides, there were problems with supply voltage fluctuations, so the power supply unit was changed in the next tests.

For the third test, the predictions show a very good correlation with the experimental results, figure 5.11. However, a closer look at the results reveals that at larger crack lengths the life predictions were pretty bad since the LEFM assumptions were violated (figure 5.9).

The remaining service lives were determined from these curves, and are shown in figures 5.12 and 5.13. Prediction errors for the remaining lives were calculated and plotted in figures 5.14 and 5.15.

The prediction error plots show that the predicted curves are able to approximate remaining lives to within 50 % error for crack ratios of less than 0.55, which is slightly above half the section thickness of the structure. For all the tests, the results show

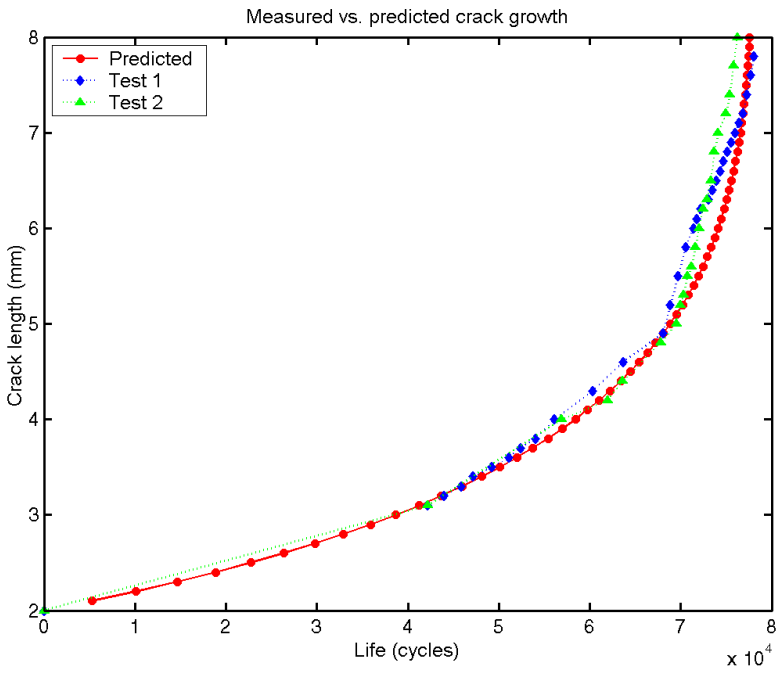

Fig. 5.10: Correspondence between measured crack propagation curves and predicted curve

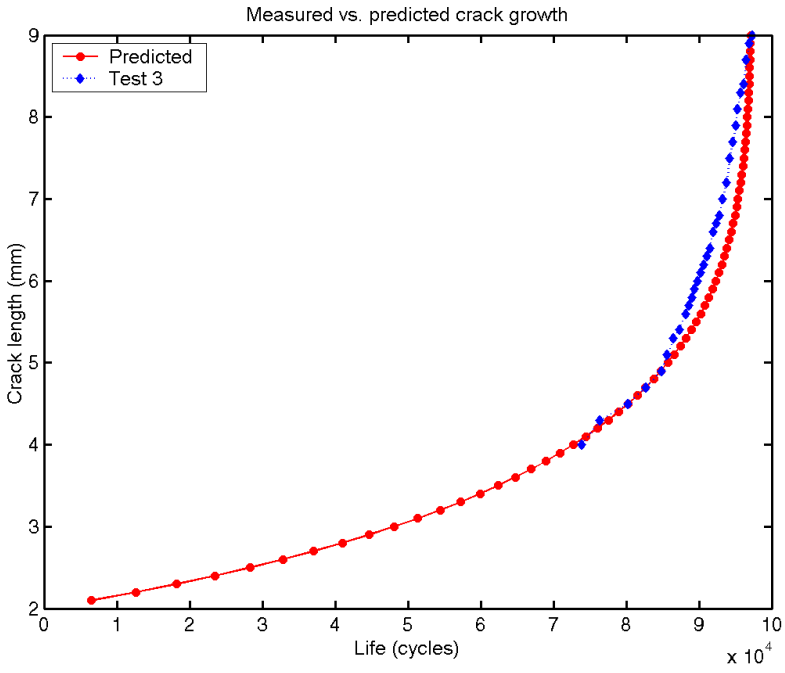

Fig. 5.11: Correlation between measured curve and the predicted propagation curve.

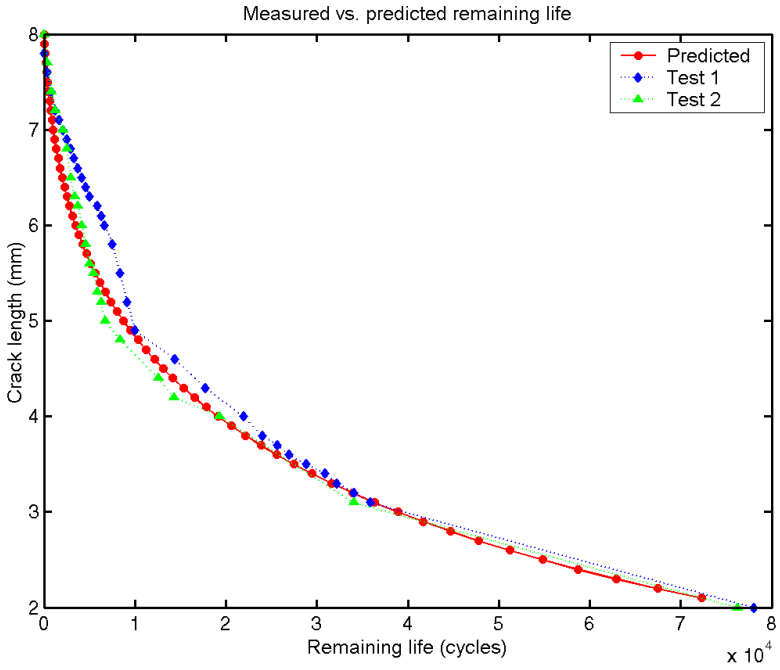

Fig. 5.12: Curve for estimating remaining service life.

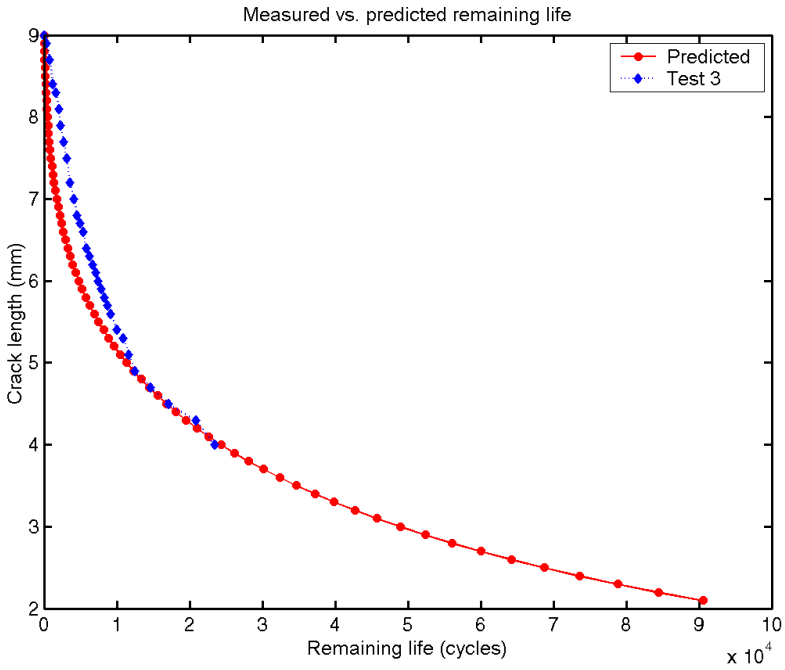

Fig. 5.13: Remaining service life prediction for test 3

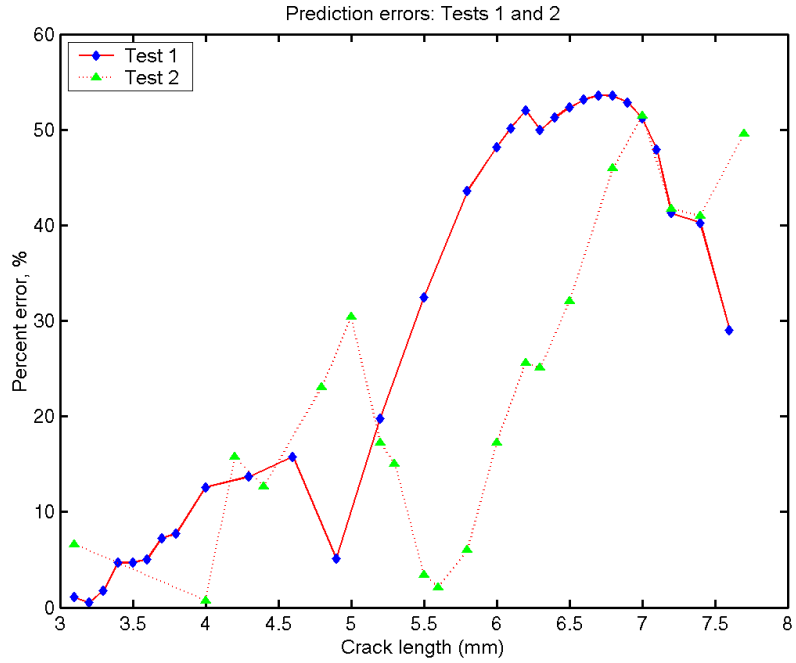

Fig. 5.14: Prediction errors for remaining service life at each crack length for tests 1 and 2

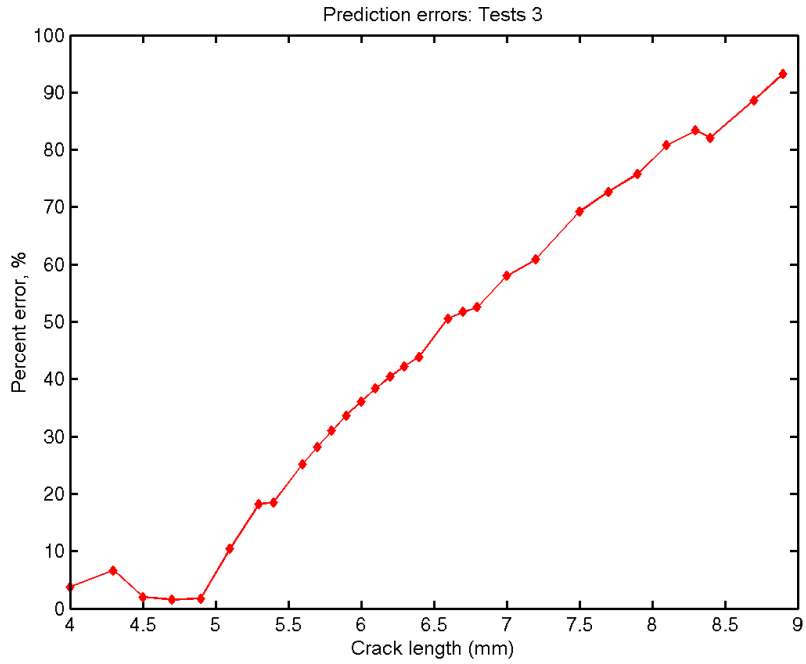

Fig. 5.15: Prediction errors for remaining service life at each crack length for test 3

that beyond this crack ratio it was extremely difficult to obtain close remaining life estimates. This agrees with figures 5.8 and 5.9 in section 5.4 where it is shown that at crack ratios beyond 0.55 LEFM assumptions would be violated for this case.

5.5.2 *Changes of time responses (acceleration)*

The essence of the present work is the use of time response data to assess structural damage. The FEM was used to calculate the acceleration responses for each damage scenario given in section 5.4. These accelerations were filtered around the excitation signal's frequency of 7 Hz. Then, their root mean square values were computed and plotted against crack lengths. The trend in the plotted root mean square values represents an increase with crack length.

The root mean square values calculated from measured data for each test were plotted over those from the model predictions. The results presented in figures 5.16 and 5.17 show that the predicted curve closely approximated test 2 results. The predictions were equally good for test 1 at some of the crack lengths but performed quite poorly around a crack length of 4 mm. This was due to loose screws, which eventually failed around that crack length. A loose screw was observed to introduce some nonlinearities in the measured acceleration signal. In the subsequent tests the screws were checked for tightness after each 60 s of testing and were replaced every 30 $mins$ to offset this effect.

The third test (figure 5.18) shows good correlation in the initial stages of crack growth, but predictions became very poor at advanced stages of crack growth. The root mean square values were random in this region and could not be predicted accurately.

5.5.3 *Changes in χ_0^2 values*

The χ_0^2 values are used in statistics to check internal data variability caused by changes in the treatment process or the operating conditions. Thus in the present work, it is inherently assumed that if all factors which influence changes in the measured time responses are kept constant, then these values can be used as damage indicators. The notable factors which must be harnessed are: force levels, boundary conditions, couplings and joints, material properties, structural geometry and crack geometry and location.

Therefore, the χ_{0m}^2 values calculated from measured data were plotted over those from

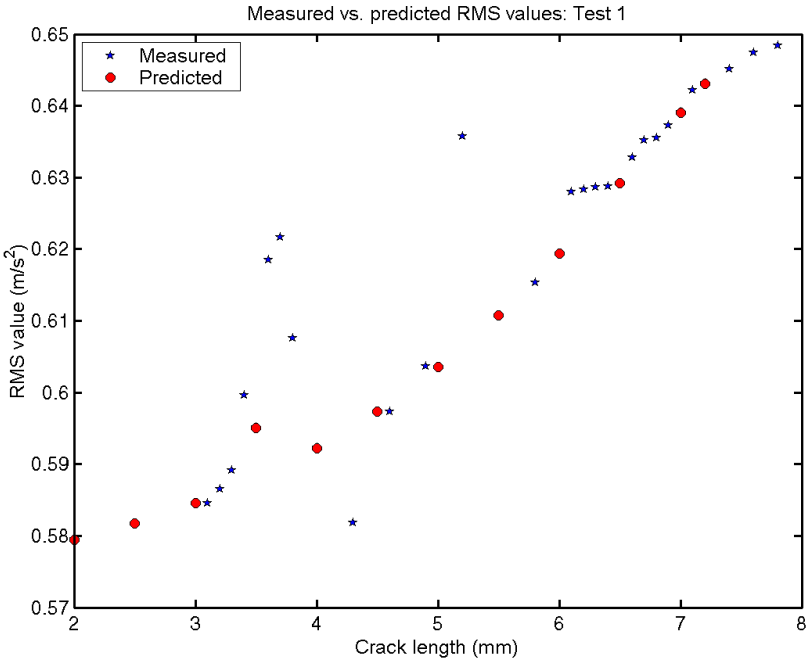

Fig. 5.16: Plot of predicted and measured root mean square values for first test

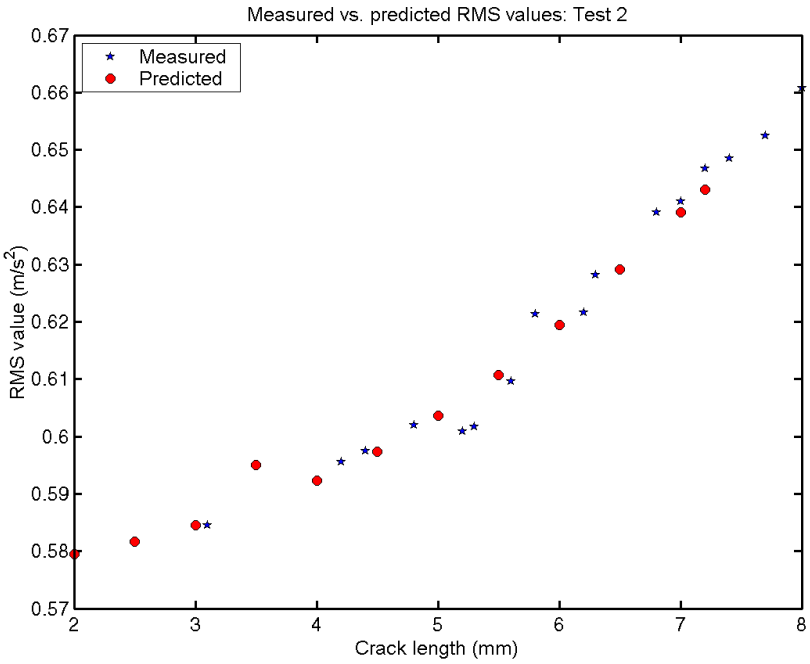

Fig. 5.17: Plot of measured and predicted root mean square values for second test

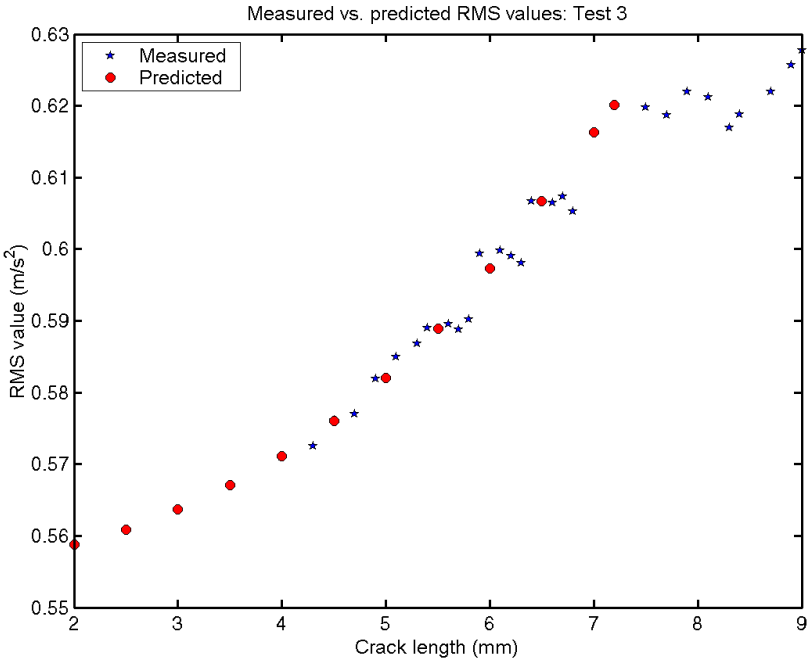

Fig. 5.18: Plot of measured and predicted root mean square values for third test

model predictions, denoted χ^2_{0p} (figures 5.19, 5.20 and 5.21). There is good correlation between experimental and predicted results especially in test 2 and shorter crack lengths for test 3. However, the problems of loose screws and supply voltage fluctuations, marred the performance of the predicted curve for test 1 in the region where LEFM theory was applicable. In the third test, the predictions at longer crack lengths were very random due to extreme violation of LEFM and unstable effects at that crack growth stage.

Thus it can be noted that by calculating the χ^2_{0m} value for a given measured response, the predicted curve can be used to obtain the corresponding crack length. Then, the remaining service life can be determined from the predicted remaining service life curves. This completes the damage identification procedure.

5.6 *Summary*

It has been shown by an experimental study that the technique can be used for complete identification of structural damage. Initially damage scenarios should be identified on the FEM. Then using the FEM both the crack propagation curves and the time responses are calculated. The calculated responses are then filtered around the interest

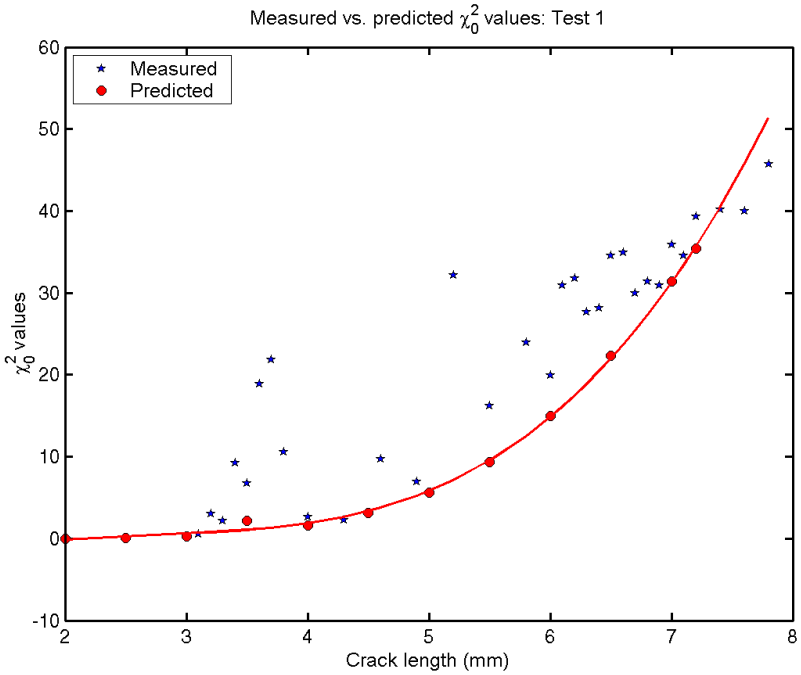

Fig. 5.19: Comparison of test statistics calculated from predicted and measured data for first test

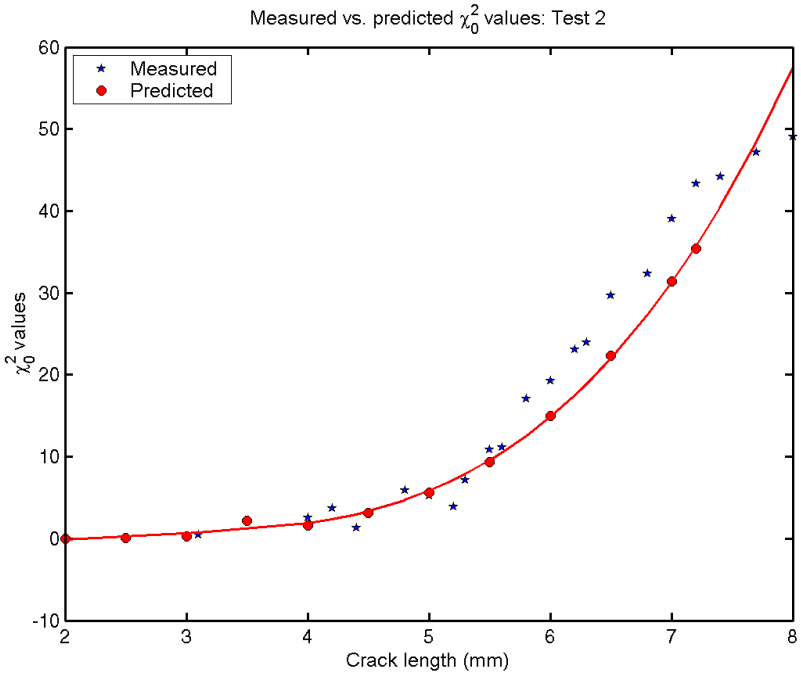

Fig. 5.20: Comparison of test statistics calculated from predicted and measured data for second test

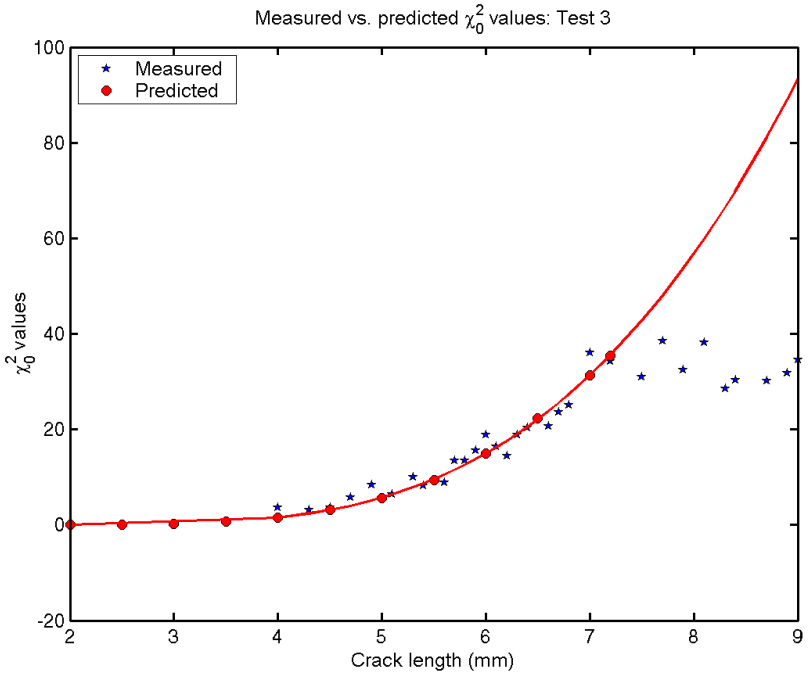

Fig. 5.21: Comparison of test statistics calculated from predicted and measured data for third test

band width after which the χ^2_{0p} values are calculated.

As the measured data is obtained the corresponding χ^2_{0m} values are calculated. Then the crack lengths are read off from the predicted curve. The remaining service life is then obtained from the predicted remaining life curves which are derived from the crack propagation curves.

It can be noted that after the FEM is used to calculate the time responses, the rest of the process requires very little computational effort. For example, to determine both the propagation life curve and the χ^2_{0p} value curve for each test it took 106 s on a Pentium 4 personal computer with 1.7 GHz and 256 MB of random access memory. Each test consisted of 32 selected responses with each response signal containing 12,000 data units. Thus, to process a single measured time response, it would take much less time than this.

6. CONCLUSIONS AND RECOMMENDATIONS

In this chapter, some conclusions and recommendations for future study are drawn. Section 6.1 delineates how each level is identified, its limitations and application. Section 6.2 draws some recommendations for further development of the technique's capability.

6.1 Conclusions

A time response based structural damage detection technique has been shown to provide a complete identification of structural damage. The technique involves the finite element modelling of the structural system from which a multivariable state-space model is identified. The multivariable state-space model is inverted using time domain based techniques so that operational forces can be determined. The calculated operational forces are applied to the structural FEM to identify high stress spots on the real structural.

The new technique identifies level 1 by using changes in the measured operational responses via test statistic values. The test statistics are compared with a threshold value which is calculated at 1 % of undamaged structure's response. The mere change in the value of the test statistics from this threshold value is taken to indicate the presence of structural damage.

Level 2 is identified through the locations of stress hot spots on the structural FEM. It is expected that these spots are the most likely damage locations. This is considered conservative.

In this this technique, structural damage is modelled in terms of crack length to allow the application of LEFM theory. Thus, several damage scenarios are inputted on the structural FEM in the identified damage locations. Then structural time responses are predicted for each scenario using FEM. The test statistic values are calculated for each damage scenario. Therefore, a test statistic value obtained from each measured response is compared with any of these calculated values to find its closest match. This identifies level 3.

The Paris law is used to predict remaining service life for each damage scenario. Thus having determined the severity of damage in level 3, the corresponding remaining service life is simultaneously determined which identifies the final level.

This technique has been verified through a numerical and an experimental case studies.

Through the numerical case study, it has been observed that more accurate estimates are obtainable by performing a sensitivity based procedure, which minimises an error between the measured response and a closest match to the predicted response. The results in both case studies show that the remaining life predictions at lower levels of structural damage are more accurate than at larger crack lengths.

The analysis on the experimental case study showed that the predictions were accurate to within an error margin of 50 % for crack ratios of less than 0.55. This result tied in well with the observations on the limits of applicability of the LEFM theory. The limit of applicability of LEFM theory was noted to lie between the crack ratios of 0.55 and 0.6. Since it was also observed that the crack grew very rapidly beyond this limit, it could be considered as the transition region into unstable crack growth phase. Therefore, it can be concluded that the technique is capable of identifying the four levels of damage identification up to the crack ratio of 0.55.

The technique has the practical attraction of requiring less computational effort during the damage identification phase hence is suitable for continuous monitoring of structural health. A further advantage lies in its better sensitivity to structural damage than the popularly used method of frequency shift monitoring. Through the numerical study the proposed technique was shown to be over three times as much sensitive as the natural frequency shift technique. Therefore, the technique could prove to be useful for complete identification of damage in structures like bridges, telegraph towers and long suspension systems where sensitivity is a real problem.

It is important to note some precautionary measures in the application of the technique. Since the operational time responses are not a property of the structural system, there are a few factors which must be attended to. Firstly, the finite element model must be able to predict the measured responses accurately. The force levels must be properly controlled so that no fluctuations occur. Finally, the boundary constraints, joints and couplings must remain in their designed functional state.

6.2 Recommendations

It might be recommended that in identifying level 1, thorough investigation into the threshold value of the test statistic value be performed. In the present study purely numerical investigation was used but this could be further enhanced by an experimental study.

The location of damage is perfomed by identifying the high stress points on the structural FEM. This approach was considered more applicable with this technique where structural operational responses are used for damage identification. Since the main focus of the work was to extend on the existing methods to identify all the four levels, this was considered satisfactory although it might be recommended that other damage location methods be investigated to work with this technique.

In the present technique, a homogeneous structure was studied. I recommend that for further study a more practical heterogeous or composite structure be studied. This might result in changes in some of the applied concepts (like the LEFM, particularly the Paris law) although the fundamental procedure may remain the same. It would be interesting to note how other structural damage concepts would work with the procedure compared to the present one.

Other important areas for future study may include investigation into development of the technique under load varying operating conditions. It is under very limited and highly controlled (e.g. laboratory situations) where load levels may remain unvarying. But in most practical structural systems, the load levels are random in nature and cannot remain constant. Besides, in this work, attention was given to the open mode of fracture (bending only or mode I of fracture). Practical structures may not strictly fracture in this mode only. Therefore, it might be necessary to consider developing techniques for other modes of fracture or their combinations. As a result, techniques for identification of branched crack geometries may be developed.

7. REFERENCES

Bannantine, J.A., Comer, J.J. & Handrock, J.L. (1990). *Fundamentals of Metal Fatigue Analysis*. Englewood Cliffs, N.J: Prentice-Hall Inc.

Bathe, K. (1996). *Finite Element Procedures*. New York: Prentice-Hall Inc.

Bement, M. J. & Farrar, C. R. (2000). *Issues for the application of statistical models in damage detection*. Conference proceedings of the 18^{th} IMAC. San Antonio, Texas.

Bendat, J.J & Piersol, A.G. (2000). *Random data: Analysis and measurement procedures*. New York: John Wiley & Sons.

Bodeux, J. B. & Golinval, J. C. (2003). Modal identification and damage detection using the data-driven stochastic subspace and ARMAV methods. *Mechanical Systems and Signal Processing,* 17(1):83–89.

Broek, D. (1989). *The practical use of fracture mechanics*. Boston: Kluwer Academic Publishers.

Chou, J. & Ghaboussi, J. (2001). Genetic algorithms in structural damage detection. *Computers and Structures,* 79:1335–1353.

Doebling, S. W., Farrar, C. R., Prime, M. B. & Shevitz, D. W. (1996). Damage identification and health monitoring of structural and mechanical systems from changes in their vibration characteristics: a literature review. Los Alamos National Laboratory Report LA-13070-MS, UC-900.

Dowling, N. E. (1999). *Mechanical behaviour of materials: Engineering methods for deformation, fracture and fatigue*. Englewood Cliffs, N.J: Prentice-Hall Inc.

Ewins, D.J. (1984). *Modal testing: Theory and practice*. London: Research studies press Ltd.

Farrar, C. R. & Doebling, S. W. (1997). An overview of modal-based damage detection identification methods. Engineering Analysis Group, Los Alamos National Laboratory, New Mexico.

Farrar, C. R., Doebling, S. W. & Duffey, T. A. (1997). Vibration-based damage detection. Los Alamos National Laboratory MS P-946.

Farrar, C. R. & Doebling, S. W. (1998). Lessons learned from applications of vibration-based damage identification methods to a large bridge structure. Engineering Analysis Group, Los Alamos National Laboratory, New Mexico.

Friswell, M.I. & Mottershead, J.E. (1995). *Finite element model updating in structural dynamics*. Dordrecht: Kluwer academic publishers.

Friswell, M. I., Penny, J. E. T. & Garvey, S. D. (1998). A combined genetic and eigensensitivity algorithm for the location of damage in structures. *Computers and Structures,* 69:547–556.

Fritzen, C. P., Jennewein, D. & Kiefer, T. (1998). Damage detection based on model updating methods. *Mechanical Systems and Signal Processing,* 12(1):163–186.

Fritzen, C. P. & Bohle, K. (2003). Global damage identification of the Steel Quake structure using modal data. *Mechanical Systems and Signal Processing,* 17(1):111–117.

Garibaldi, L., Marchesiello, S. & Bonisoli, E. (2003). Identification and updating over the Z24-bridge benchmark, *Mechanical Systems and Signal Processing,* 17(1):153–161.

Görl, E. & Link, M. (2003). Damage detection using changes of eigenfrequencies and mode shapes. *Mechanical Systems and Signal Processing,* 17(1):103–110.

Groenwold, A.A. (2002). *Study Guide: Finite element methods (MEE732).* RSA,University of Pretoria.

Haftka, R.T., Gürdal, Z. & Kamat, M.P. (1990). *Elements of structural optimisation.* Dordrecht: Kluwer academic publishers.

He, L. (1999). Damage detection evaluation I. In *Modal Analysis and Testing.* Edited by Silva, M. M. J. & Maia, M. M. N. NATO Science Series, Dordrecht: Kluwer Academic Publishers.

Heyns, P.S. (2002). *Study Guide: Mechanical Vibration: Measurement and Analysis.*

RSA, University of Pretoria.

Hughes, T.J.R. (1987). *The finite element method: Linear static and dynamic finite element analysis*. Englewood Cliffs, N.J: Prentice-Hall Inc.

Krawczuk, M., $\dot{Z}$ak, A., & Ostachowicz, W. (2000). Elastic beam finite element with a transverse elasto-plastic crack, *Finite Element in Analysis and Design*, 34:61–73.

Kullaa, J. (2003). Damage detection of the Z24-bridge using control charts. *Mechanical Systems and Signal Processing,* 17(1):163–170.

Lam, H. F., Ko, J. M. & Wong, C. W. (1998). Localisation of damaged structural connections based on experimental modal and sensitivity analysis. *Journal of Sound and Vibration* 210(1):91-115.

Li, Z. X., Chan, T. H. T. & Ko, J. M. (2001). Fatigue analysis and life prediction of bridges with structural health monitoring data–Part I: methodology and strategy. *International Journal of Fatigue,* 23:45-53.

Lin, R. M. & Ewins, D. J. (1990). *Model updating using FRF data*. Proceedings of the 15^{th} International Seminar on Modal Analysis. Leuven, Belgium.

Maeck, J. & De Roeck, G. (2003). Damage assessment using vibration analysis on the Z24-bridge. *Mechanical Systems and Signal Processing,* 17(1):133–142.

Messina, A., Williams, E.J. & Contursi, T. (1998). Structural damage detection by a sensitivity and statistical-based method. *Journal of Sound and Vibration,* 216(5):791-808.

Montgomery, D.C. (1996). *Design and analysis of experiments*. New York: John Wiley and Sons.

Mottershead, J. E. & Friswell, M. I. (1993). Model updating in structural dynamics: a survey. *Journal of Sound and Vibration,* 167(2):347–355.

Narayaja, K. K. & Jebaraj, C. (1999). Sensitivity analysis of local/global modal parameters for identification of a crack in a beam. *Journal of Sound and Vibration,* 228(5):977–994.

Raath, A. D. (1992). *Structural dynamic response reconstruction in the time domain*. PhD Thesis. RSA: University of Pretoria.

Raich, A. & Liszkai, T. (2003). A model parameter updating damage detection technique using genetic algorithm. In *Metal Structures- Design, Fabrication, Economy. Edited by Jármai & Farkas,* Millpress: Rotterdam.

Rao, S.S. (1989). *The finite element method in engineering.* New York: Pergamon Press.

Rao, S.S. (1995). *Mechanical vibrations.* Reading, Mass.: Addison-Wesley Publishing Company.

Rytter, A. (1993). *Vibration-based inspection of civil engineering structures.* Ph D Thesis. Denmark: Aalborg University.

Shigley, J.E., Mischke, C.R., & Budynas, R.G. (2003). *Mechanical Engineering Design.* Boston: McGraw Hill Higher Education.

Sohn, H. & Farrar, C. R. (2001). Damage diagnosis using time series analysis of vibration signals. *Journal of Smart Materials and Structures,* 10:1-6.

Sohn, H., Fugate, M. L. & Farrar, C. R. (2000). *Continuous structural monitoring using statistical process control.* Conference proceedings of the 18^{th} IMAC. San Antonio, Texas.

Sohn, H. & Law, K. H. (1998). Bayesian probabilistic damage detection of reinforced-concrete bridge column. *Earthquake Engineering and Structural Dynamics.*

Van Tonder, F. (2004). *Experimental strain measurement using strain gages*(Brochure). RSA: University of Pretoria.

Wang, Z., Lin, R. M. & Lim, M. K. (1997). Structural damage detection using measured FRF data. *Computer Methods in Applied Mechanics and Engineering,* 147:187–197.

Worden, K., Manson, G. & Fieller, N. R. J. (2000). Damage detection using outlier analysis. *Journal of Sound and Vibration,* 229(3):647–667.

Worden, K., Manson, G. & Allman, D. (2003). Experimental validation of a health monitoring methodology: Part I. novelty detection on a laboratory structure. *Journal of Sound and Vibration,* 259(2):323–343.

Yoon, M. K., Heider, D., Gillespie Jr., J. W., Ratcliffe, C. P. & Crane, R. M. (in press).

Local damage detection using the two-dimensional gapped smoothing method, *Journal of Sound and Vibration*. Elsevier ltd (available online).

Zapico, J. L., González, M. P. & Worden, K. (2003). Damage assessment using neural networks. *Mechanical Systems and Signal Processing,* 17(1):119–125.

Ziaei-Rad, S. & Imregun, M. (1996). On the accuracy required of experimental data for finite element model updating. *Journal of Sound and Vibration*, 196(3):323–336.

Zienkiewicz, O.C. (1977). *The finite element method*. New York: McGraw-Hill publishing Co. Ltd.

APPENDIX

A. THE FORMULATION OF A CRACK MODEL BY ELEMENT SEPARATION

Consider figure A.1, where the two four-noded quadrilaterals are separated along the red line at node 3 (top diagram). The cracked structure is shown on the bottom diagram and has one more node added (node 5), which evidently changes the node numbering beyond the crack. Now, the changes to the structure of the stiffness matrix are reflected in the reduced number of coupled cross stiffness elements within the modified system stiffness matrix (from 16 to 4) (see tables A.1 A.2). From the structures presented

Tab. A.1: Structure of undamaged system stiffness matrix

DOF	1	2	3	4	5	6	7	8	9	10	11	12
1	k^1_{11}	k^1_{12}	k^1_{13}	k^1_{14}	k^1_{15}	k^1_{16}	k^1_{17}	k^1_{18}	0	0	0	0
2	k^1_{21}	k^1_{22}	k^1_{23}	k^1_{24}	k^1_{25}	k^1_{26}	k^1_{27}	k^1_{28}	0	0	0	0
3	k^1_{31}	k^1_{32}	k^1_{33}	k^1_{34}	k^1_{35}	k^1_{36}	k^1_{37}	k^1_{38}	0	0	0	0
4	k^1_{41}	k^1_{42}	k^1_{43}	k^1_{44}	k^1_{45}	k^1_{46}	k^1_{47}	k^1_{48}	0	0	0	0
5	k^1_{51}	k^1_{52}	k^1_{53}	k^1_{54}	$k^1_{55}+k^2_{11}$	$k^1_{56}+k^2_{12}$	$k^1_{57}+k^2_{13}$	$k^1_{58}+k^2_{14}$	k^2_{15}	k^2_{16}	k^2_{17}	k^2_{18}
6	k^1_{61}	k^1_{62}	k^1_{63}	k^1_{64}	$k^1_{65}+k^2_{21}$	$k^1_{66}+k^2_{22}$	$k^1_{67}+k^2_{23}$	$k^1_{68}+k^2_{24}$	k^2_{25}	k^2_{26}	k^2_{27}	k^2_{28}
7	k^1_{71}	k^1_{72}	k^1_{73}	k^1_{74}	$k^1_{75}+k^2_{31}$	$k^1_{76}+k^2_{32}$	$k^1_{77}+k^2_{33}$	$k^1_{78}+k^2_{34}$	k^2_{35}	k^2_{36}	k^2_{37}	k^2_{38}
8	k^1_{81}	k^1_{82}	k^1_{83}	k^1_{84}	$k^1_{85}+k^2_{41}$	$k^1_{86}+k^2_{42}$	$k^1_{87}+k^2_{43}$	$k^1_{88}+k^2_{44}$	k^2_{45}	k^2_{46}	k^2_{47}	k^2_{48}
9	0	0	0	0	k^2_{51}	k^2_{52}	k^2_{53}	k^2_{54}	k^2_{55}	k^2_{56}	k^2_{57}	k^2_{58}
10	0	0	0	0	k^2_{61}	k^2_{62}	k^2_{63}	k^2_{64}	k^2_{65}	k^2_{66}	k^2_{67}	k^2_{68}
11	0	0	0	0	k^2_{71}	k^2_{72}	k^2_{73}	k^2_{74}	k^2_{75}	k^2_{76}	k^2_{77}	k^2_{78}
12	0	0	0	0	k^2_{81}	k^2_{82}	k^2_{83}	k^2_{84}	k^2_{85}	k^2_{86}	k^2_{87}	k^2_{88}

in tables A.1 and A.2, it is noted that the stiffness matrix symmetry and bandedness are preserved. The half band width of both stiffness matrices are 5. Thus the cracked stiffness matrix requires 12 more computer storage locations during the analysis (84 vs. 72). The computational cost difference is insignificant.

Now, consider the effect of the cyclic load on the structure modelled by two elements

Tab. A.2: Structure of damaged system stiffness matrix

DOF	1	2	3	4	5	6	7	8	9	10	11	12	13	14
1	k^1_{11}	k^1_{12}	k^1_{13}	k^1_{14}	k^1_{15}	k^1_{16}	k^1_{17}	k^1_{18}	0	0	0	0	0	0
2	k^1_{21}	k^1_{22}	k^1_{23}	k^1_{24}	k^1_{25}	k^1_{26}	k^1_{27}	k^1_{28}	0	0	0	0	0	0
3	k^1_{31}	k^1_{32}	k^1_{33}	k^1_{34}	k^1_{35}	k^1_{36}	k^1_{37}	k^1_{38}	0	0	0	0	0	0
4	k^1_{41}	k^1_{42}	k^1_{43}	k^1_{44}	k^1_{45}	k^1_{46}	k^1_{47}	k^1_{48}	0	0	0	0	0	0
5	k^1_{51}	k^1_{52}	k^1_{53}	k^1_{54}	k^1_{55}	k^1_{56}	k^1_{57}	k^1_{58}	0	0	0	0	0	0
6	k^1_{61}	k^1_{62}	k^1_{63}	k^1_{64}	k^1_{65}	k^1_{66}	k^1_{67}	k^1_{68}	0	0	0	0	0	0
7	k^1_{71}	k^1_{72}	k^1_{73}	k^1_{74}	k^1_{75}	k^1_{76}	$k^1_{77}+k^2_{11}$	$k^1_{78}+k^2_{12}$	k^2_{13}	k^2_{14}	k^2_{15}	k^2_{16}	k^2_{17}	k^2_{18}
8	k^1_{81}	k^1_{82}	k^1_{83}	k^1_{84}	k^1_{85}	k^1_{86}	$k^1_{87}+k^2_{21}$	$k^1_{88}+k^2_{22}$	k^2_{23}	k^2_{24}	k^2_{25}	k^2_{26}	k^2_{27}	k^2_{28}
9	0	0	0	0	0	0	k^2_{31}	k^2_{32}	k^2_{33}	k^2_{34}	k^2_{35}	k^2_{36}	k^2_{37}	k^2_{38}
10	0	0	0	0	0	0	k^2_{41}	k^2_{42}	k^2_{43}	k^2_{44}	k^2_{45}	k^2_{46}	k^2_{47}	k^2_{48}
11	0	0	0	0	0	0	k^2_{51}	k^2_{52}	k^2_{53}	k^2_{54}	k^2_{55}	k^2_{56}	k^2_{57}	k^2_{58}
12	0	0	0	0	0	0	k^2_{61}	k^2_{62}	k^2_{63}	k^2_{64}	k^2_{65}	k^2_{66}	k^2_{67}	k^2_{68}
13	0	0	0	0	0	0	k^2_{71}	k^2_{72}	k^2_{73}	k^2_{74}	k^2_{75}	k^2_{76}	k^2_{77}	k^2_{78}
14	0	0	0	0	0	0	k^2_{81}	k^2_{82}	k^2_{83}	k^2_{84}	k^2_{85}	k^2_{86}	k^2_{87}	k^2_{88}

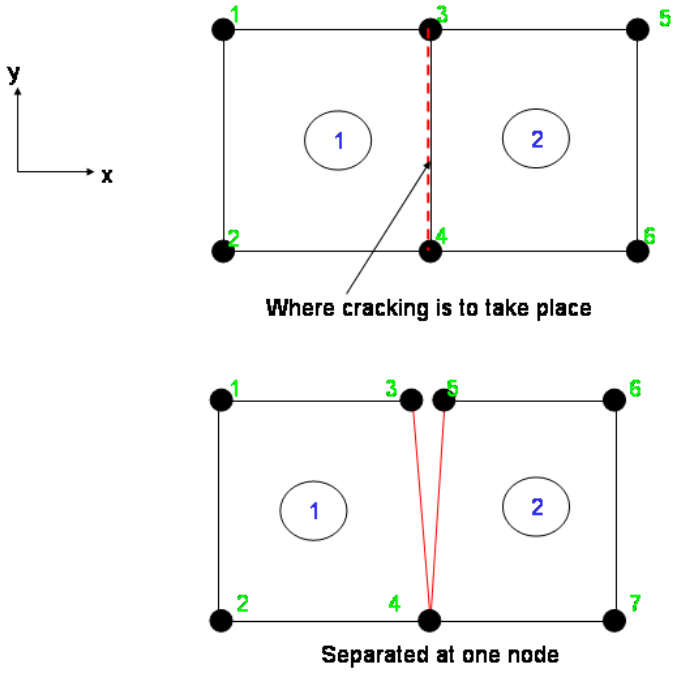

Fig. A.1: Four-noded quadrilateral elements separated along their boundary to model crack

as given in figure A.2. The structure is assumed constrained at nodes 1 and 2. When a cyclic load is applied, the crack opens during tension (view B) and closes during compression (view D). Thus in tension, only the cross stiffness elements at node 4 offer the constraining forces, while in compression, node 3 and 5 come in contact and behave as if there is no crack. Therefore, when using this approach to model cracks in MSC/Nastran, it is important to place a contact surface between the two cracked faces to guard against the non-physical penetration of elements.

Thus the effect of the crack is more significant on tensile reversals than compressive reversals. The structure behaves as if there is no damage at all on the compressive reversal. However, this is only true during stable crack growth, because when the crack has gone beyond its fracture toughness limit, the volume of material beyond the crack tip is largely plastic, and therefore, can undergo permanent deformation, which might change substantially the behaviour of the cracked structure on both the tensile and compressive reversals.

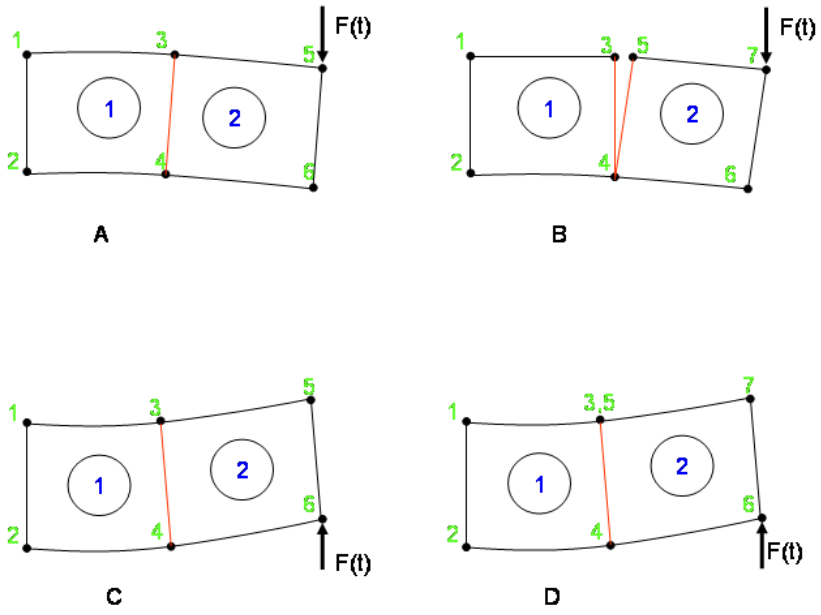

Fig. A.2: Behaviour of non-cracked and cracked structure under cyclic loading

In view of the foregoing discussion, the damaged stiffness matrix can be written as:

$$[K]_{dam} = \sum_{i=1}^{N} \left[\sum_{j=1}^{n} \sum_{k=1}^{n} ke_{j,k} \right]_{I,J} \tag{A.1}$$

where again the summations represent the assembling operation and subscripts (I, J)

represent the position within the system stiffness matrix where the first diagonal element of the assembled element stiffness matrix is to be placed. The values of (I, J) are obtained from the connectivity matrix.

Therefore, the equation of motion can be modified as:

$$[M]\{\ddot{x}(t)\} + \left([\widetilde{K}] + i[H]\right)\{x(t)\} = \{f(t)\}e^{i\omega t} \tag{A.2}$$

where $[\widetilde{K}]$, is equal to $[K]$ during compression and equal to $[K]_{dam}$ during tension.

Thus, in the state-space formulation, the time responses are determined from equation A.3(Haftka, et al. 1990):

$$\{\dot{\chi}\} = [E]_{dam}\{\chi\} + \{D\} \tag{A.3}$$

where,

$$[E]_{dam} = \begin{bmatrix} [0] & [I] \\ -[M]^{-1}\left([\widetilde{K}] + i[H]\right) & [0] \end{bmatrix}$$

Structural time responses will result in amplitude changes being more conspicuous on one side depending on the location of the surface crack and the direction of the force. For the configuration shown in figure A.2, the response magnitude changes are more appreciable on the negative side of the response history.

B. INVERSION OF THE DYNAMIC MATRIX

There are four methods proposed by Raath (1992), to realise the inverse model (actually, he developed the first three methods and adopted the fourth one in cases of persisting instabilities of the plant dynamics). The choice of any method depends on the stability of the system as dictated by the location of its zeros and poles:

1. **First method:** An ARX model is identified for each output channel. The identified ARX models are combined into a multivariable (MIMO) state space model. And, finally, the (MIMO) state space model is inverted.
2. **Second method:** An ARX model for each output channel is identified. Each identified ARX model is inverted. And, finally, the inverted ARX models are combined into one multivariable (MIMO) state space model.
3. **Third method:** The inversion process is performed during identification. A direct inverse ARX model is identified for each input channel. The identified ARX models are combined into one multivariable (MIMO) state space model.
4. **Fourth method :** Where it is impossible to implement any of the above methods because of persisting instabilities, a classical linear quadratic optimal servo-controller is used (see figure B.2).

The flowchart illustrating the model inversion process for the first three methods is displayed in figure B.1.

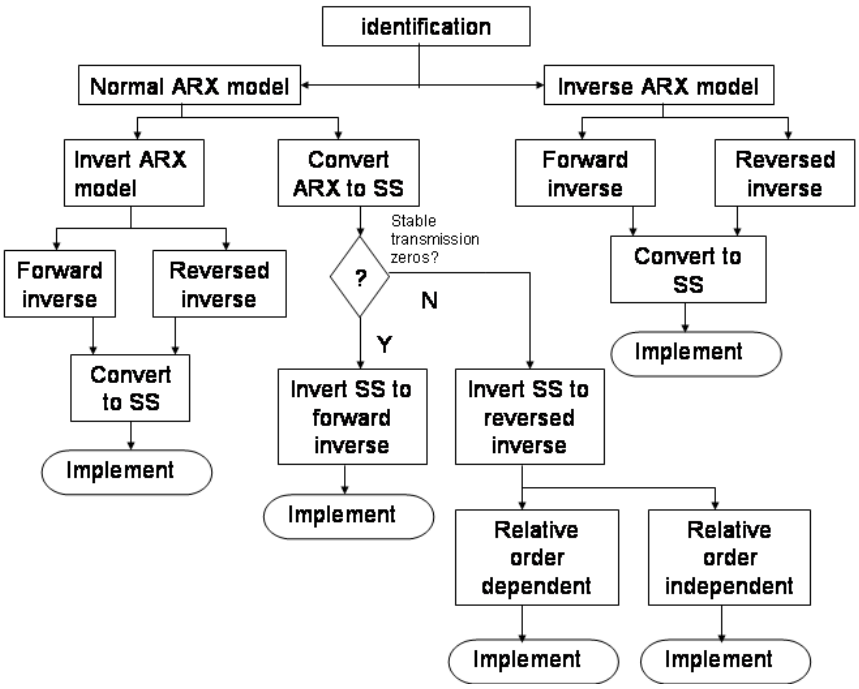

Fig. B.1: Summarised procedure in selecting the appropriate inverting technique

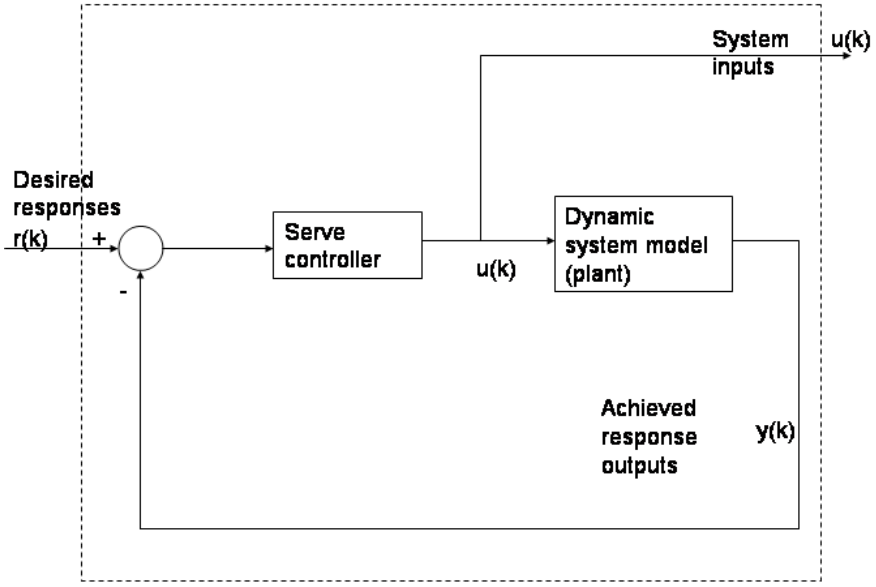

Fig. B.2: Application of a servo-controller to determine the system inputs from the desired system responses

C. THE FORMULATION OF THE OPEN CRACKED BEAM ELEMENT

This appendix draws from the work of Krawczuk et al. (2000). In their work they derived finite element matrices for an open cracked elastoplastic beam element. The underlying theory is that materials develop plastic strains as they yield beyond their yield strengths. Thus, in the vicinity of the crack tip materials tend to have a plastic zone. The existence of this plastic zone increases the local flexibility of the material. This may sometimes affect the dynamic behaviour of the material. For example, natural frequencies are noted to shift because of the existence of cracks in vibrating structures.

The extent to which this increase of flexibility affects the dynamic behaviour depends on the size of the plastic zone. The size of the plastic zone around the crack tip for an open fracture mode is given by:

$$r_y = \frac{1}{2\pi}\left(\frac{K_I}{\sigma_y}\right)^2 \tag{C.1}$$

where K_I is the remote stress intensity factor, σ_y is the material yield strength.

The stress intensity factor for a crack with a plastic zone around the tip is given by, (Krawczuk, et al. 2000):

$$K_{Ip} = f(g)\sigma\sqrt{a + r_y} \tag{C.2}$$

where a is the crack length, $f(g)$ is a correction factor which takes into account the body and crack geometry, while σ is the applied nominal stress.

By substituting C.1 into C.2, the stress intensity factor becomes:

$$K_{Ip} = K_I\sqrt{1 + \frac{f(g)^2}{2\pi}\left(\frac{\sigma}{\sigma_y}\right)^2} \tag{C.3}$$

Irwin suggested that the local flexibilities of the body due to the crack are given by the expression:

$$c_{ij} = \frac{\partial^2}{\partial P_i P_j}\int_A J_c dA \tag{C.4}$$

where J_c denotes the strain energy density function, P is a corresponding force at the cracked cross-section, while A is the crack area. Equation C.4 is derived from the fact that flexibility is the quotient of the strain energy and the square of the applied force.

For an open fracture mode, the strain energy density function is given by:

$$J_c = \frac{1}{E'}\left(\sum_{i=1}^{i=6} K_{Ipi}\right) \tag{C.5}$$

where $E' = E/(1-\nu^2)$ for plane state of stress, E is the Young's modulus and ν is the Poisson's ratio.

If the beam is subjected to bending only, the stress intensity factor may be calculated as:

$$K_{Ip} = \frac{6M}{BH^2}\sqrt{1 + \frac{f(g)^2}{2\pi}\left(\frac{\sigma}{\sigma}\right)^2} \tag{C.6}$$

where B and H denote the width and thickness of the beam, respectively. M is the applied bending moment.

When C.5 and C.6 are substituted into C.4 the following expression for the flexibility results:

$$c = \frac{72}{EB^2H^4}\int_A f(g)^2 a dA + \frac{216}{E\pi B^2H^4}\left(\frac{\sigma}{\sigma}\right)^2 \int_A f(g)^4 a dA \tag{C.7}$$

Equation C.7 can be rewritten in terms of crack ratio $\bar{a} = a/H$ as:

$$c = \frac{72}{EBH^2}\int_0^{\bar{a}_k} \bar{f}(g)^2 \bar{a} d\bar{a} + \frac{216}{E\pi BH^2}\left(\frac{\sigma}{\sigma}\right)^2 \int_0^{\bar{a}_k} \bar{f}(g)^4 \bar{a} d\bar{a} \tag{C.8}$$

where a is the crack length and $\bar{f}(g)$ is the correction factor expressed in terms of the crack ratio.

The expression for the flexibility just obtained is applied to the stiffness matrix equation which is given as:

$$K_{ce} = EJ\begin{bmatrix} \frac{12}{L^3} & \frac{6}{L^2} & -\frac{12}{L^3} & \frac{6}{L^2} \\ \frac{6}{L^2} & \frac{4L^2+6LK+3K^2}{L(L+K)^2} & -\frac{6}{L^2} & \frac{2L^2+6LK+3K^2}{L(L+K)^2} \\ -\frac{12}{L^3} & -\frac{6}{L^2} & \frac{12}{L^3} & -\frac{6}{L^2} \\ \frac{6}{L^2} & \frac{2L^2+6LK+3K^2}{L(L+K)^2} & -\frac{6}{L^2} & \frac{4L^2+6LK+3K^2}{L(L+K)^2} \end{bmatrix} \tag{C.9}$$

where $K = EJc$ and J denotes the geometric moment of inertia of the beam cross-section.

The stiffness matrix in equation C.8 is a function of the crack ratio $\bar{a}$. The form of the stiffness matrix is reduced to the non-cracked form if $K = 0$, which is equivalent to $a = 0$. A schematic diagram of the cracked beam element is shown in figure C.1.

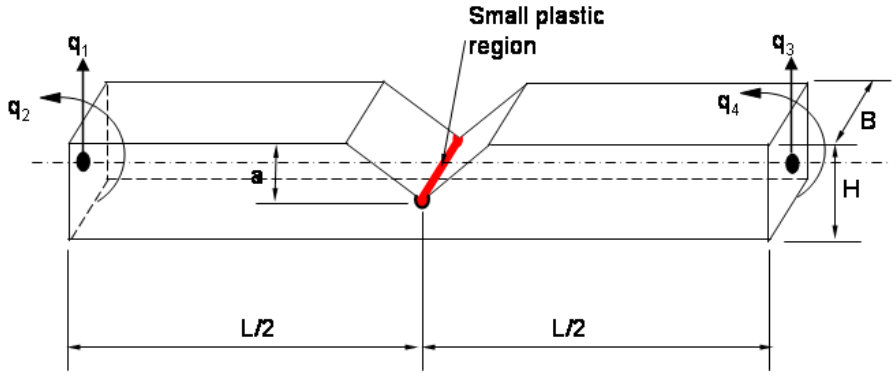

Fig. C.1: The diagram of the cracked beam finite element model

D. CALCULATING THE STRESS

Given the beam structure shown in figure D.1, the stress on the beam at any section x was desired. The calculations were based on statically indeterminate beam solutions.

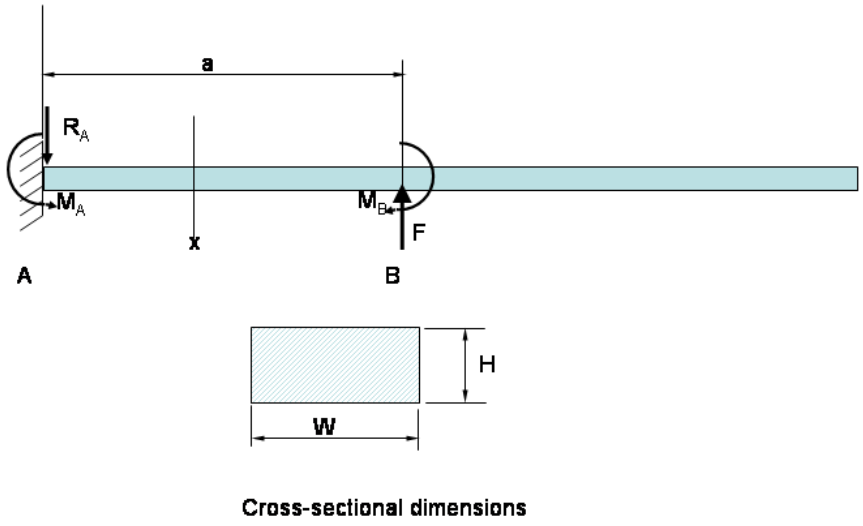

Fig. D.1: Schematic diagram of the beam configuration

The equilibrium of vertical forces on the beam yield:

$$R_A - F = 0 \tag{D.1}$$

The equilibrium of moments about A is:

$$M_A + Fa - M_B = 0 \tag{D.2}$$

At the point x along the beam, the bending moment is given by:

$$EI\frac{d^2v}{dx^2} = M_A + R_A x \tag{D.3}$$

Integrating equation D.3 yields the following forms:

$$EI\frac{dv}{dx} = M_A x + R_A\frac{x^2}{2} + A \tag{D.4}$$

$$EIv = M_A\frac{x^2}{2} + R_A\frac{x^3}{6} + Ax + B \tag{D.5}$$

Considering the following boundary conditions: $v(0) = 0$; $dv/dx(0) = 0$; $v(a) = \delta$ and $dv/dx(a) = 0$, the constants A and B are zero, while $M_A = -Fa/2$.

Thus equation D.5 becomes:

$$EI\delta = M_A\frac{a^2}{2} + R_A\frac{a^3}{6} \tag{D.6}$$

By substituting $M_A = -Fa/2$ into equation D.6 and solving for the applied force F, equation D.7 is obtained.

$$F = -\frac{12EI\delta}{a^3} \tag{D.7}$$

The bending moment at x is determined by:

$$M = \frac{12EI\delta}{a^3}\left(\frac{a}{2} - x\right) \tag{D.8}$$

From which the bending strain and stress are obtained as:

$$\epsilon = \frac{MH}{2EI} \tag{D.9}$$

$$\sigma = E'\epsilon \tag{D.10}$$

where $E' = E/(1-\nu^2)$ for the plane stress state.